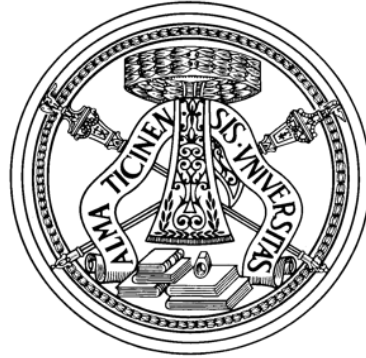


UNIVERSITÀ DEGLI STUDI DI PAVIA
FACOLTÀ DI INGEGNERIA
DIPARTIMENTO DI INGEGNERIA CIVILE E ARCHITETTURA
CORSO DI LAUREA MAGISTRALE IN INGEGNERIA CIVILE



TESI DI LAUREA

FINITE ELEMENT FORMULATIONS FOR ISOTROPIC AND
ANISOTROPIC MATERIALS: A COMPARISON BETWEEN
DIFFERENT APPROACHES

Candidato: Giuseppe Sineri

Relatore: Prof. Ferdinando Auricchio

Correlatrice: Dr. Giulia Scalet

Anno Accademico 2014/2015

Abstract

In engineering, thanks to the increasing and intensive use of fibers for reinforcement purposes, it is possible to obtain composite materials which have high mechanical strength and lightness. Such materials exhibit different physical properties and anisotropy, depending on the orientation of the fibers in the matrix. In the present thesis, in the context of small strain, we analyze anisotropic materials with a single family of inextensible fibers. The aim is to propose novel finite element formulations to be used in the simulation of structures composed of fiber-reinforced materials. We propose new formulations for the modeling of these materials, based on the use of well-known optimization methods to treat the inextensible constraint such as the Lagrange Multiplier, Penalty, and Perturbed Lagrangian approach. For each formulation various finite elements are developed, depending on the number of nodes (four-node and nine-node quadrangular element), and on the adopted interpolation for the Lagrange multiplier and displacement field. The proposed finite elements are tested on several numerical tests, to determine their performance.

Abstract

In ingegneria, grazie al crescente ed intensivo utilizzo di fibre d'armatura, è possibile ottenere materiali compositi dotati di alta resistenza meccanica e leggerezza. Tali materiali esibiscono diverse proprietà fisiche ed anisotropia, in base all'orientamento delle fibre all'interno della matrice. Nella presente tesi, nel contesto delle piccole deformazioni, analizziamo materiali anisotropi aventi un'unica famiglia di fibre inestensibili. L'obiettivo è quello di proporre nuove formulazioni agli elementi finiti per la simulazione di strutture composte da materiali fibro-rinforzati. Proponiamo nuove formulazioni per la modellazione di questi materiali, basate sull'utilizzo di ben noti metodi di ottimizzazione vincolata, quali Lagrange Multiplier, Penalty e Perturbed Lagrangian. Per ogni formulazione sviluppiamo vari elementi finiti, in base al numero di nodi (elemento quadrangolare a quattro e a nove nodi) e all'interpolazione adottata per il moltiplicatore di Lagrange e per il campo degli spostamenti. Gli elementi finiti proposti sono testati attraverso vari test numerici, per determinare le loro prestazioni.

Contents

1	Introduction	14
2	Finite element procedure	17
2.1	Strong form	18
2.1.1	3D linear elasticity	18
2.1.2	2D linear elasticity	20
2.2	Weak form	21
2.3	Algebraic form	24
2.3.1	Isoparametric elements and approximations	24
2.4	Some basic formulations	30
2.4.1	Displacement-based formulations	30
2.4.2	Two-field mixed formulations	30
2.4.3	Three-field mixed formulations	32
3	Finite element formulations for isotropic materials	34
3.1	Q1-DB and T1-DB: displacement-based elements	35
3.2	Q1-PS: Pian-Sumihara assumed-stress element	37
3.3	Q1-E4 and Q1-E5: enhanced-strain elements	40
3.4	MINI: mixed Stokes flow element	42
4	Finite element formulations for anisotropic materials	45
4.1	Transverse isotropy	45
4.2	Proposed formulations	50

4.2.1	Lagrange Multiplier formulation	51
4.2.2	Penalty formulation	54
4.2.3	Perturbed Lagrangian formulation	55
4.2.4	Developed finite elements	57
5	Numerical tests	59
5.1	Programming environment overview	60
5.1.1	AceGen	60
5.1.2	AceFEM	61
5.2	Traction test	63
5.2.1	Isotropic material	65
5.2.2	Anisotropic material	65
5.3	Bending test	70
5.3.1	Isotropic material	71
5.3.2	Anisotropic material	73
5.4	Cook's membrane test	82
5.4.1	Isotropic material	83
5.4.2	Anisotropic material	84
5.5	Two-element distortion test	92
5.5.1	Isotropic material	93
5.5.2	Anisotropic material	93
6	Conclusions and future work	101
A	Analytical solutions	105
A.1	Traction test	105
A.2	Bending test	106

List of Figures

1.1	Examples of fiber-reinforced composite materials. Left: unidirectional reinforcement. Right: bidirectional reinforcement (fabric form). . . .	15
2.1	Superparametric representation.	25
2.2	Isoparametric representation.	25
2.3	Quadrilateral and triangular isoparametric elements.	26
3.1	MINI element approximations as proposed in [14].	44
4.1	Fiber-reinforced material.	46
4.2	Developed finite elements. Displacements and Lagrange multiplier interpolations.	58
5.1	Hybrid system for multi-language and multi-environment finite element code generation [25].	60
5.2	Traction test. Geometry and boundary conditions.	63
5.3	Traction test for anisotropic material, with fiber direction (left) $\mathbf{a} = (1, 0)$, (middle) $\mathbf{a} = (0, 1)$, (right) $\mathbf{a} = (\sqrt{2}/2, \sqrt{2}/2)$. The three tests are denoted, respectively, as T1, T2 and T3.	64
5.4	Traction test T1: sensitivity to C_C for the Penalty Formulation. . . .	68
5.5	Traction test T2: sensitivity to C_C for the Penalty Formulation. . . .	68
5.6	Traction test T3: sensitivity to C_C for the Penalty Formulation. . . .	68
5.7	Traction test T1: sensitivity to C_C for the Perturbed Lagrangian Formulation.	69

5.8	Traction test T2: sensitivity to C_C for the Perturbed Lagrangian Formulation.	69
5.9	Traction test T3: sensitivity to C_C for the Perturbed Lagrangian Formulation.	69
5.10	Bending test. Geometry and boundary conditions.	70
5.11	Bending test for anisotropic material, with fiber direction (left) $\mathbf{a} = (1, 0)$, (middle) $\mathbf{a} = (0, 1)$, (right) $\mathbf{a} = (\sqrt{2}/2, \sqrt{2}/2)$. The three tests are denoted, respectively, as B1, B2 and B3.	71
5.12	Bending test sensitivity to mesh setting $\nu = 0.3$: isotropic formulations.	72
5.13	Bending test B1: sensitivity to mesh for the Lagrange Multiplier Formulation.	75
5.14	Bending test B2: sensitivity to mesh for the Lagrange Multiplier Formulation.	76
5.15	Bending test B3: sensitivity to mesh for the Lagrange Multiplier Formulation.	76
5.16	Bending test B1: sensitivity to mesh for the Penalty Formulation.	76
5.17	Bending test B2: sensitivity to mesh for the Penalty Formulation.	77
5.18	Bending test B3: sensitivity to mesh for the Penalty Formulation.	77
5.19	Bending test B1: sensitivity to mesh for the Perturbed Lagrangian Formulation.	77
5.20	Bending test B2: sensitivity to mesh for the Perturbed Lagrangian Formulation.	78
5.21	Bending test B3: sensitivity to mesh for the Perturbed Lagrangian Formulation.	78
5.22	Bending test B1: sensitivity to C_C for the Penalty Formulation.	79
5.23	Bending test B2: sensitivity to C_C for the Penalty Formulation.	80
5.24	Bending test B3: sensitivity to C_C for the Penalty Formulation.	80
5.25	Bending test B1: sensitivity to C_C for the Perturbed Lagrangian Formulation.	80

5.26	Bending test B2: sensitivity to C_C for the Perturbed Lagrangian Formulation.	81
5.27	Bending test B3: sensitivity to C_C for the Perturbed Lagrangian Formulation.	81
5.28	Cook's membrane test. Geometry and boundary conditions.	82
5.29	Cook's membrane test for anisotropic material, with fiber direction (left) $\mathbf{a} = (1, 0)$, (middle) $\mathbf{a} = (0, 1)$, (right) $\mathbf{a} = (\sqrt{2}/2, \sqrt{2}/2)$. The three tests are denoted, respectively, as C1, C2 and C3.	82
5.30	Cook's membrane test sensitivity to mesh setting $\nu = 0.3$: isotropic formulations.	84
5.31	Cook's membrane test C1: sensitivity to mesh for the Lagrange Multiplier Formulation.	86
5.32	Cook's membrane test C2: sensitivity to mesh for the Lagrange Multiplier Formulation.	86
5.33	Cook's membrane test C3: sensitivity to mesh for the Lagrange Multiplier Formulation.	86
5.34	Cook's membrane test C1: sensitivity to mesh for the Penalty Formulation.	87
5.35	Cook's membrane test C2: sensitivity to mesh for the Penalty Formulation.	87
5.36	Cook's membrane test C3: sensitivity to mesh for the Penalty Formulation.	87
5.37	Cook's membrane test C1: sensitivity to mesh for the Perturbed Lagrangian Formulation.	88
5.38	Cook's membrane test C2: sensitivity to mesh for the Perturbed Lagrangian Formulation.	88
5.39	Cook's membrane test C3: sensitivity to mesh for the Perturbed Lagrangian Formulation.	88
5.40	Cook's membrane test C1: sensitivity to C_C for the Penalty Formulation.	89
5.41	Cook's membrane test C2: sensitivity to C_C for the Penalty Formulation.	90

5.42	Cook's membrane test C3: sensitivity to C_C for the Penalty Formulation.	90
5.43	Cook's membrane test C1: sensitivity to C_C for the Perturbed Lagrangian Formulation.	90
5.44	Cook's membrane test C2: sensitivity to C_C for the Perturbed Lagrangian Formulation.	91
5.45	Cook's membrane test C3: sensitivity to C_C for the Perturbed Lagrangian Formulation.	91
5.46	Two-element Distortion test. Geometry and boundary conditions. . .	92
5.47	Two-elements distortion test for anisotropic material, with fiber direction (left) $\mathbf{a} = (1, 0)$, (middle) $\mathbf{a} = (0, 1)$, (right) $\mathbf{a} = (\sqrt{2}/2, \sqrt{2}/2)$. The three tests are denoted, respectively, as D1, D2 and D3.	93
5.48	Two-elements distortion test sensitivity to mesh distortion: isotropic formulations.	93
5.49	Distortion test D1: sensitivity to mesh distortion for the Lagrange Multiplier Formulation.	95
5.50	Distortion test D2: sensitivity to mesh distortion for the Lagrange Multiplier Formulation.	95
5.51	Distortion test D3: sensitivity to mesh distortion for the Lagrange Multiplier Formulation.	96
5.52	Distortion test D1: sensitivity to mesh distortion for the Penalty Formulation.	96
5.53	Distortion test D2: sensitivity to mesh distortion for the Penalty Formulation.	96
5.54	Distortion test D3: sensitivity to mesh distortion for the Penalty Formulation.	97
5.55	Distortion test D1: sensitivity to mesh distortion for the Perturbed Lagrangian Formulation.	97
5.56	Distortion test D2: sensitivity to mesh distortion for the Perturbed Lagrangian Formulation.	97

5.57 Distortion test D3: sensitivity to mesh distortion for the Perturbed Lagrangian Formulation.	98
5.58 Distortion test D1: sensitivity to C_C for the Penalty Formulation. . .	98
5.59 Distortion test D2: sensitivity to C_C for the Penalty Formulation. . .	99
5.60 Distortion test D3: sensitivity to C_C for the Penalty Formulation. . .	99
5.61 Distortion test D1: sensitivity to C_C for the Perturbed Lagrangian Formulation.	99
5.62 Distortion test D2: sensitivity to C_C for the Perturbed Lagrangian Formulation.	100
5.63 Distortion test D3: sensitivity to C_C for the Perturbed Lagrangian Formulation.	100
6.1 Finite elements for anisotropic materials.	101
A.1 Pure bending of a beam	106

List of Tables

2.1	Two-dimensional shape functions.	27
2.2	Two-dimensional Gauss-Legendre quadrature.	29
5.1	Traction test numerical results: isotropic formulations.	65
5.2	Traction test numerical results: anisotropic formulations. When the constraint is effective, the results are indicated in green , while the incorrect results are indicated in red . Instead, when the constraint is ineffective, the results are indicated in black.	66
5.3	Traction test numerical results: sensitivity to mesh.	67
5.4	Bending test numerical results: isotropic formulations.	72
5.5	Bending test: solutions for anisotropic formulations setting $\mathbf{a} = (0, 0)$	73
5.6	Bending test numerical results: anisotropic formulations. When the constraint is effective, the results are indicated in green , while the incorrect results are indicated in red . Instead, when the constraint is ineffective, the results are indicated in black.	74
5.7	Cook's membrane test numerical results: isotropic formulations.	83
5.8	Cook's membrane test numerical results: anisotropic formulations. When the constraint is effective, the results are indicated in green , while the incorrect results are indicated in red . Instead, when the constraint is ineffective, the results are indicated in black.	85

5.9	Two-elements distortion test numerical results: anisotropic formulations. When the constraint is effective, the results are indicated in green , while the incorrect results are indicated in red . Instead, when the constraint is ineffective, the results are indicated in black.	94
6.1	Traction test results.	102
6.2	Bending test results.	102
6.3	Cook's membrane test results.	103
6.4	Two-element distortion test results.	103

Chapter 1

Introduction

The use of fiber reinforcements for the development of new and more efficient materials can be traced back to the 1960s. During the years, the high stiffness and the specific resistance of the fibers have been exploited to create composite materials, binding the reinforcement to a continuous matrix [1].

The interest towards advanced composite materials stems from the mechanical properties of the reinforcement fibers used, which confer a significant increase in structural efficiency. Historically, one of the first composite materials used in the context of civil constructions can be considered the reinforced concrete, in which the matrix is composed of concrete and the fibers are identified by the longitudinal reinforcement. A recent composite material used in the rehabilitation of existing structures is the fiber-reinforced polymer, which is composed of fibers (glass, carbon, steel etc.), embedded in a polymer matrix.

The basic element of fiber-reinforced materials is given by a single unidirectional fiber layer immersed in a matrix. The superimposition of more layers can give rise to materials with multidirectional reinforcement. As an example, Figure 1.1 shows two types of fiber-reinforced systems consisting of unidirectional and bidirectional reinforcements.

A great advantage of fiber-reinforced materials lies in the high resistance and stiffness compared to a low specific weight, while a limit for their exploitation is that the fibers, by themselves, can only transmit tensile uniaxially loads: hence, the

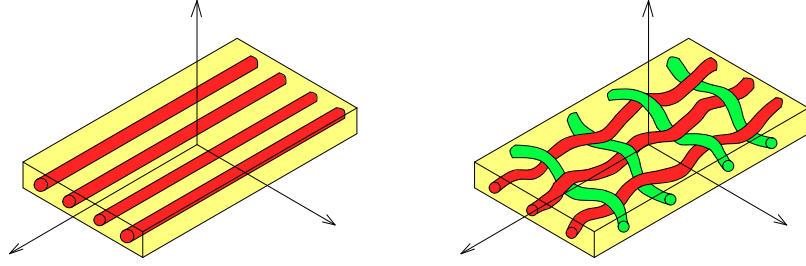


Figure 1.1: Examples of fiber-reinforced composite materials. Left: unidirectional reinforcement. Right: bidirectional reinforcement (fabric form).

necessity of a continuous matrix.

Given the widespread use of fiber-reinforced materials, it is clear the need for new modeling approaches and finite element formulations for the design of structural components. To this purpose, it is necessary to take into account the specific properties of these materials, i.e., the high anisotropy and strength ratio between matrix and fibers. Fiber-reinforced materials generally present anisotropic physical properties: for this reason they show a material directional constraint in the mathematical formulation, due to the matrix-reinforcement welding. The present thesis focuses on the case of inextensible fibers, where the stiffness ratio between matrix and fibers tends to infinity, due to the presence of a constraint associated to the fibers inextensibility. To treat the presence of constraints in the modeling formulation, we propose to adopt methods from constrained optimization [2, 3]. In particular, we adopt the following three methods:

1. Lagrange Multiplier method
2. Penalty method
3. Perturbed Lagrangian method

From the numerical point of view, this leads to boundary value problems that cannot be solved through classical displacement-based finite elements. Locking phenomena are in fact very well-known in the literature, as in the case of incompressible linear elasticity [4]. Therefore, we adopt mixed finite element formulations which are stable and well-performing in the small strain and isotropic regime.

To verify the response of these formulations and to determine their limits, we first perform various benchmark tests for isotropic linear elasticity, by using well-known finite element formulations, such as displacement-based, hybrid assumed-stress (mixed two-field formulation), enhanced-strain (mixed three-field formulation) and mixed MINI (mixed Stokes flow formulation). Then, we test the mixed formulations for anisotropic materials on the same benchmark tests.

The thesis is organized as follows:

- *Chapter 2. Finite element procedure.* Starting from the differential form of linear elasticity, the classical finite element procedure is described, which allows to find the solution of the problem. Particular emphasis is given to the classical variational principles, which are the basis of the formulations discussed in Chapter 3.
- *Chapter 3. Finite element formulations for isotropic materials.* Regarding isotropic materials, as previously mentioned, some of the well-known FEM formulations are implemented. These formulations are presented in this chapter.
- *Chapter 4. Finite element formulations for anisotropic materials.* This chapter treats the main part of the thesis, i.e., the proposed formulations for the modeling of anisotropic materials. A recall to the classic modeling procedure, based on the invariants derived from the tensor and vector fields, is also provided.
- *Chapter 5. Numerical tests.* This chapter summarizes the results of the performed benchmark tests and describes the characteristics of the used programming environment.
- *Chapter 6. Conclusions and future work.* A conclusion on the performance of each proposed formulation, together with future research direction, is provided.

Chapter 2

Finite element procedure

In order to evaluate the correctness of the performed benchmark tests, we will use well-known classical finite element formulations that refer to homogeneous isotropic linear elastic materials. In addition, some concepts, such as multi-field variational basis, isoparametric elements, and numerical integration procedures, will be also useful in the study of the formulations that we will discuss in Chapter 4, for transversely isotropic materials. For this reason, in this chapter we recall some finite element basic concepts [5, 6, 7]. The finite element method (FEM) is a general approach to compute the approximate solution for any general differential equation that describes a physical problem (in our case the elasticity problem). Consequently, this chapter is structured following the classical finite element procedure, which consists of the following steps:

Convert *differential* to *integral* form

↓

Convert *integral* to *algebraic* form (introduction of approximation fields)

↓

Solution of *algebraic* problem (numerical integration procedure)

2.1 Strong form

In this section, we recall the differential form of the linear elastic problem.

2.1.1 3D linear elasticity

Linear elasticity is the mathematical study of how solid objects deform and become internally stressed due to prescribed loading conditions. The fundamental assumptions for linear elasticity are: small strains and linear relationships between the components of stress and strain. The equations governing a linear elastic boundary value problem (differential equation together with a set of additional constraints, called boundary conditions) are based on three tensor partial differential equations for the equilibrium between internal stress and external loads (*equilibrium* equations) and six infinitesimal strain-displacement relations (*compatibility* equations). The system of differential equations is completed by a set of linear algebraic *constitutive* relations. Let us now turn to a more formal description of the linear elasticity problem.

We consider a three-dimensional deformable continuous body, consisting of a domain $\Omega \subset \mathbb{R}^3$ and a boundary $\partial\Omega$, subdivided in turn into $\partial\Omega_u$ and $\partial\Omega_t$, representing respectively the constrained and the free boundary such that $\partial\Omega_u \cup \partial\Omega_t = \partial\Omega$.

With reference to the Cauchy continuum, assuming small strains, the linear elasticity problem is expressed by the following three tensor partial differential equations (also known as *field* equations):

$$\begin{aligned} \textit{equilibrium} \quad \operatorname{div} \boldsymbol{\sigma} + \mathbf{b} &= \mathbf{0} & \text{in } \Omega \\ \textit{constitutive} \quad \boldsymbol{\sigma} &= \mathbb{D} \boldsymbol{\varepsilon} & \text{in } \Omega \\ \textit{compatibility} \quad \boldsymbol{\varepsilon} &= \nabla^s \mathbf{u} & \text{in } \Omega \end{aligned} \tag{2.1}$$

where $\boldsymbol{\sigma}$ is the symmetric Cauchy stress tensor, $\boldsymbol{\varepsilon}$ is the symmetric infinitesimal strain tensor, \mathbf{u} is the displacement vector, \mathbb{D} is the fourth-order elasticity tensor, \mathbf{b} is the body force per unit volume vector, and ∇^s is the symmetric gradient operator, such as:

$$\boldsymbol{\varepsilon} = \nabla^s \mathbf{u} = \frac{1}{2} [\nabla \mathbf{u} + (\nabla \mathbf{u})^T] \quad (2.2)$$

In order to find the particular solution of Problem (2.1), we introduce the following boundary conditions:

$$\begin{aligned} \textit{imposed displacements} \quad \mathbf{u} &= \bar{\mathbf{u}} & \text{on} \quad \partial\Omega_u \\ \textit{imposed forces} \quad \boldsymbol{\sigma} \mathbf{n} &= \bar{\mathbf{t}} & \text{on} \quad \partial\Omega_t \end{aligned} \quad (2.3)$$

where $\bar{\mathbf{u}}$ and $\bar{\mathbf{t}}$ are the assigned displacement and surface force field, respectively, and \mathbf{n} is the outward normal vector. Equation (2.3)₁ is an *essential* boundary condition (representing the kinematics congruence between displacements and imposed displacements on $\partial\Omega_u$), while Equation (2.3)₂ is a *natural* boundary condition (representing the equilibrium between internal stress and external surface stress on $\partial\Omega_t$). Equations (2.1) have been introduced in tensor notation, but for the purpose of the FEM programming (discussed in the following chapters), it is useful to use the engineering notation. Taking advantage of the Voigt notation (you can use it by exploiting the symmetries of $\boldsymbol{\varepsilon}$, $\boldsymbol{\sigma}$, and \mathbb{D} tensors), the field equations become:

$$\begin{aligned} \textit{equilibrium} \quad [\mathbf{L}]^T \{\boldsymbol{\sigma}\} + \{\mathbf{b}\} &= \{\mathbf{0}\} & \text{in} \quad \Omega \\ \textit{constitutive} \quad \{\boldsymbol{\sigma}\} &= [\mathbb{D}][\mathbb{M}]\{\boldsymbol{\varepsilon}\} & \text{in} \quad \Omega \\ \textit{compatibility} \quad \{\boldsymbol{\varepsilon}\} &= [\mathbf{L}]\{\mathbf{u}\} & \text{in} \quad \Omega \end{aligned} \quad (2.4)$$

where the differential operator $[\mathbf{L}]^T$, which corresponds to *divergence*, is defined as:

$$[\mathbf{L}]^T = \begin{bmatrix} \frac{\partial}{\partial x} & 0 & 0 & \frac{\partial}{\partial y} & 0 & \frac{\partial}{\partial z} \\ 0 & \frac{\partial}{\partial y} & 0 & \frac{\partial}{\partial x} & \frac{\partial}{\partial z} & 0 \\ 0 & 0 & \frac{\partial}{\partial z} & 0 & \frac{\partial}{\partial y} & \frac{\partial}{\partial x} \end{bmatrix} \quad (2.5)$$

and the algebraic operator $[\mathbb{M}]$, which corresponds to *double-contraction*, is:

$$[\mathbb{M}] = \begin{bmatrix} 1 & 0 & 0 & 0 & 0 & 0 \\ 0 & 1 & 0 & 0 & 0 & 0 \\ 0 & 0 & 1 & 0 & 0 & 0 \\ 0 & 0 & 0 & 2 & 0 & 0 \\ 0 & 0 & 0 & 0 & 2 & 0 \\ 0 & 0 & 0 & 0 & 0 & 2 \end{bmatrix} \quad (2.6)$$

For a homogeneous linear-isotropic material, the stress can be express by the Hooke's law, as follows:

$$\{\boldsymbol{\sigma}\} = [\mathbb{D}^M] \{\boldsymbol{\varepsilon}\} = \lambda \operatorname{tr}(\boldsymbol{\varepsilon})\{\mathbf{1}\} + 2\mu\{\boldsymbol{\varepsilon}\} \quad (2.7)$$

where $\lambda = \frac{E\nu}{(1+\nu)(1-2\nu)}$ and $\mu = \frac{E}{2(1+\nu)}$ are, respectively, the first and second Lamé constants, E is the Young's Modulus, ν is the Poisson's ratio, and \mathbb{D} is the following *elasticity tensor*:

$$\mathbb{D} = [\lambda(\mathbf{1} \otimes \mathbf{1}) + 2\mu\mathbb{I}] = \begin{bmatrix} \lambda + 2\mu & \lambda & \lambda & 0 & 0 & 0 \\ \lambda & \lambda + 2\mu & \lambda & 0 & 0 & 0 \\ \lambda & \lambda & \lambda + 2\mu & 0 & 0 & 0 \\ 0 & 0 & 0 & \mu & 0 & 0 \\ 0 & 0 & 0 & 0 & \mu & 0 \\ 0 & 0 & 0 & 0 & 0 & \mu \end{bmatrix} \quad (2.8)$$

2.1.2 2D linear elasticity

In this thesis, we will restrict ourself to isotropic and anisotropic materials in the two-dimensional context. For this reason it is useful to express all the tensors, vectors, and matrices treated previously in two-dimensional form.

Specifically, the kinematic quantities take the following form:

$$\mathbf{u} = \begin{bmatrix} u \\ v \end{bmatrix}, \quad \boldsymbol{\varepsilon} = \begin{bmatrix} \varepsilon_{xx} \\ \varepsilon_{yy} \\ \varepsilon_{xy} \end{bmatrix} \quad (2.9)$$

while the static quantities:

$$\mathbf{b} = \begin{bmatrix} b_x \\ b_y \end{bmatrix}, \quad \mathbf{t} = \begin{bmatrix} t_x \\ t_y \end{bmatrix} = \begin{bmatrix} \sigma_{xx}n_x + \sigma_{xy}n_y \\ \sigma_{xy}n_x + \sigma_{yy}n_y \end{bmatrix}, \quad \boldsymbol{\sigma} = \begin{bmatrix} \sigma_{xx} \\ \sigma_{yy} \\ \sigma_{xy} \end{bmatrix} \quad (2.10)$$

where

$$\mathbf{n} = \begin{bmatrix} n_x \\ n_y \end{bmatrix} \quad (2.11)$$

The elasticity tensor takes the form:

$$\mathbb{D} = \begin{bmatrix} \lambda + 2\mu & \lambda & 0 \\ \lambda & \lambda + 2\mu & 0 \\ 0 & 0 & \mu \end{bmatrix} = \frac{E}{(1+\nu)(1-2\nu)} \begin{bmatrix} 1-\nu & \nu & 0 \\ \nu & 1-\nu & 0 \\ 0 & 0 & \frac{1}{2}(1-2\nu) \end{bmatrix} \quad (2.12)$$

and the operators:

$$[\mathbf{L}]^T = \begin{bmatrix} \frac{\partial}{\partial x} & 0 & \frac{\partial}{\partial y} \\ 0 & \frac{\partial}{\partial y} & \frac{\partial}{\partial x} \end{bmatrix}, \quad [\mathbb{M}] = \begin{bmatrix} 1 & 0 & 0 \\ 0 & 1 & 0 \\ 0 & 0 & 2 \end{bmatrix} \quad (2.13)$$

2.2 Weak form

The equilibrium differential Equation (2.1)₁ represents the *strong* form of the linear elasticity problem. When the problem is expressed in this form, it is difficult to obtain general closed-form solutions. For this reason we resort to numerical approxi-

mation methods. Here, we adopt the FEM to construct a *weak* form (also known as *integral* form) starting from Equation (2.1)₁. Subsequently, by introducing appropriate approximation fields, we can construct the so-called *algebraic* form (also known as *matrix* form), which is easy to solve. To our purpose, we make use of the principle of virtual work and the general variational principles theory.

The principle of virtual work constitutes an integral formulation of equilibrium. It states that:

Given a force system $F(\boldsymbol{\sigma}, \mathbf{b}, \bar{\mathbf{t}})$ and a displacement system $D(\delta\mathbf{u}, \delta\boldsymbol{\varepsilon})$, if for any system D which satisfies compatibility the following equality holds:

$$\delta\mathcal{L}^{ext} = \delta\mathcal{L}^{int} \quad (2.14)$$

then system F satisfies equilibrium.

The expressions of the internal and external work are, respectively:

$$\begin{aligned} \delta\mathcal{L}^{int} &= \int_{\Omega} (\boldsymbol{\sigma} : \delta\boldsymbol{\varepsilon}) dV \\ \delta\mathcal{L}^{ext} &= \int_{\Omega} (\mathbf{b} \cdot \delta\mathbf{u}) dV + \int_{\partial\Omega_t} (\bar{\mathbf{t}} \cdot \delta\mathbf{u}) dA \end{aligned} \quad (2.15)$$

Among all the displacement fields compatible with the kinematic constraints, the elastic problem solution is the one that makes steady the associated total potential energy functional of the system.

The internal potential energy is defined as the integral over the entire volume of the internal energy density W (or strain energy):

$$\Pi_{int}(\boldsymbol{\varepsilon}) = \int_{\Omega} W(\boldsymbol{\varepsilon}) dV = \frac{1}{2} \int_{\Omega} [\boldsymbol{\sigma} : \boldsymbol{\varepsilon}] dV \quad (2.16)$$

If both the constitutive and compatibility equations are implicitly satisfied, the internal energy can be rewritten as:

$$\Pi_{int}(\mathbf{u}) = \frac{1}{2} \int_{\Omega} [\mathbb{D}\boldsymbol{\varepsilon}(\mathbf{u}) : \boldsymbol{\varepsilon}(\mathbf{u})] dV \quad (2.17)$$

Similarly, the external potential energy is defined by:

$$\Pi_{ext}(\mathbf{u}) = - \int_{\Omega} [\mathbf{b} \cdot \mathbf{u}] dV - \oint_{\partial\Omega_t} [\bar{\mathbf{t}} \cdot \mathbf{u}] dA \quad (2.18)$$

To simplify the discussion, we omit the integral related to the external surface forces $\bar{\mathbf{t}}$. The total potential energy of the system is thus defined as the sum of the internal energy and external potential energy, as follows:

$$\Pi(\mathbf{u}) = \frac{1}{2} \int_{\Omega} [\mathbb{D}\boldsymbol{\varepsilon}(\mathbf{u}) : \boldsymbol{\varepsilon}(\mathbf{u})] dV - \int_{\Omega} [\mathbf{b} \cdot \mathbf{u}] dV \quad (2.19)$$

The stationarity of the total potential energy ensures that, a displacement field \mathbf{u} , satisfying the boundary condition (2.3)₁, is a solution of the elastic equilibrium problem (2.1) if it makes stationary the potential energy functional (2.19), as follows:

$$d\Pi(\mathbf{u}, \delta\mathbf{u}) = \int_{\Omega} [\mathbb{D}\boldsymbol{\varepsilon}(\mathbf{u}) : \boldsymbol{\varepsilon}(\delta\mathbf{u})] dV - \int_{\Omega} [\mathbf{b} \cdot \delta\mathbf{u}] dV = 0 \quad (2.20)$$

Applying this potential energy approach, only the equilibrium is respected, but not the compatibility and constitutive equations.

To overcome this problem, alternatives variational formulations have been proposed. The most generic is the Hu-Washizu functional [8], obtained by imposing the a-priori fulfilment of the compatibility conditions on the boundary and condition (2.3)₂ and all other equations in weak form. In this way we obtain a functional in three variables \mathbf{u} , $\boldsymbol{\varepsilon}$ and $\boldsymbol{\sigma}$, as follows:

$$\Pi_{HW}(\mathbf{u}, \boldsymbol{\varepsilon}, \boldsymbol{\sigma}) = \frac{1}{2} \int_{\Omega} [\boldsymbol{\varepsilon} : \mathbb{D}\boldsymbol{\varepsilon}] dV - \int_{\Omega} [\boldsymbol{\sigma} : (\boldsymbol{\varepsilon} - \nabla^s \mathbf{u})] dV - \Pi_{ext} \quad (2.21)$$

Taking the variation of this functional with respect to \mathbf{u} , $\boldsymbol{\varepsilon}$ and $\boldsymbol{\sigma}$, it is possible to recover the equilibrium, constitutive, and compatibility equations.

By requiring the compliance of the constitutive equation (2.1)₂, we obtain the two variable mixed functional of Hellinger-Reissner [9, 10], defined as:

$$\Pi_{HR}(\mathbf{u}, \boldsymbol{\sigma}) = -\frac{1}{2} \int_{\Omega} [\boldsymbol{\sigma} : \mathbb{D}^{-1} \boldsymbol{\sigma}] dV + \int_{\Omega} [\boldsymbol{\sigma} : \nabla^s \mathbf{u}] dV - \Pi_{ext} \quad (2.22)$$

Taking the variation of the functional with respect to \mathbf{u} and $\boldsymbol{\sigma}$, it is possible to recover the equilibrium equation and a combination of the constitutive and compatibility equations.

2.3 Algebraic form

In this section we introduce the concepts related to the algebraic form, which provides the introduction of the field approximation based on the domain discretization, and the numerical integration procedure.

2.3.1 Isoparametric elements and approximations

We introduce the concepts of *isoparametric element* and *numerical quadrature*. It was created to overcome the following difficulties with the classic method for the construction of the stiffness matrix:

1. The construction of shape functions that satisfy consistency requirements for higher order elements with curved boundaries becomes increasingly complicated;
2. Integrals that appear in the expressions of the element stiffness matrix and consistent nodal force vector can no longer be evaluated in simple closed form.

Moreover, the isoparametric method leads to a simple computer program formulation and it is generally applicable to two- and three-dimensional analyses and non-structural problems. For these reasons, isoparametric elements gave rise to a large number of formulations.

The most important concept is related to the approximations to both the geometry and the displacement field. In the *superparametric* element (term that emphasizes an unequal treatment), shape functions are used to approximate only the displacement

field, as shown in Figure 2.1. Evidently, geometry and displacements are not treated equally. If we proceed to higher order elements, only the displacement field is well-approximate, whereas the geometry definition remains the same.

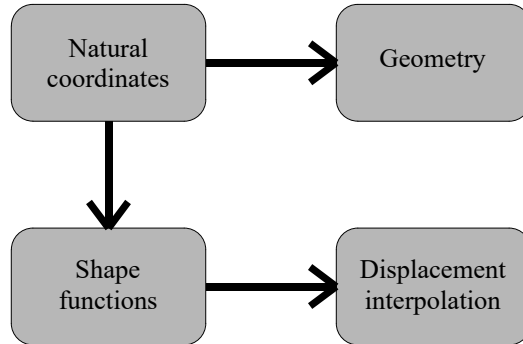


Figure 2.1: Superparametric representation.

Instead, using *isoparametric* elements, geometry and displacements are treated in the same way (i.e. interpolated with the same set of shape functions), as shown in Figure 2.2.

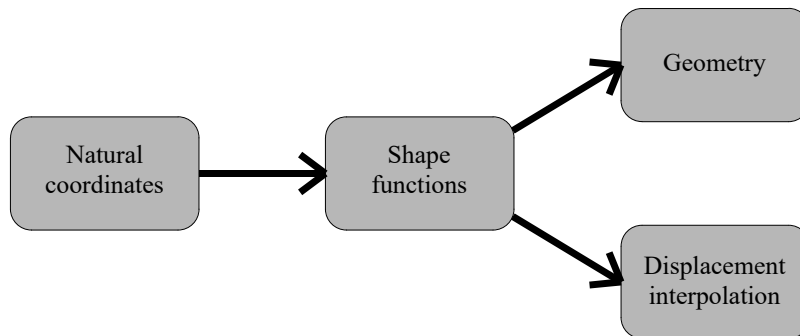


Figure 2.2: Isoparametric representation.

Now, we focus on two-dimensional isoparametric representation for quadrilateral elements. This formulation is general enough to be applied to more complicated (higher order) elements such as a quadratic plane element with three nodes along an edge, which can have straight or quadratic curved sides. Higher-order elements have additional nodes and use different shape functions as compared to linear elements, but the steps in the development of the stiffness matrices are the same.

Figure (2.3) show the isoparametric elements (or reference frame) using in this discussion. Isoparametric elements refer to the (ξ, η) coordinates system.

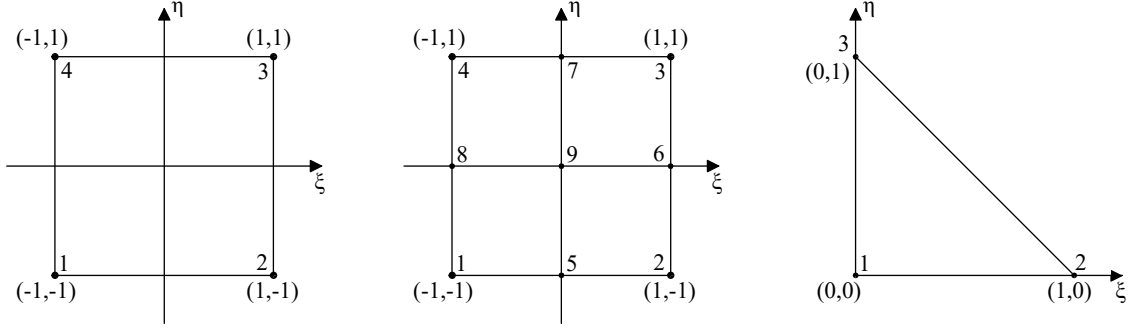


Figure 2.3: Quadrilateral and triangular isoparametric elements.

Hence, using the same shape functions for displacements and coordinates, we obtain the following discrete fields:

$$\begin{aligned}
 \mathbf{u} &= \begin{bmatrix} u \\ v \end{bmatrix} \rightarrow \begin{cases} u \approx u_h = \sum_{i=1}^n N_i \hat{u}_i \\ v \approx v_h = \sum_{i=1}^n N_i \hat{v}_i \end{cases} \\
 \mathbf{x} &= \begin{bmatrix} x \\ y \end{bmatrix} \rightarrow \begin{cases} x = \sum_{i=1}^n N_i \bar{x}_i \\ y = \sum_{i=1}^n N_i \bar{y}_i \end{cases}
 \end{aligned} \tag{2.23}$$

where (\bar{x}, \bar{y}) are the nodal coordinates of actual frame. Now, shape functions are defined on the reference frame (i.e. $N_i = N_i(\xi, \eta)$). It is easier to define the shape functions on the reference frame because it has a known geometry; possible choices are shown in Table 2.1.

For each element, the element stiffness matrix can be written as $\mathbf{K}^e = \int_{\Omega} [\mathbf{B}^T \mathbb{D} \mathbf{B}] d\Omega$; then, matrices \mathbf{B} and \mathbf{N} are (point-to-point):

$$\mathbf{B}_i = \begin{bmatrix} N_{i,x} & 0 \\ 0 & N_{i,y} \\ N_{i,y} & N_{i,x} \end{bmatrix} \quad \mathbf{N}_i = \begin{bmatrix} N_i & 0 \\ 0 & N_i \end{bmatrix} \tag{2.24}$$

Matrix \mathbf{B} requires the derivatives of the shape functions respect to x and y ; whereas we need $N_i(\xi, \eta)$, a change of coordinates from the (ξ, η) parametric space to the (x, y) physical space is necessary. For this purpose we can use the Jacobian Matrix \mathbf{F} :

Table 2.1: Two-dimensional shape functions.

Element type	Approximation type	Shape functions
Quadrilateral	Constant	$N_1 = 1$
	Bilinear	$N_1 = \frac{1}{4}(1 - \xi)(1 - \eta)$
		$N_2 = \frac{1}{4}(1 + \xi)(1 - \eta)$
		$N_3 = \frac{1}{4}(1 + \xi)(1 + \eta)$
		$N_4 = \frac{1}{4}(1 - \xi)(1 + \eta)$
	Biquadratic	$N_1 = \frac{1}{4}\xi(\xi - 1)\eta(\eta - 1)$
		$N_2 = \frac{1}{4}\xi(\xi + 1)\eta(\eta - 1)$
		$N_3 = \frac{1}{4}\xi(\xi + 1)\eta(\eta + 1)$
		$N_4 = \frac{1}{4}\xi(\xi - 1)\eta(\eta + 1)$
		$N_5 = \frac{1}{2}(1 - \xi^2)\eta(\eta - 1)$
		$N_6 = \frac{1}{2}\xi(\xi + 1)(1 - \eta^2)$
		$N_7 = \frac{1}{2}(1 - \xi^2)\eta(\eta + 1)$
		$N_8 = \frac{1}{2}\xi(\xi - 1)(1 - \eta^2)$
	$N_9 = (1 - \xi^2)(1 - \eta^2)$	
Triangular	Constant	$N_1 = 1$
	Linear	$N_1 = \xi$
		$N_2 = \eta$
		$N_3 = 1 - \xi - \eta$
	Linear (MINI)	$N_1 = \xi$
		$N_2 = \eta$
		$N_3 = 1 - \xi - \eta$
		$N_4 = 27\xi\eta(1 - \xi - \eta)$
	Quadratic	$N_1 = \xi(2\xi - 1)$
		$N_2 = \eta(2\eta - 1)$
		$N_3 = (1 - 2\xi - 2\eta)(1 - \xi - \eta)$
$N_4 = 4\xi\eta$		
$N_5 = 4\eta(1 - \xi - \eta)$		
$N_6 = 4\xi(1 - \xi - \eta)$		

$$\begin{bmatrix} \frac{\partial N_i}{\partial x} \\ \frac{\partial N_i}{\partial y} \end{bmatrix} = \mathbf{F} \begin{bmatrix} \frac{\partial N_i}{\partial \xi} \\ \frac{\partial N_i}{\partial \eta} \end{bmatrix} = \begin{bmatrix} \frac{\partial \xi}{\partial x} & \frac{\partial \eta}{\partial x} \\ \frac{\partial \xi}{\partial y} & \frac{\partial \eta}{\partial y} \end{bmatrix} \begin{bmatrix} \frac{\partial N_i}{\partial \xi} \\ \frac{\partial N_i}{\partial \eta} \end{bmatrix} \quad (2.25)$$

For the inverse change of coordinates we can use the following matrix:

$$\mathbf{G} = \begin{bmatrix} \frac{\partial x}{\partial \xi} & \frac{\partial x}{\partial \eta} \\ \frac{\partial y}{\partial \xi} & \frac{\partial y}{\partial \eta} \end{bmatrix} \quad (2.26)$$

Now, matrix \mathbf{B} is defined in the physical space, but the domain is still defined on the parametric space. Evidently it must be a passage of the reference system: this mapping is made possible by:

$$\int_{\Omega^e} f(x) dA = \int_{\square} f[x(\xi)] J d\xi \quad (2.27)$$

where $J = \det(\mathbf{G})$ is the determinant of the Jacobian matrix and the symbol \square (square) indicates the domain of the isoparametric element. Finally, we can write the expression of the stiffness matrix on the physical space as:

$$\mathbf{K}^e = \int_{\Omega^e} \mathbf{B}^T \mathbb{D} \mathbf{B} J d\Omega \quad (2.28)$$

Thanks to Equation (2.28), we have the algebraic form of the stiffness matrix, but there is not a closed form solution for this expression. For this reason, we rely on specific numerical integration methods (quadrature formulas).

2.3.1.1 Gauss-Legendre quadrature

Integration stiffness matrices and load vectors can not be performed analytically for the general case of isoparametric elements. Instead, stiffness matrices and load vectors are typically evaluated numerically using Gauss-Legendre quadrature. A quadrature rule is an approximation of the definite integral of a function, usually stated as a weighted sum of function values of specified points within the domain of integration [11]. An n -point Gauss-Legendre quadrature rule is constructed to yield an exact

result for polynomials of degree $2n - 1$ or less. For the two-dimensional case we use the following formula:

$$I = \int_{-1}^1 \int_{-1}^1 f(\xi, \eta) d\xi d\eta = \sum_{i=1}^n \sum_{j=1}^n f(\xi_i, \eta_j) w_i w_j \quad (2.29)$$

where ξ_i, η_j are abscissae and w_i are the weighting coefficients of the Gauss integration rule. For different element types and approximations, the Gauss points and weights are shown in Table 2.2.

Table 2.2: Two-dimensional Gauss-Legendre quadrature.

Element type	Approximation type	Gauss points	Gauss weights
Quadrilateral	Bilinear	(0.577350,0.577350)	1.0000000
		(0.577350,-0.577350)	1.0000000
		(-0.577350,0.577350)	1.0000000
		(-0.577350,-0.577350)	1.0000000
	Biquadratic	(-0.774597,-0.774597)	-0.308642
		(0,-0.774597)	0.493827
		(0.774597,-0.774597)	0.308642
		(-0.774597,0)	0.493827
		(0,0)	0.790123
		(0.774597,0)	0.493827
		(-0.774597,0.774597)	0.308642
		(0,0.774597)	0.493827
		(0.774597,0.774597)	0.308642
Triangular	Linear	(0.500000,0.500000)	0.166667
		(0,0.500000)	0.166667
		(0.500000,0)	0.166667
	Linear (MINI)	(0.101286,0.101286)	0.062970
		(0.101286,0.797427)	0.062970
		(0.797427,0.101286)	0.062970
		(0.470142,0.470142)	0.066197
		(0.059716,0.470142)	0.066197
		(0.470142,0.059716)	0.066197
		(0.333333,0.333333)	0.112500
		(0.333333,0.333333)	-0.281250
	Quadratic	(0.600000,0.200000)	0.260417
		(0.200000,0.600000)	0.260417
		(0.200000,0.200000)	0.260417
(0.200000,0.200000)		0.260417	

Using the Gauss-Legendre quadrature, the element stiffness matrix becomes:

$$K^e = \sum_{ig=1}^{ng} \sum_{jg=1}^{ng} \mathbf{B}^T \mathbb{D} \mathbf{B} J w_{ig} w_{jg} \quad (2.30)$$

2.4 Some basic formulations

2.4.1 Displacement-based formulations

The most well known approach, implemented in numerical codes for the elastic problem solution, is based on the principle of minimum total potential energy. Consider the *total potential energy functional* (2.19). Its stationarity gives:

$$\int_{\Omega} \delta \boldsymbol{\varepsilon}^T \boldsymbol{\sigma} d\Omega - \int_{\Omega} \delta \mathbf{u}^T \mathbf{b} d\Omega = 0 \quad (2.31)$$

after exploiting the constitutive relation and the compatibility equation.

Substituting the approximation fields ($\mathbf{u} \approx \mathbf{N}_u \hat{\mathbf{u}}$ and $\boldsymbol{\varepsilon} \approx \mathbf{B} \hat{\mathbf{u}}$) in the weak form (2.31), we obtain the following algebraic form of the displacement-based formulation:

$$\int_{\Omega} [\mathbf{B}^T \mathbb{D} \mathbf{B}] \hat{\mathbf{u}} d\Omega - \int_{\Omega} \mathbf{N}_u^T \mathbf{b} d\Omega = 0 \quad (2.32)$$

where the element stiffness matrix and the nodal force vector are:

$$\begin{aligned} \mathbf{K} &= \int_{\Omega} [\mathbf{B}^T \mathbb{D} \mathbf{B}] d\Omega \\ \mathbf{f} &= \int_{\Omega} [\mathbf{N}_u^T \mathbf{b}] d\Omega \end{aligned} \quad (2.33)$$

2.4.2 Two-field mixed formulations

In the previous paragraph we used an irreducible formulation, using the displacement \mathbf{u} as the primary variable. Now, we assume that the virtual work principle is still valid, but we approximate $\boldsymbol{\sigma}$ independently.

Using this variational approach, the constitutive relation becomes :

$$\boldsymbol{\sigma} = \mathbb{D} \nabla^s \mathbf{u} \quad (2.34)$$

We proceed with the classical finite element (FE) computational procedure. We associate to the Hellinger-Reissner functional (2.22) the following variational equations:

$$\begin{aligned} \int_{\Omega} \delta \boldsymbol{\sigma}^T (\nabla^s \mathbf{u} - \mathbb{D}^{-1} \boldsymbol{\sigma}) d\Omega &= 0 \\ \int_{\Omega} \delta \boldsymbol{\varepsilon}^T \boldsymbol{\sigma} d\Omega - \int_{\Omega} \delta \mathbf{u}^T \mathbf{b} d\Omega &= 0 \end{aligned} \quad (2.35)$$

In order to obtain the algebraic form of the variational problem we introduce the approximations ($\mathbf{u} \approx \mathbf{N}_u \hat{\mathbf{u}}$, $\boldsymbol{\varepsilon} \approx \mathbf{B} \hat{\mathbf{u}}$, and $\boldsymbol{\sigma} \approx \mathbf{N}_\sigma \hat{\boldsymbol{\sigma}}$) to write the discrete form of the problem. Hence, Equations (2.35) become:

$$\begin{aligned} - \int_{\Omega} [\mathbf{N}_\sigma^T \mathbb{D}^{-1} \mathbf{N}_\sigma] \hat{\boldsymbol{\sigma}} d\Omega + \int_{\Omega} [\mathbf{N}_\sigma^T \mathbf{B}] \hat{\mathbf{u}} d\Omega &= 0 \\ \int_{\Omega} [\mathbf{B}^T \mathbf{N}_\sigma] \hat{\boldsymbol{\sigma}} d\Omega - \int_{\Omega} [\mathbf{N}_u^T \mathbf{b}] d\Omega &= 0 \end{aligned} \quad (2.36)$$

We can thus write the two-field mixed problem in a simple matrix form as:

$$\begin{bmatrix} \mathbf{K}^{\sigma\sigma} & \mathbf{K}^{\sigma u} \\ \mathbf{K}^{u\sigma} & \mathbf{0} \end{bmatrix} \begin{bmatrix} \hat{\boldsymbol{\sigma}} \\ \hat{\mathbf{u}} \end{bmatrix} = \begin{bmatrix} \mathbf{0} \\ \mathbf{f} \end{bmatrix} \quad (2.37)$$

where the element stiffness matrix and nodal force vector are:

$$\begin{aligned} \mathbf{K}^{\sigma\sigma} &= - \int_{\Omega} \mathbf{N}_\sigma^T \mathbb{D}^{-1} \mathbf{N}_\sigma d\Omega \\ \mathbf{K}^{\sigma u} &= \int_{\Omega} \mathbf{N}_\sigma^T \mathbf{B} d\Omega \\ \mathbf{K}^{u\sigma} &= (\mathbf{K}^{\sigma u})^T \\ \mathbf{f} &= \int_{\Omega} \mathbf{N}_u^T \mathbf{b} d\Omega \end{aligned} \quad (2.38)$$

In this form, the shape functions \mathbf{N}_u have still to be continuous, though \mathbf{N}_σ can be discontinuous.

Later, a mixed assumed-stress formulation will be discussed, based on the decomposition of the displacement field into two components ($\mathbf{u} = \mathbf{u} + \mathbf{u}_\lambda$). With this approach, incompatible displacements \mathbf{u}_λ represent the difference between the dis-

placement field obtainable through the integration of $\boldsymbol{\sigma}$ and the actual displacements. Despite this formulation is more accurate, it is not very effective in generating new finite elements, because of the excessive number of parameters. For this reason, it has been proposed the Pian-Sumihara [12] finite element, based on a different approach, as we will discuss later.

2.4.3 Three-field mixed formulations

It is possible to use an independent approximation to all the essential variables entering the elasticity problem. We can then use the variational equations resulting from the stationarity of the three-field Hu-Washizu functional (2.21):

$$\begin{aligned} \int_{\Omega} \delta \boldsymbol{\varepsilon}^T (\mathbb{D} \boldsymbol{\varepsilon} - \boldsymbol{\sigma}) d\Omega &= 0 \\ \int_{\Omega} \delta \boldsymbol{\sigma}^T (\nabla^s \mathbf{u} - \boldsymbol{\varepsilon}) d\Omega &= 0 \\ \int_{\Omega} \delta (\nabla^s \mathbf{u})^T \boldsymbol{\sigma} d\Omega - \int_{\Omega} \delta \mathbf{u}^T \mathbf{b} d\Omega &= 0 \end{aligned} \quad (2.39)$$

We can proceed directly by taking the following approximations:

$$\mathbf{u} \approx \mathbf{N}_u \hat{\mathbf{u}} \quad \boldsymbol{\sigma} \approx \mathbf{N}_\sigma \hat{\boldsymbol{\sigma}} \quad \boldsymbol{\varepsilon} \approx \mathbf{N}_\varepsilon \hat{\boldsymbol{\varepsilon}} \quad \nabla^s \mathbf{u} \approx \mathbf{B} \hat{\mathbf{u}} \quad (2.40)$$

which yield an equation system of the following form:

$$\begin{bmatrix} \mathbf{K}^{\varepsilon\varepsilon} & \mathbf{K}^{\varepsilon\sigma} & \mathbf{0} \\ \mathbf{K}^{\sigma\varepsilon} & \mathbf{0} & \mathbf{K}^{\sigma u} \\ \mathbf{0} & \mathbf{K}^{u\sigma} & \mathbf{0} \end{bmatrix} \begin{bmatrix} \hat{\boldsymbol{\varepsilon}} \\ \hat{\boldsymbol{\sigma}} \\ \hat{\mathbf{u}} \end{bmatrix} = \begin{bmatrix} \mathbf{0} \\ \mathbf{0} \\ \mathbf{f} \end{bmatrix} \quad (2.41)$$

where:

$$\begin{aligned}
\mathbf{K}^{\varepsilon\varepsilon} &= \int_{\Omega} \mathbf{N}_{\varepsilon}^T \mathbb{D} \mathbf{N}_{\varepsilon} d\Omega \\
\mathbf{K}^{\varepsilon\sigma} &= - \int_{\Omega} \mathbf{N}_{\varepsilon}^T \mathbf{N}_{\sigma} d\Omega \\
\mathbf{K}^{\sigma\varepsilon} &= (\mathbf{K}^{\varepsilon\sigma})^T \\
\mathbf{K}^{\sigma u} &= \int_{\Omega} \mathbf{N}_{\sigma}^T \mathbf{B} d\Omega \\
\mathbf{K}^{u\sigma} &= (\mathbf{K}^{\sigma u})^T
\end{aligned} \tag{2.42}$$

The most important application of the three-field mixed formulation is the so-called *enhanced-strain*, based on the enrichment of strain field. In the following chapter we will discuss in detail the enhanced-strain approach.

Chapter 3

Finite element formulations for isotropic materials

In this chapter we focus on the presentation of plane isotropic finite elements, used to verify the conducted benchmark tests. For this purpose, we decide to use some classical formulations, such as:

- Q1-DB: classical displacement-based four-node element;
- Q1-E4: standard four-node enhanced-strain element with four enhanced modes [13];
- Q1-E5: standard four-node enhanced-strain element with five enhanced modes [13];
- Q1-PS: hybrid-stress four-node element with five stress modes [12];
- T1-DB: classical displacement-based three-node element;
- MINI: mixed three-node Stokes flow element [14].

The choice of these formulations is due to the fact that these elements are well-known and established results are available. In the following, we briefly describe the main characteristics of the finite elements listed above.

3.1 Q1-DB and T1-DB: displacement-based elements

In the context of linear elasticity problems, the most used finite elements are certainly those with four and three nodes. Their extensive use is due to the simple numerical implementation. The formulation is based on the concept of stationarity of potential energy (as discussed in the previous chapter), which coincides with the principle of virtual work. Hence, the reference potential energy functional and its variational equations are the following:

$$\Pi(\mathbf{u}) = \frac{1}{2} \int_{\Omega} [\mathbb{D}\boldsymbol{\varepsilon}(\mathbf{u}) : \boldsymbol{\varepsilon}(\mathbf{u})] d\Omega - \int_{\Omega} [\mathbf{b} \cdot \mathbf{u}] d\Omega \quad (3.1)$$

$$\int_{\Omega} (\nabla^s \delta \mathbf{u})^T \mathbb{D} \nabla^s \mathbf{u} d\Omega - \int_{\Omega} \delta \mathbf{u}^T \mathbf{b} d\Omega = 0 \quad (3.2)$$

By introducing the approximations for \mathbf{u} ($\mathbf{u} = \mathbf{N}_u \hat{\mathbf{u}}$ and $\boldsymbol{\varepsilon} = \mathbf{B} \hat{\mathbf{u}}$), we obtain the algebraic form of displacement-based problem:

$$\int_{\Omega} [\mathbf{B}^T \mathbb{D} \mathbf{B}] \hat{\mathbf{u}} d\Omega - \int_{\Omega} [\mathbf{N}_u^T \mathbf{b}] d\Omega = 0 \quad (3.3)$$

where the stiffness matrix is:

$$\mathbf{K} = \int_{\Omega} [\mathbf{B}^T \mathbb{D} \mathbf{B}] d\Omega \quad (3.4)$$

Using for both the four-node and three-node formulations (respectively, *Q1* and *T1*), the concept of isoparametric element, the only differences is in the associated shape functions:

- Q1 displacement-based formulation

$$\begin{aligned}
N_1 &= \frac{1}{4}(1 - \xi)(1 - \eta) \\
N_2 &= \frac{1}{4}(1 + \xi)(1 + \eta) \\
N_3 &= \frac{1}{4}(1 + \xi)(1 - \eta) \\
N_4 &= \frac{1}{4}(1 - \xi)(1 + \eta)
\end{aligned} \tag{3.5}$$

- T1 displacement-based formulation

$$\begin{aligned}
N_1 &= \xi \\
N_2 &= \eta \\
N_3 &= 1 - \xi - \eta
\end{aligned} \tag{3.6}$$

Experience has shown that, in the presence of incompressible material, these finite elements, show the numerical pathology known as *volumetric locking*. This is related to a certain incompressibility constraint (volume must remain constant during the deformation) that the low-performance finite elements can not satisfy. Numerically, placing $\nu \rightarrow 0.5$, we note that the bulk modulus tends to infinity and the displacements tends to zero:

$$\nu \rightarrow 0.5 \quad \Rightarrow \quad K = \frac{E}{3(1 - 2\nu)} \rightarrow \infty \quad \Rightarrow \quad \mathbf{u} \rightarrow 0$$

3.2 Q1-PS: Pian-Sumihara assumed-stress element

This formulation, initiated by Pian [15], is also known as *hybrid stress* finite element. The Pian-Sumihara element [12] is considered a milestone in the finite element history: thanks to its good performance, it has been used by other authors for the construction of new formulations. The Pian-Sumihara formulation can be derived on the basis of the Hellinger-Reissner functional and on the use of incompatible displacements \mathbf{u}_λ :

$$H(\mathbf{u}, \mathbf{u}_\lambda, \boldsymbol{\sigma}) = -\frac{1}{2} \int_{\Omega} [\boldsymbol{\sigma} : \mathbb{D}^{-1} \boldsymbol{\sigma}] d\Omega + \int_{\Omega} [\boldsymbol{\sigma} : (\nabla^s \mathbf{u} + \nabla^s \mathbf{u}_\lambda)] d\Omega - \Pi_{ext} \quad (3.7)$$

Requiring the stationarity of Equation (3.7), we obtain the following variational equations:

$$\begin{aligned} - \int_{\Omega} \delta \boldsymbol{\sigma}^T (\mathbb{D}^{-1} \boldsymbol{\sigma}) d\Omega + \int_{\Omega} \delta \boldsymbol{\sigma}^T (\nabla^s \mathbf{u}) d\Omega + \int_{\Omega} \delta \boldsymbol{\sigma}^T (\nabla^s \mathbf{u}_\lambda) d\Omega &= 0 \\ \int_{\Omega} \delta (\nabla^s \mathbf{u})^T \boldsymbol{\sigma} d\Omega - \int_{\Omega} \delta \mathbf{u}^T \mathbf{b} d\Omega &= 0 \\ \int_{\Omega} \delta (\nabla^s \mathbf{u}_\lambda)^T \boldsymbol{\sigma} d\Omega &= 0 \end{aligned} \quad (3.8)$$

A direct solution of this system of equations is not however comfortable. Therefore, the additional step to take is to impose condition (3.8)₃ a-priori. This corresponds to assume a stress field that annuls on average the typical incompatibility error of the mixed formulations. Furthermore, Equation (3.8)₃ requires that the strains for the incompatible displacement field should be orthogonal to the assumed stresses.

Furthermore, condition (3.8)₃ is used to choose the *assumed stress*, such as the one taken orthogonal to the incompatible displacement field:

$$\int_{\Omega} \delta (\nabla^s \mathbf{u}_\lambda)^T \boldsymbol{\sigma} d\Omega = 0 \quad \Rightarrow \quad \boldsymbol{\sigma}^* \quad (3.9)$$

Hence, Equations (3.8) reduce to:

$$\begin{aligned}
-\int_{\Omega} (\delta \boldsymbol{\sigma}^*)^T (\mathbb{D}^{-1} \boldsymbol{\sigma}^*) d\Omega + \int_{\Omega} (\delta \boldsymbol{\sigma}^*)^T (\nabla^s \mathbf{u}) d\Omega &= 0 \\
\int_{\Omega} \delta (\nabla^s \mathbf{u})^T \boldsymbol{\sigma}^* d\Omega - \int_{\Omega} \delta \mathbf{u}^T \mathbf{b} d\Omega &= 0
\end{aligned} \tag{3.10}$$

For the displacement, strain, and assumed stress fields, we introduce the following approximations:

$$\mathbf{u} \approx \mathbf{N}_u \hat{\mathbf{u}} \quad \boldsymbol{\varepsilon} \approx \mathbf{B} \hat{\mathbf{u}} \quad \boldsymbol{\sigma}^* \approx \mathbf{N}_\sigma^* \hat{\boldsymbol{\sigma}}^* \tag{3.11}$$

Equations (3.10) can be rewritten in the approximate form:

$$\begin{aligned}
-\int_{\Omega} [(\mathbf{N}_\sigma^*)^T \mathbb{D}^{-1} \mathbf{N}_\sigma^*] \hat{\boldsymbol{\sigma}}^* d\Omega + \int_{\Omega} [(\mathbf{N}_\sigma^*)^T \mathbf{B}] \hat{\mathbf{u}} d\Omega &= 0 \\
\int_{\Omega} [\mathbf{B}^T \mathbf{N}_\sigma^*] \hat{\boldsymbol{\sigma}}^* d\Omega - \int_{\Omega} [\mathbf{N}_u^T \mathbf{b}] d\Omega &= 0
\end{aligned} \tag{3.12}$$

In matrix form, the problem becomes:

$$\begin{bmatrix} \mathbf{K}^{\sigma^* \sigma^*} & \mathbf{K}^{\sigma^* u} \\ \mathbf{K}^{u \sigma^*} & \mathbf{0} \end{bmatrix} \begin{bmatrix} \hat{\boldsymbol{\sigma}}^* \\ \hat{\mathbf{u}} \end{bmatrix} = \begin{bmatrix} \mathbf{0} \\ \mathbf{f} \end{bmatrix} \tag{3.13}$$

where:

$$\begin{aligned}
\mathbf{K}^{\sigma^* \sigma^*} &= - \int_{\Omega} [(\mathbf{N}_\sigma^*)^T \mathbb{D}^{-1} \mathbf{N}_\sigma^*] \hat{\boldsymbol{\sigma}}^* d\Omega \\
\mathbf{K}^{\sigma^* u} &= \int_{\Omega} [(\mathbf{N}_\sigma^*)^T \mathbf{B}] \hat{\mathbf{u}} d\Omega \\
\mathbf{K}^{u \sigma^*} &= (\mathbf{K}^{\sigma^* u})^T
\end{aligned} \tag{3.14}$$

Now, we discuss the structures of the shape functions to be taken for the Q1PS four-node element used in the numerical tests. The field of compatible displacement is approximated with the classical shape functions deriving from the isoparametric element, i.e.:

$$\mathbf{N}_u = \begin{bmatrix} N_1 & 0 & N_2 & 0 & N_3 & 0 & N_4 & 0 \\ 0 & N_1 & 0 & N_2 & 0 & N_3 & 0 & N_4 \end{bmatrix} \tag{3.15}$$

where:

$$N_i(\xi, \eta) = \frac{1}{4}(1 + \xi_i\xi)(1 + \eta_i\eta) \quad i = 1, \dots, 4 \quad (3.16)$$

The stress interpolation is restricted to each element individually and, thus, can be discontinuous between adjacent elements. To satisfy the stability condition of two-field mixed formulations in elasticity ($n_\sigma \geq n_u$, where n_σ and n_u stand, respectively, for numbers of freedom in appropriate variables), we need at least five stress parameters in each element. A possible choice is:

$$\boldsymbol{\sigma} = \begin{bmatrix} 1 & 0 & 0 & \eta & 0 \\ 0 & 1 & 0 & 0 & \xi \\ 0 & 0 & 1 & 0 & 0 \end{bmatrix} \begin{bmatrix} \alpha_1 \\ \alpha_2 \\ \alpha_3 \\ \alpha_4 \\ \alpha_5 \end{bmatrix} \quad (3.17)$$

The problem remains to deduce an approximation for the assumed stress field for the quadrilateral element. Pian and Sumihara used the following approximation:

$$\boldsymbol{\sigma}^* = \begin{bmatrix} 1 & 0 & 0 & a_1^2\eta & a_3^2\xi \\ 0 & 1 & 0 & b_1^2\eta & b_3^2\xi \\ 0 & 0 & 1 & a_1b_1\eta & a_3b_3\xi \end{bmatrix} \begin{bmatrix} \alpha_1 \\ \alpha_2 \\ \alpha_3 \\ \alpha_4 \\ \alpha_5 \end{bmatrix} \quad (3.18)$$

where a_1 , b_1 , a_3 and b_3 are defined as:

$$\begin{aligned} a_1 &= \frac{1}{4}x_i\xi_i & a_3 &= \frac{1}{4}x_i\eta_i \\ b_1 &= \frac{1}{4}y_i\eta_i & b_3 &= \frac{1}{4}y_i\xi_i \end{aligned} \quad (3.19)$$

with $i = 1, \dots, 4$.

3.3 Q1-E4 and Q1-E5: enhanced-strain elements

The enhanced-strain formulation, proposed by Simo and Rifai [13], is based on the Hu-Washizu functional rewritten by decomposing the strain field as follows:

$$\boldsymbol{\varepsilon} = \nabla^s \mathbf{u} + \tilde{\boldsymbol{\varepsilon}} \quad (3.20)$$

The strain field is split in two parts: the first one is the usual displacement-gradient (compatible) part, while the second one is an added or *enhanced-strain* (incompatible) part. The latter allows to improve the rigid response of the standard element (i.e., displacement-based), therefore allowing to obtain a high performance finite element. Hence, the Hu-Washizu functional and its variational equations can be rewritten as:

$$\tilde{\Pi}_{HW}(\mathbf{u}, \tilde{\boldsymbol{\varepsilon}}, \boldsymbol{\sigma}) = \frac{1}{2} \int_{\Omega} [(\nabla^s \mathbf{u} + \tilde{\boldsymbol{\varepsilon}}) : \mathbb{D}(\nabla^s \mathbf{u} + \tilde{\boldsymbol{\varepsilon}})] d\Omega + \int_{\Omega} [\boldsymbol{\sigma} : \tilde{\boldsymbol{\varepsilon}}] d\Omega - \int_{\Omega} [\mathbf{b} \cdot \mathbf{u}] d\Omega \quad (3.21)$$

and

$$\begin{aligned} \int_{\Omega} \delta \tilde{\boldsymbol{\varepsilon}}^T [\mathbb{D}(\nabla^s \mathbf{u} + \tilde{\boldsymbol{\varepsilon}})] d\Omega - \int_{\Omega} \delta \tilde{\boldsymbol{\varepsilon}}^T \boldsymbol{\sigma} d\Omega &= 0 \\ \int_{\Omega} \delta (\nabla^s \mathbf{u})^T [\mathbb{D}(\nabla^s \mathbf{u} + \tilde{\boldsymbol{\varepsilon}})] d\Omega - \int_{\Omega} \delta \mathbf{u}^T \mathbf{b} d\Omega &= 0 \\ \int_{\Omega} \delta \boldsymbol{\sigma}^T \tilde{\boldsymbol{\varepsilon}} d\Omega &= 0 \end{aligned} \quad (3.22)$$

The enhanced-strain formulation must meet the following conditions:

1. $\nabla^s \mathbf{u} \cap \tilde{\boldsymbol{\varepsilon}} = \emptyset$. This requirement is quite natural, given that $\tilde{\boldsymbol{\varepsilon}}$ is intended as an enrichment of the strain field. Furthermore, it is shown in [13] as it is essential to ensure the solvency of the discrete system.
2. $\int_{\Omega} \delta \tilde{\boldsymbol{\varepsilon}} : \boldsymbol{\sigma} dV = 0$. It is the orthogonality condition between stress and enhanced-strain fields.
3. $\int_{\Omega} \tilde{\boldsymbol{\varepsilon}} dV = 0$. The enhanced-strain field is orthogonal with respect to any constant field.

We introduce, respectively, for displacement, strain, stress, and enhanced-strain fields, the following approximations:

$$\boldsymbol{\varepsilon} \approx \mathbf{B}\hat{\mathbf{u}} \quad \boldsymbol{\sigma} \approx \mathbf{N}_\sigma\hat{\boldsymbol{\sigma}} \quad \mathbf{u} \approx \mathbf{N}_u\hat{\mathbf{u}} \quad \tilde{\boldsymbol{\varepsilon}} \approx \mathbf{N}_{en}\hat{\tilde{\boldsymbol{\varepsilon}}} \quad (3.23)$$

Now, by substituting Equations (3.23) in Equations (3.22) we obtain:

$$\begin{aligned} \int_{\Omega} [\mathbf{N}_{en}^T \mathbb{D} \mathbf{B}] \hat{\mathbf{u}} d\Omega + \int_{\Omega} [\mathbf{N}_{en}^T \mathbb{D} \mathbf{N}_{en}] \hat{\tilde{\boldsymbol{\varepsilon}}} d\Omega - \int_{\Omega} [\mathbf{N}_{en}^T \mathbf{N}_\sigma] \hat{\boldsymbol{\sigma}} d\Omega &= 0 \\ \int_{\Omega} [\mathbf{B}^T \mathbb{D} \mathbf{B}] \hat{\mathbf{u}} d\Omega + \int_{\Omega} [\mathbf{B}^T \mathbb{D} \mathbf{N}_{en}] \hat{\tilde{\boldsymbol{\varepsilon}}} d\Omega - \int_{\Omega} \mathbf{N}_u^T \mathbf{b} d\Omega &= 0 \\ \int_{\Omega} [\mathbf{N}_\sigma^T \mathbf{N}_{en}] \hat{\tilde{\boldsymbol{\varepsilon}}} d\Omega &= 0 \end{aligned} \quad (3.24)$$

The problem can be expressed with the matrix form:

$$\begin{bmatrix} \mathbf{K}^{\tilde{\varepsilon}\tilde{\varepsilon}} & \mathbf{K}^{\tilde{\varepsilon}\sigma} & \mathbf{K}^{\tilde{\varepsilon}u} \\ \mathbf{K}^{\sigma\tilde{\varepsilon}} & 0 & 0 \\ \mathbf{K}^{u\tilde{\varepsilon}} & 0 & \mathbf{K}^{uu} \end{bmatrix} \begin{bmatrix} \hat{\tilde{\boldsymbol{\varepsilon}}} \\ \hat{\boldsymbol{\sigma}} \\ \hat{\mathbf{u}} \end{bmatrix} = \begin{bmatrix} 0 \\ 0 \\ \mathbf{f} \end{bmatrix} \quad (3.25)$$

where:

$$\begin{aligned} \mathbf{K}^{\tilde{\varepsilon}\tilde{\varepsilon}} &= \int_{\Omega} [\mathbf{N}_{en}^T \mathbb{D} \mathbf{N}_{en}] d\Omega \\ \mathbf{K}^{\tilde{\varepsilon}\sigma} &= - \int_{\Omega} [\mathbf{N}_{en}^T \mathbf{N}_\sigma] d\Omega \\ \mathbf{K}^{\tilde{\varepsilon}u} &= \int_{\Omega} [\mathbf{N}_{en}^T \mathbb{D} \mathbf{B}] d\Omega \\ \mathbf{K}^{\sigma\tilde{\varepsilon}} &= (\mathbf{K}^{\tilde{\varepsilon}\sigma})^T \\ \mathbf{K}^{u\tilde{\varepsilon}} &= (\mathbf{K}^{\tilde{\varepsilon}u})^T \\ \mathbf{K}^{uu} &= \int_{\Omega} [\mathbf{B}^T \mathbb{D} \mathbf{B}] d\Omega \end{aligned} \quad (3.26)$$

3.4 MINI: mixed Stokes flow element

For clarity we recall some basic Stokes equations concepts. The steady state of an incompressible Newtonian fluid can be formulated as a $(\mathbf{u}, \boldsymbol{\varepsilon}, \boldsymbol{\sigma}, p)$ four-field problem as follows:

$$\begin{aligned}
 \text{equilibrium} \quad & \text{div} \boldsymbol{\sigma} + \mathbf{b} = \mathbf{0} & \text{in } \Omega \\
 \text{constitutive} \quad & \boldsymbol{\sigma} = 2\mu \boldsymbol{\varepsilon} - p \mathbf{1} & \text{in } \Omega \\
 \text{compatibility} \quad & \boldsymbol{\varepsilon} = \nabla^s \mathbf{u} & \text{in } \Omega \\
 \text{incompressibility constraint} \quad & \text{div} \mathbf{u} = 0 & \text{in } \Omega
 \end{aligned} \tag{3.27}$$

The constitutive equation relates the stress $\boldsymbol{\sigma}$ to the symmetric part of the velocity gradient $\boldsymbol{\varepsilon}$ through a material constant μ , known as viscosity, and a volumetric pressure-like scalar contribution p .

The set of Equations (3.27) is completed by the following boundary condition:

$$\mathbf{u} = \mathbf{0} \quad \text{on } \partial\Omega \tag{3.28}$$

Equations (3.27) can be simplified by eliminating $\boldsymbol{\varepsilon}$ and $\boldsymbol{\sigma}$, thus obtaining a (\mathbf{u}, p) two-field problem:

$$\begin{aligned}
 \mu \Delta \mathbf{u} - \nabla p + \mathbf{b} &= \mathbf{0} & \text{in } \Omega \\
 \text{div} \mathbf{u} &= 0 & \text{in } \Omega
 \end{aligned} \tag{3.29}$$

This equation can be derived from the following potential energy functional:

$$\Pi(\mathbf{u}) = \frac{1}{2} \mu \int_{\Omega} [\nabla \mathbf{u} : \nabla \mathbf{u}] d\Omega - \int_{\Omega} [\mathbf{b} \cdot \mathbf{u}] d\Omega \tag{3.30}$$

where the field \mathbf{u} satisfies the constraint (3.27)₄. To remove this constraint, we modify Equation (3.30), by introducing the following Lagrangian function:

$$\mathcal{L}(\mathbf{u}, p) = \frac{1}{2} \mu \int_{\Omega} [\nabla \mathbf{u} : \nabla \mathbf{u}] d\Omega - \int_{\Omega} [\mathbf{b} \cdot \mathbf{u}] d\Omega - \int_{\Omega} [p \text{div} \mathbf{u}] d\Omega \tag{3.31}$$

Requiring the stationarity of this functional. we obtain:

$$\begin{aligned}
\mu \int_{\Omega} [(\nabla \delta \mathbf{u}) : \nabla \mathbf{u}] d\Omega - \int_{\Omega} [\delta \mathbf{u} \cdot \mathbf{b}] d\Omega - \int_{\Omega} [\operatorname{div}(\delta \mathbf{u}) p] d\Omega &= 0 \\
- \int_{\Omega} [\delta p \operatorname{div} \mathbf{u}] d\Omega &= 0
\end{aligned} \tag{3.32}$$

After introducing the following approximation fields:

$$\mathbf{u} \approx \mathbf{N}_u \hat{\mathbf{u}} \quad p \approx \mathbf{N}_p \hat{p} \tag{3.33}$$

the variational equations (3.32) can be rewritten in matrix form, as follows:

$$\begin{bmatrix} \mathbf{K}^{uu} & \mathbf{K}^{up} \\ \mathbf{K}^{pu} & \mathbf{0} \end{bmatrix} \begin{bmatrix} \hat{\mathbf{u}} \\ \hat{p} \end{bmatrix} = \begin{bmatrix} \mathbf{f} \\ \mathbf{0} \end{bmatrix} \tag{3.34}$$

where:

$$\begin{aligned}
\mathbf{K}^{uu} &= \mu \int_{\Omega} [\nabla \mathbf{N}_u : \nabla \mathbf{N}_u] d\Omega \\
\mathbf{K}^{up} &= - \int_{\Omega} [\operatorname{div} \mathbf{N}_u^T \mathbf{N}_p] d\Omega \\
\mathbf{f} &= \int_{\Omega} [\mathbf{N}_u \cdot \mathbf{b}] d\Omega
\end{aligned} \tag{3.35}$$

Various examples of interpolating functions can be found in the literature. We focus on the MINI element proposed by Arnold, Brezzi and Fortin [14].

The MINI element is a velocity-pressure finite element for the computation of Stokes flow. The displacement field is discretized with continuous piecewise linear functions enriched by bubble functions and the pressure with piecewise linear functions. Given a triangular mesh of Ω , we require that:

1. the components of $\hat{\mathbf{u}}$ are the sum of a linear function plus a standard cubic bubble function;
2. the components of $\hat{\mathbf{u}}$ are globally continuous functions on Ω .

For the generic element, the elemental degrees of freedom for $\hat{\mathbf{u}}$ are its values at the triangle vertexes and barycenter. Furthermore, a set of elemental degrees of

freedom for \hat{p} is given by its values at the triangle vertexes. The degrees of freedom for the MINI element are schematically depicted in Figure 3.1.

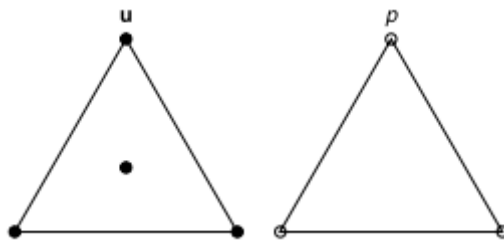


Figure 3.1: MINI element approximations as proposed in [14].

The bubble functions are internal modes, so that they can be eliminated on the element level by means of the so-called *static condensation* procedure.

Chapter 4

Finite element formulations for anisotropic materials

The mechanics of fiber-reinforced solids is based on the concept of anisotropic materials in which the response depends on the fiber direction. In this thesis we will discuss transversely isotropic materials and we will limit ourselves to the case of one family of inextensible fibers. In the first part of this chapter we will present the classical anisotropic formulation, proposed by Spencer [16]. Then, we will introduce the main argument of this work, namely the proposed finite element formulations based on constrained optimization methods, in order to impose the inextensibility constraint in the fiber direction.

4.1 Transverse isotropy

A transversely isotropic material presents physical properties which are symmetric about an axis that is normal to a plane of isotropy. Such a transverse plane has infinite planes of symmetry and thus, within this plane, the material properties are the same in all the directions. This type of material exhibits hexagonal symmetry (though technically this ceases to be true for tensors of rank 6 and higher), so the number of independent constants in the (fourth-rank) elasticity tensor are reduced to 5 (from a total of 21 independent constants in the case of a fully anisotropic solid).

We consider a material with an isotropic matrix, in which we immerse a family of fibers that have different mechanical properties than the matrix. Transversely isotropic materials are characterized by a preferred direction. Thus, the material response is invariant with respect to arbitrary rotations around this preferred direction, to reflections at fibers parallel planes, and to the reflection at that plane, whose normal is \mathbf{a} .

We introduce a fixed rectangular cartesian coordinate system and a unit vector \mathbf{a} in the undeformed configuration as shown in Figure 4.1, that describes the local fiber direction, and we require that the strain energy depend on this vector, i.e., $W = W(\boldsymbol{\varepsilon}, \mathbf{a})$.

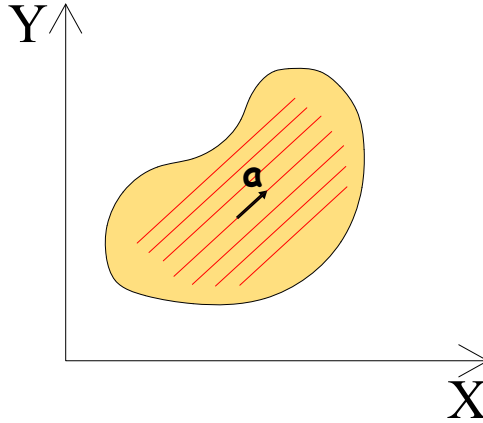


Figure 4.1: Fiber-reinforced material.

Starting from \mathbf{a} , we can construct the structural tensor of transverse isotropy or *fabric tensor* \mathbf{M} , as:

$$\mathbf{M} = \mathbf{a} \otimes \mathbf{a} \quad (4.1)$$

where \otimes represents the tensor outer product. The fiber stretch λ_a can be determined in terms of the deformation gradient and the fiber direction in the undeformed configuration:

$$\lambda_a^2 = \mathbf{a} \cdot \boldsymbol{\varepsilon} \mathbf{a} \quad (4.2)$$

In case of transverse isotropy, the free energy function is formulated as a function

of the isotropic invariants of the strain tensor $\boldsymbol{\varepsilon}$ and the fabric tensor \boldsymbol{M} . Under such an assumption, Spencer [17] presented relations for the strain energy at the material point in terms of five scalar quantities (invariants) derived from the tensor and vector fields:

$$W(\boldsymbol{\varepsilon}, \boldsymbol{a}) = W(I_1(\boldsymbol{\varepsilon}), I_2(\boldsymbol{\varepsilon}), I_3(\boldsymbol{\varepsilon}), I_4(\boldsymbol{\varepsilon}, \boldsymbol{a}), I_5(\boldsymbol{\varepsilon}, \boldsymbol{a})) \quad (4.3)$$

where the set of invariants is defined as:

$$\begin{aligned} I_1 &= tr(\boldsymbol{\varepsilon}) & \partial I_1 / \partial \boldsymbol{\varepsilon} &= \boldsymbol{I} \\ I_2 &= \frac{1}{2} [tr(\boldsymbol{\varepsilon})^2 - tr(\boldsymbol{\varepsilon}^2)] & \partial I_2 / \partial \boldsymbol{\varepsilon} &= I_1 \boldsymbol{I} - \boldsymbol{\varepsilon} \\ I_3 &= det(\boldsymbol{\varepsilon}) & \partial I_3 / \partial \boldsymbol{\varepsilon} &= I_3 \boldsymbol{\varepsilon}^{-1} \\ I_4 &= \boldsymbol{a} \cdot \boldsymbol{\varepsilon} \boldsymbol{a} & \partial I_4 / \partial \boldsymbol{\varepsilon} &= \boldsymbol{a} \otimes \boldsymbol{a} \\ I_5 &= \boldsymbol{a} \cdot \boldsymbol{\varepsilon}^2 \boldsymbol{a} & \partial I_5 / \partial \boldsymbol{\varepsilon} &= \boldsymbol{a} \otimes (\boldsymbol{\varepsilon} \boldsymbol{a}) + (\boldsymbol{a} \boldsymbol{\varepsilon}) \otimes \boldsymbol{a} \end{aligned} \quad (4.4)$$

where I_1 , I_2 , and I_3 are the standard invariants of the right Cauchy-Green deformation tensor, associated with isotropic material behaviour, while I_4 and I_5 arise from the anisotropy introduced by the reinforcing fiber family. These invariants represent contributions to the strain energy from the properties of the fibers and their interaction with the other material constituents; I_4 , for instance, is the square of the stretch along the fiber direction, as in Equation (4.2). The form (4.3) chosen for the strain energy, assures the satisfaction of material frame indifference and the material symmetry restrictions for transverse isotropy.

We now focus on *linear transverse isotropic* materials in which the strain energy becomes:

$$W(\boldsymbol{\varepsilon}, \boldsymbol{a}) = W(I_1(\boldsymbol{\varepsilon}), I_2(\boldsymbol{\varepsilon}), I_4(\boldsymbol{\varepsilon}, \boldsymbol{a}), I_5(\boldsymbol{\varepsilon}, \boldsymbol{a})) \quad (4.5)$$

To derive a representation of W and the infinitesimal stress tensor $\boldsymbol{\sigma}$ as isotropic tensor-function, the functional basis of the two symmetric second order tensorial argument $\boldsymbol{\sigma}$ and \boldsymbol{M} is needed. Assuming the stress to be a linear function of the strains and providing a stress-free undistorted initial configuration, such terms are

neglected, which are linear or cubic in the strains. Hence, in the context of *plane strain*, for elastic material with one family of fibers, we have the following strain energy:

$$W(\boldsymbol{\varepsilon}, \mathbf{a}) = \frac{1}{2}\lambda(I_1)^2 + \mu_T \text{tr}(\boldsymbol{\varepsilon}^2) + \alpha I_4 I_1 + 2(\mu_L - \mu_T)I_5 + \frac{1}{2}\beta(I_4)^2 \quad (4.6)$$

with only five independent material parameters (elasticity constants) that describe the transversely isotropic material behaviour. Particularly, λ and μ_T are Lamé constants relative to isotropic response of the *matrix*, μ_L is the shear modulus relative to response in the *fiber* direction, α is a coupling parameter, and β measures elastic response in the *fiber* direction.

We obtain the following expression for the stress:

$$\begin{aligned} \boldsymbol{\sigma} = & [\lambda \text{tr}(\boldsymbol{\varepsilon})\mathbf{I} + 2\mu_T \boldsymbol{\varepsilon}] \\ & + \alpha(\mathbf{a} \cdot \boldsymbol{\varepsilon} \mathbf{a})\mathbf{I} + (\alpha \text{tr}(\boldsymbol{\varepsilon}) + \beta \mathbf{a} \cdot \boldsymbol{\varepsilon} \mathbf{a})[\mathbf{a} \otimes \mathbf{a}] \\ & + 2(\mu_L - \mu_T)[(\mathbf{a} \otimes \mathbf{a})\boldsymbol{\varepsilon} + \boldsymbol{\varepsilon}(\mathbf{a} \otimes \mathbf{a})] \end{aligned} \quad (4.7)$$

and the elasticity tensor is rewritten as:

$$\begin{aligned} \mathbb{D} = & \lambda(\mathbf{I} \otimes \mathbf{I}) + 2\mu_T \mathbb{I}^I + \alpha[(\mathbf{a} \otimes \mathbf{a}) \otimes \mathbf{I} + \mathbf{I} \otimes (\mathbf{a} \otimes \mathbf{a})] \\ & + \beta \mathbf{M} + 2(\mu_L - \mu_T) \mathbb{I}^M \end{aligned} \quad (4.8)$$

The introduced fourth-order tensor \mathbb{I}^M in index notation reads as $\mathbf{M}_{im} \mathbb{I}_{jmkl} + \mathbf{M}_{jm} \mathbb{I}_{mikl}$.

In matrix notation, the fourth-order elasticity tensor of transversely isotropic material for a preferred X_1 -direction in a Cartesian coordinate system, i.e. $\mathbf{a} = (1, 0, 0)^T$, reads:

$$\mathbb{D} = \begin{bmatrix} \lambda + 2\alpha + \beta + 4\mu_L - 2\mu_T & \lambda + \alpha & \lambda + \alpha & 0 & 0 & 0 \\ \lambda + \alpha & \lambda + 2\mu_T & \lambda & 0 & 0 & 0 \\ \lambda + \alpha & \lambda & \lambda + 2\mu_T & 0 & 0 & 0 \\ 0 & 0 & 0 & \mu_L & 0 & 0 \\ 0 & 0 & 0 & 0 & \mu_T & 0 \\ 0 & 0 & 0 & 0 & 0 & \mu_L \end{bmatrix} \quad (4.9)$$

The transformation from engineering constants to those of the invariant representation [18] and vice-versa are:

- symmetry of the elasticity tensor:

$$\frac{\nu_{12}}{E_{22}} = \frac{\nu_{21}}{E_{11}}; \quad \frac{\nu_{13}}{E_{33}} = \frac{\nu_{31}}{E_{11}}; \quad \frac{\nu_{23}}{E_{33}} = \frac{\nu_{32}}{E_{22}};$$

- constants of invariant formulation:

$$\lambda = E_{22}(\nu_{23} + \nu_{31}\nu_{13})/D$$

$$\alpha = E_{22}[\nu_{31}(1 + \nu_{32} - \nu_{13}) - \nu_{32}]/D$$

$$\beta = E_{11}(1 - \nu_{32}\nu_{23})/D - E_{22}[\nu_{23} + \nu_{13}\nu_{31}]/D - 4\mu_{12}$$

$$\mu_L = \mu_{12}$$

$$\mu_T = \mu_{23}$$

$$D = 1 - \nu_{32}^2 - 2\nu_{13}\nu_{31} - 2\nu_{32}\nu_{31}\nu_{13}$$

- engineering constants:

$$E_{22} = E_{33}; \quad \nu_{23} = \nu_{32}; \quad \nu_{12} = \nu_{13}; \quad \nu_{21} = \nu_{31}; \quad \mu_{12} = \mu_{13};$$

$$E_{11} = -(\lambda\mu_T - 4\lambda\mu_L - \lambda\beta - 2\alpha\mu_T + 2\mu_T^2 - \beta\mu_T - 2\alpha\mu_T - 4\mu_L\mu_T + \alpha^2)/(\lambda + \mu_T)$$

$$E_{22} = -4\mu_T(\lambda\mu_T - 4\lambda\mu_L - \beta\lambda + 2\mu_T^2 - \beta\mu_T - 2\alpha\mu_T - 4\mu_T\mu_L + \alpha^2)/D_T$$

$$\begin{aligned}
\nu_{12} &= 2\mu_T(\lambda + \alpha)/D_T \\
\nu_{21} &= (\lambda + \alpha)/(2\lambda + 2\mu_T) \\
\nu_{23} &= -(\alpha^2 + 2\lambda\mu_T - \beta\lambda - 4\mu_L\lambda)/D_T \\
\mu_{12} &= \mu_L \\
\mu_{23} &= \mu_T \\
D_T &= 4\mu_L\lambda + \beta\lambda - 4\mu_T^2 + 4\mu_T\alpha + 2\beta\mu_T + 8\mu_L\mu_T - \alpha^2
\end{aligned}$$

4.2 Proposed formulations

By expression (4.6) we note that strain energy is expressed as the sum of isotropic and anisotropic terms:

$$W(\boldsymbol{\varepsilon}, \mathbf{a}) = W^{ISO}(\boldsymbol{\varepsilon}) + W^{ANISO}(\boldsymbol{\varepsilon}, \mathbf{a}) \quad (4.10)$$

where W^{ISO} describes the response of the isotropic matrix, while W^{ANISO} describes the directional contribution of the reinforcement. As shown in the previous paragraph, the anisotropic component of the strain energy equation is classically expressed in terms of invariants, which are themselves functions of the strain and the unit vector \mathbf{a} . The idea behind this thesis is to replace this anisotropic term with a directional equality constraint term. Specifically, we assume that the material does not extend in the fiber direction \mathbf{a} . This means that the constraint is the following:

$$\mathbf{a} \cdot \boldsymbol{\varepsilon} \mathbf{a} = 0 \quad (4.11)$$

or, equivalently:

$$\boldsymbol{\varepsilon} : \mathbf{M} = tr(\boldsymbol{\varepsilon} \mathbf{M}) = 0 \quad (4.12)$$

For this purpose, we avail of classical constrained optimization methods [2], such as:

1. Lagrange Multiplier method

2. Penalty method
3. Perturbed Lagrange method

Constrained optimization is the process of optimizing an objective function $f(\mathbf{x})$ with respect to some variables in the presence of constraint $g(\mathbf{x})$. The basic problem that we consider in this chapter is the minimization of a function subject to equality constraints:

$$\begin{aligned} & \text{minimize} && f(\mathbf{x}) \\ & \text{subject to} && g(\mathbf{x}) = 0 \quad (\text{Equality Constraint}) \end{aligned} \tag{4.13}$$

In our case, we assume the isotropic strain energy as objective function. Thus, the constrained problem can be written as follows:

$$\begin{aligned} & \text{minimize} && W^{ISO}(\boldsymbol{\epsilon}) \\ & \text{subject to} && \text{tr}(\boldsymbol{\epsilon}\mathbf{M}) = 0 \quad (\text{Equality Constraint}) \end{aligned} \tag{4.14}$$

The constrained problem can be convert into an unconstrained problem by adopting the following methods [2]:

1. Lagrange Multiplier (LM) Formulation
2. Penalty (PM) Formulation
3. Perturbed Lagrange (PLM) Formulation

4.2.1 Lagrange Multiplier formulation

In mathematical optimization, the Lagrange multiplier method is a strategy for finding the local minimal/maximal of a function subject to equality constraint:

$$\begin{aligned} & \text{minimize/maximize} && f(\mathbf{x}) \\ & \text{subject to} && g(\mathbf{x}) = 0 \end{aligned} \tag{4.15}$$

We require that $f(\mathbf{x})$ and $g(\mathbf{x})$ functions must have continuous first partial derivatives (i.e. C^1 functions). We introduce a new variable p , called as Lagrange multiplier, and a Lagrange function, defined as:

$$\mathcal{L}(\mathbf{x}, p) = f(\mathbf{x}) + p g(\mathbf{x}) \quad (4.16)$$

If $f(\mathbf{x}_0)$ is a minimum/maximum of $f(\mathbf{x})$, then there exists p_0 such that (\mathbf{x}_0, p_0) is a *stationary point* for the Lagrange function. Generally, a point is defined stationary for a certain function, when all possible partial derivatives of the function, evaluated at that point, are zero. In other words, a point (\mathbf{x}_0, p_0) is stationary for the Lagrange function, when:

$$\nabla \mathcal{L}(\mathbf{x}_0, p_0) = \mathbf{0} \quad (4.17)$$

Now, we apply these mathematical concepts to the constrained optimization problem (4.14). We start with a function $W^{ISO}(\boldsymbol{\varepsilon})$ that we wish to minimize, subject to the constraint $tr(\boldsymbol{\varepsilon}\mathbf{M}) = 0$. Following the lagrange multiplier method, the constraint is introduced by adding a term to the internal strain energy component of the total potential energy, as follows:

$$\Pi(\boldsymbol{\varepsilon}, p) = \int_{\Omega} [W^{ISO}(\boldsymbol{\varepsilon}) + tr(\boldsymbol{\varepsilon}\mathbf{M})p] d\Omega + \Pi_{ext}(\boldsymbol{\varepsilon}) \quad (4.18)$$

where Π_{ext} is the potential energy of external loads and $W^{ISO}(\boldsymbol{\varepsilon})$ is the isotropic strain energy. Therefore, we define a new strain energy function as:

$$W(\boldsymbol{\varepsilon}, p) = \frac{\lambda}{2} [tr(\boldsymbol{\varepsilon})]^2 + \mu tr(\boldsymbol{\varepsilon}^2) + tr(\boldsymbol{\varepsilon}\mathbf{M})p \quad (4.19)$$

Following the classical finite element approach, we write the variations of the functional W respect to the two fields, obtaining the residual equations in weak form

$$\begin{aligned} \int_{\Omega} \delta \boldsymbol{\varepsilon}^T [\lambda tr(\boldsymbol{\varepsilon}) \mathbf{1} + 2\mu \boldsymbol{\varepsilon} + \mathbf{M}p] d\Omega - \int_{\Omega} \delta \mathbf{u}^T \mathbf{b} d\Omega &= 0 \\ \int_{\Omega} \delta p^T [tr(\boldsymbol{\varepsilon}\mathbf{M})] d\Omega &= 0 \end{aligned} \quad (4.20)$$

Introducing the approximations for \mathbf{u} and p , Equations (4.20) can be rewritten, obtaining the strong form of the problem:

$$\begin{aligned} \int_{\Omega} [\mathbf{B}^T \mathbb{D} \mathbf{B}] \hat{\mathbf{u}} d\Omega + \int_{\Omega} [\mathbf{B}^T \mathbf{M} \mathbf{N}^p] \hat{p} d\Omega - \int_{\Omega} [(\mathbf{N}^u)^T \mathbf{b}] d\Omega &= 0 \\ \int_{\Omega} [(\mathbf{N}^p)^T \mathbf{M}^T \mathbf{B}] \hat{\mathbf{u}} d\Omega &= 0 \end{aligned} \quad (4.21)$$

We can thus express the problem in matrix form as:

$$\begin{bmatrix} \mathbf{K}^{uu} & \mathbf{K}^{up} \\ \mathbf{K}^{pu} & \mathbf{0} \end{bmatrix} \begin{bmatrix} \hat{\mathbf{u}} \\ \hat{p} \end{bmatrix} = \begin{bmatrix} \hat{\mathbf{f}} \\ \mathbf{0} \end{bmatrix} \quad (4.22)$$

where the components of the stiffness matrix are:

$$\begin{aligned} \mathbf{K}^{uu} &= \int_{\Omega} [\mathbf{B}^T \mathbb{D} \mathbf{B}] d\Omega \\ \mathbf{K}^{up} &= \int_{\Omega} [\mathbf{B}^T \mathbf{M} \mathbf{N}^p] d\Omega \\ \mathbf{K}^{pu} &= \int_{\Omega} [(\mathbf{N}^p)^T \mathbf{M}^T \mathbf{B}] d\Omega \end{aligned} \quad (4.23)$$

It is interesting to highlight the constitutive law related to this formulation. To do this, it is necessary to calculate the gradient of the strain energy functional, obtaining the following relations:

$$\begin{aligned} \frac{\partial W}{\partial \boldsymbol{\varepsilon}}(\boldsymbol{\varepsilon}, p) &= \lambda \text{tr}(\boldsymbol{\varepsilon}) \mathbf{1} + 2\mu \boldsymbol{\varepsilon} + \mathbf{M} p = \boldsymbol{\sigma} \\ \frac{\partial W}{\partial p}(\boldsymbol{\varepsilon}, p) &= \text{tr}(\boldsymbol{\varepsilon} \mathbf{M}) = 0 \end{aligned} \quad (4.24)$$

In this way we obtain a system of four equations in four variables:

$$\begin{bmatrix} \sigma_{xx} \\ \sigma_{yy} \\ \sigma_{xy} \\ 0 \end{bmatrix} = \begin{bmatrix} \lambda + 2\mu & \lambda & 0 & a_x^2 \\ \lambda & \lambda + 2\mu & 0 & a_y^2 \\ 0 & 0 & 2\mu & a_x a_y \\ a_x^2 & a_y^2 & 2a_x a_y & 0 \end{bmatrix} \begin{bmatrix} \varepsilon_{xx} \\ \varepsilon_{yy} \\ \varepsilon_{xy} \\ p \end{bmatrix} \quad (4.25)$$

4.2.2 Penalty formulation

The Penalty method consist in adding a term (the so-called penalty function) to the objective function, that consists of a *penalty parameter* C_C , multiplied by a measure of the constraint violation. The penalty parameter is a non-negative scalar multiplier to determinate the penalty magnitude. As C_C takes higher values, the approximation becomes increasingly accurate. More rigorously, this method consists in rewriting the equality constrained problem 4.13 on an unconstrained minimization as the following problem:

$$\text{minimize } f(\mathbf{x}) + \frac{1}{2}C_C|g(\mathbf{x})|^2 \quad (4.26)$$

Now, we apply penalty method to our problem. Once again, we want to minimize the isotropic strain energy $W^{ISO}(\boldsymbol{\varepsilon})$ subject to $tr(\boldsymbol{\varepsilon}\mathbf{M}) = 0$. Hence, the total potential energy becomes:

$$\Pi(\boldsymbol{\varepsilon}) = \int_{\Omega} \left[W(\boldsymbol{\varepsilon}) + \frac{1}{2}C_C[tr(\boldsymbol{\varepsilon}\mathbf{M})]^2 \right] d\Omega + \Pi_{ext}(\boldsymbol{\varepsilon}) \quad (4.27)$$

where the strain energy is:

$$W(\boldsymbol{\varepsilon}) = \frac{\lambda}{2}[tr(\boldsymbol{\varepsilon})]^2 + \mu tr(\boldsymbol{\varepsilon}^2) + \frac{1}{2}C_C[tr(\boldsymbol{\varepsilon}\mathbf{M})]^2 \quad (4.28)$$

We follow the classical finite element method to derive the formulation. First of all, we write the residual equation:

$$\int_{\Omega} \delta\boldsymbol{\varepsilon}^T [\lambda tr(\boldsymbol{\varepsilon})\mathbf{1} + 2\mu\boldsymbol{\varepsilon} + C_C tr(\boldsymbol{\varepsilon}\mathbf{M})\mathbf{M}] d\Omega - \int_{\Omega} \delta\mathbf{u}^T \mathbf{b} d\Omega = 0 \quad (4.29)$$

By introducing the approximations for \mathbf{u} , the residual equation can be rewritten as:

$$\int_{\Omega} [(\mathbf{B}^T \mathbb{D} \mathbf{B}) + (C_C \mathbf{M}^T \mathbf{B} \mathbf{M})] \hat{\mathbf{u}} d\Omega - \int_{\Omega} (\mathbf{N}^u)^T \mathbf{b} d\Omega = 0 \quad (4.30)$$

where the stiffness matrix is:

$$\mathbf{K} = \int_{\Omega} [(\mathbf{B}^T \mathbb{D} \mathbf{B}) + (C_C \mathbf{M}^T \mathbf{B} \mathbf{M})] d\Omega \quad (4.31)$$

We note that in the Penalty Formulation, the constraint is imposed, in an approximated way, by introducing some extra stiffness terms in the global stiffness matrix, according to the fibers orientation.

Differentiating the strain energy with respect to $\boldsymbol{\varepsilon}$ we calculate the stress tensor and, consequently, we obtain the constitutive law:

$$\begin{bmatrix} \sigma_{xx} \\ \sigma_{yy} \\ \sigma_{xy} \end{bmatrix} = \begin{bmatrix} \lambda + 2\mu + C_C a_x^4 & \lambda + C_C a_x^2 a_y^2 & 2C_C a_x^3 a_y \\ \lambda + C_C a_x^2 a_y^2 & \lambda + 2\mu + C_C a_y^4 & 2C_C a_x a_y^3 \\ 2C_C a_x^3 a_y & 2C_C a_x a_y^3 & 2\mu + 2C_C a_x^2 a_y^2 \end{bmatrix} \begin{bmatrix} \varepsilon_{xx} \\ \varepsilon_{yy} \\ \varepsilon_{xy} \end{bmatrix} \quad (4.32)$$

The Penalty method enables one to transform the constrained problem into an unconstrained one without introducing additional variables. The constraint condition is satisfied only approximately for finite values of the penalty parameter. The main difficulty associated with this method, however, lies in the poor conditioning of the problem as the penalty is increased to more accurately enforce the constraint condition. This is a well-understood phenomenon, particularly in the context of incompressible and nearly incompressible problems and fluid mechanics. Augmented Lagrangian (Perturbed) procedures have been thus proposed as a promising way to partially overcome these difficulties and regularize the penalty formulation.

4.2.3 Perturbed Lagrangian formulation

Perturbed Lagrangian methods have similarities to penalty methods since they replace a constrained optimization problem by a series of unconstrained problems and add a penalty term to the objective function; the difference is that the Perturbed Lagrangian method adds yet another term (quadratic positive term) in the Lagrange multiplier function, designed to mimic a Lagrange multiplier. As in the treatment of the incompressibility constraint, several approximation schemes are pos-

sible within the context of a perturbed Lagrangian formulation. The Perturbed Lagrangian method consists on a sequential unconstrained minimization of the form:

$$\text{minimize } f(\mathbf{x}) + p g(\mathbf{x}) - \frac{1}{2C_C} p^2 \quad (4.33)$$

In our case, the strain energy function is defined as:

$$W = \frac{\lambda}{2} [tr(\boldsymbol{\varepsilon})]^2 + \mu tr(\boldsymbol{\varepsilon}^2) + tr(\boldsymbol{\varepsilon} \mathbf{M}) p - \frac{1}{2C_C} p^2 \quad (4.34)$$

where p is the Lagrange multiplier and C_C is the penalty parameter. If the Lagrange multiplier is removed in the element level through static condensation, the Perturbed Lagrangian formulation becomes identical to the Penalty formulation.

Now, we develop the variational equations governing the problem. We write the residuals for the two fields:

$$\begin{aligned} \int_{\Omega} \delta \boldsymbol{\varepsilon}^T [\lambda tr(\boldsymbol{\varepsilon}) \mathbf{1} + 2\mu \boldsymbol{\varepsilon} + \mathbf{M} p] d\Omega - \int_{\Omega} \delta \mathbf{u}^T \mathbf{b} d\Omega &= 0 \\ \int_{\Omega} \delta p^T [tr(\boldsymbol{\varepsilon} \mathbf{M}) - \frac{1}{C_C} p] d\Omega &= 0 \end{aligned} \quad (4.35)$$

Introducing the approximations for \mathbf{u} and p , the residual equations become:

$$\begin{aligned} \int_{\Omega} [\mathbf{B}^T \mathbb{D} \mathbf{B}] \hat{\mathbf{u}} d\Omega + \int_{\Omega} [\mathbf{B}^T \mathbf{M} \mathbf{N}^p] \hat{p} d\Omega - \int_{\Omega} [(\mathbf{N}^u)^T \mathbf{b}] d\Omega &= 0 \\ \int_{\Omega} [(\mathbf{N}^p)^T \mathbf{M}^T \mathbf{B}] \hat{\mathbf{u}} d\Omega - \int_{\Omega} [(\mathbf{N}^p)^T \frac{1}{C_C} \mathbf{N}^p] \hat{p} d\Omega &= 0 \end{aligned} \quad (4.36)$$

Now, we can express the problem in matrix form as follows:

$$\begin{bmatrix} \mathbf{K}^{uu} & \mathbf{K}^{up} \\ \mathbf{K}^{pu} & \mathbf{K}^{pp} \end{bmatrix} \begin{bmatrix} \hat{\mathbf{u}} \\ \hat{p} \end{bmatrix} = \begin{bmatrix} \hat{\mathbf{f}} \\ \mathbf{0} \end{bmatrix} \quad (4.37)$$

where:

$$\begin{aligned}
\mathbf{K}^{uu} &= \int_{\Omega} [\mathbf{B}^T \mathbb{D} \mathbf{B}] d\Omega \\
\mathbf{K}^{up} &= \int_{\Omega} [\mathbf{B}^T \mathbf{M} \mathbf{N}^p] d\Omega \\
\mathbf{K}^{pu} &= (\mathbf{K}^{up})^T \\
\mathbf{K}^{pp} &= - \int_{\Omega} [(\mathbf{N}^p)^T \frac{1}{C_C} \mathbf{N}^p] d\Omega
\end{aligned} \tag{4.38}$$

In order to show the constitutive relation, we now compute the gradient of the strain energy functional. We obtain the following relations:

$$\begin{bmatrix} \sigma_{xx} \\ \sigma_{yy} \\ \sigma_{xy} \\ 0 \end{bmatrix} = \begin{bmatrix} \lambda + 2\mu & \lambda & 0 & a_x^2 \\ \lambda & \lambda + 2\mu & 0 & a_y^2 \\ 0 & 0 & 2\mu & a_x a_y \\ a_x^2 & a_y^2 & 2a_x a_y & -\frac{1}{C_C} \end{bmatrix} \begin{bmatrix} \varepsilon_{xx} \\ \varepsilon_{yy} \\ \varepsilon_{xy} \\ p \end{bmatrix} \tag{4.39}$$

4.2.4 Developed finite elements

We now introduce an important concept, concerning the different approximation that can be used for the Lagrange multiplier p , introduced in Lagrange Multiplier and Perturbed Lagrangian formulations, and for the displacement field \mathbf{u} . In this chapter, we provide a general form for these formulations, without get into specifics of the approximations.

Specifically, we focus on quadrilateral elements with both four and nine nodes. For the four-nodes element (Q1), we adopt bilinear shape functions to approximate \mathbf{u} , while for the nine-node element (Q2) we use biquadratic shape functions for \mathbf{u} . For both elements, we make use of the following approximations for p :

- bilinear approximation

$$p = \sum_{i=1}^4 \frac{1}{4} (1 + \xi \bar{\xi}_i) (1 + \eta \bar{\eta}_i) \hat{p}_i$$

- linear approximation

$$p = \hat{p}_0 + a_x \xi + a_y \eta$$

- constant approximation

$$p = \hat{p}_0$$

In a qualitative way, Figure 4.2 summarizes all the considered cases and the denominations used in the following chapter. Probably, the most natural choice would be to adopt the same interpolation for p and \mathbf{u} . However, this choice is not suitable, as demonstrated by the numerical results of Chapter 5.

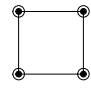
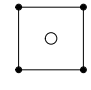
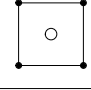
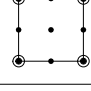
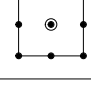
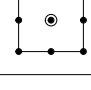
		Displacements	Lagrange Multiplier
Q1P1		Bilinear	Bilinear
Q1P0		Bilinear	Constant
Q1PL		Bilinear	Linear
Q2P1		Biquadratic	Bilinear
Q2P0		Biquadratic	Constant
Q2PL		Biquadratic	Linear
<ul style="list-style-type: none"> • Displacements node ○ Lagrange Multiplier node 			

Figure 4.2: Developed finite elements. Displacements and Lagrange multiplier interpolations.

Chapter 5

Numerical tests

This chapter presents the performed numerical tests. First, the tests have been performed to evaluate the performances of the isotropic finite elements described in Chapter 3. The obtained results are compared with results available in technical literature (see, e.g., [19, 20, 21]). Then, the same numerical tests have been used to test the performance of the anisotropic finite elements proposed in Chapter 4. In particular, we perform the following simulations:

1. Traction test to simulate a pure uniaxial traction state on a single element;
2. Bending test to simulate a bending state of a cantilever beam;
3. Cook's membrane test to simulate a bending state of a beam with unconventional geometry;
4. Two-element distortion test to evaluate the sensibility against mesh distortion for a cantilever beam in a bending state.

For each test, we assume the material to be, first, isotropic and, then, anisotropic. In the latter case, three fiber directions are considered, i.e., $\mathbf{a} = (1, 0)$, $\mathbf{a} = (0, 1)$, and $\mathbf{a} = (\sqrt{2}/2, \sqrt{2}/2)$.

5.1 Programming environment overview

To implement the formulations codes and the benchmark tests, we use the AceGen [22] and AceFEM [23] packages, written and developed by Prof. J. Korelc. Each package combines the use of Mathematica's facilities with external handling of intensive computation through compiled modules.

5.1.1 AceGen

AceGen is a multi-language and multi-environment numerical code generator. By using the *symbolic-numerical approach* [24], it derives formulas needed in numerical procedures and combines several techniques with the symbolic and algebraic capabilities of Wolfram Mathematica, as shown in Figure 5.1. The application's multi-language capabilities are useful for rapidly prototyping numerical procedures in script languages of general problem-solving environments as Wolfram Mathematica.

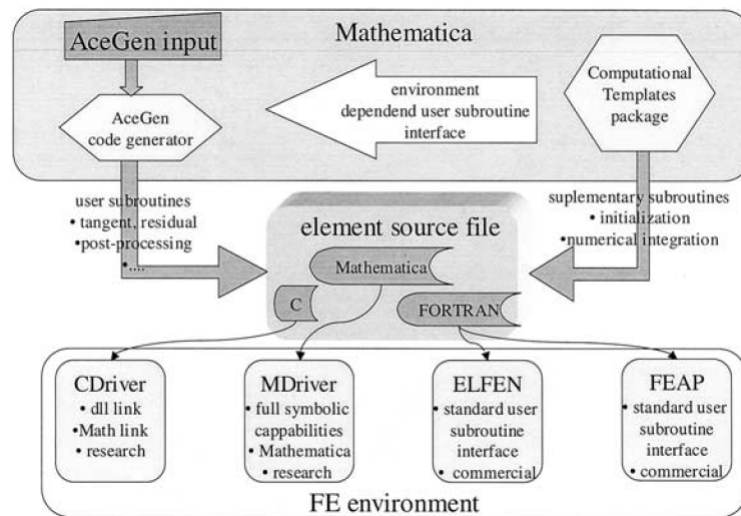


Figure 5.1: Hybrid system for multi-language and multi-environment finite element code generation [25].

In order to generate a new finite element source code, the following procedure has to be executed:

1. *AceGen Initialization* - <<"AceGEN' ". The AceGen package is loaded while Mathematica is running.

2. *Template Initialization* - **SMSTemplate**. During this phase all the constants that are needed for proper symbolic-numeric interface are initialized. The essential template constants are basically the element topology and the number of nodal degrees of freedom. In order to support the user, AceGen provides a list of standard element topology, which can be divided into three main groups: 1D, 2D and 3D. During the definition of the template constants, there are a lot of additional options, which can be easily found in the manual and include the possibility to define additional nodes (not included in the standard element topology), the number of spatial dimension, the number of degrees of freedom per node for all nodes, and arbitrary real values per node.
3. *Definition of user subroutines* - **SMSStandardModule**. The user can define his original subroutine with the default names and arguments. Moreover, the user can exploit the pre-arranged subroutines, which are able to calculate the tangent matrix and residual for the current values of nodal and element data, the post-processing quantities, or the sensitivity pseudo-load vector for the current sensitivity parameters.
4. *Code generation* - **SMSWrite**. It's the last phase of the AceGen procedure where the element source code is generated.

5.1.2 AceFEM

AceFEM includes a general finite element environment designed to solve multi-physics and multi-field problems [25]. The main part of the package includes procedures that are not numerically intensive, such as processing of the user input data, mesh generation, or control of the solution procedures. The numerical module exists as Mathematica package as well as external program written in C language (generated by AceGen). The AceFem package contains a large library of finite elements (solid, thermal, contact, ... , 2D, 3D) including full symbolic input for most of the elements. The AceFem structure could be divided into two main parts. The first one is a group of useful procedures, written and executed directly inside Mathematica, usu-

ally not numerically intensive. These procedures consist of some basic pre-processing and post-processing functions (`SMTMesh`, `SMTShowMesh`) which could help the user to visualize element geometry, meshing, boundary conditions, input data and so on. The second part of the AceFEM structure is the numerical module. The standard AceFEM procedure scheme is the following:

1. *AceFEM Inizialization* - `<<AceFEM'`". The AceFEM package is loaded while Mathematica is running.
2. *Input data* - `SMTInputData`. This phase is composed by different and obligatory commands. The users can load the needed element code and define the data common to all elements of the specific type. Later, the geometry and the mesh of the element are defined through a particular function, which define the nodes coordinates and their connectivity for topological mesh. The topological mesh is a base on which the actual finite element mesh is constructed.
3. *Analysis* - `SMTAnalysis`. This phase checks the correctness of the previously defined input data, and then compiles the element source files and creates dynamic link library files (dll file) with the user subroutines, or, in the case of MDriver reads, all the element source files into Mathematica. The `SMTAnalysis` command transcripts input data structures into analysis data base structures. When the analysis phase is initialized, it starts the iterative solution procedure using a Newton-Raphson iterative procedure. The solution procedure is executed accordingly to the Mathematica input given by the user through the `SMTConvergence`. It checks if the convergence conditions for the iterative procedure have been satisfied.
4. *Post-processing*. The graphic post-processing of the results can be part of the analysis (for instance, using `SMTShowMesh`, `SMTPostData`) or can be done later independently of the analysis, by using a special post-processing palette.

5.2 Traction test

We consider the square plate of Figure 5.2, subjected, along the edge CD , to a uniform tensile load q . This configuration generates a state of *uniaxial pure traction*. We set: $L = 10$, $q = 1$, $E = 1000$ and $\nu = 0.3$. For this test, we consider the displacement components of point C .

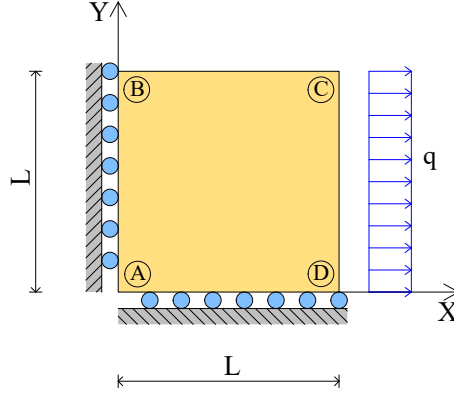


Figure 5.2: Traction test. Geometry and boundary conditions.

The pure uniaxial traction state implies, assuming the configuration of Figure 5.2, that the stress components σ_{yy} and σ_{xy} are equal to zero, i.e.:

$$\begin{aligned}\sigma_{yy} &= 0 \\ \sigma_{xy} &= 0\end{aligned}\tag{5.1}$$

We perform this test because, due to the simple problem configuration, it is easy to derive an analytical solution and to verify the accuracy of results. By inverting the elasticity matrix \mathbb{D} and by imposing conditions (5.1), we obtain, in a general form, the inverse constitutive relations as:

$$\begin{bmatrix} \varepsilon_{xx} \\ \varepsilon_{yy} \\ \varepsilon_{xy} \end{bmatrix} = \begin{bmatrix} \mathbb{S}_{11} & \mathbb{S}_{12} & \mathbb{S}_{13} \\ \mathbb{S}_{21} & \mathbb{S}_{22} & \mathbb{S}_{23} \\ \mathbb{S}_{31} & \mathbb{S}_{32} & \mathbb{S}_{33} \end{bmatrix} \begin{bmatrix} \sigma_{xx} \\ 0 \\ 0 \end{bmatrix}\tag{5.2}$$

After calculating the strain components and integrating, it is easy to calculate the displacements. In particular, for an isotropic material, the analytical solution is the following:

$$\begin{cases} u_C = 9.10E - 03 \\ v_C = -3.90E - 03 \end{cases} \quad (5.3)$$

For an anisotropic material (see Figure 5.3), the analytical solutions are respectively:

$$T1 \begin{cases} u_C = 0.00E + 00 \\ v_C = 0.00E + 00 \end{cases} \quad T2 \begin{cases} u_C = 7.43E - 03 \\ v_C = 0.00E + 00 \end{cases} \quad T3 \begin{cases} u_C = 6.50E - 03 \\ v_C = -6.50E - 03 \end{cases} \quad (5.4)$$

The explicit calculation of the analytical solutions is shown in Appendix A.

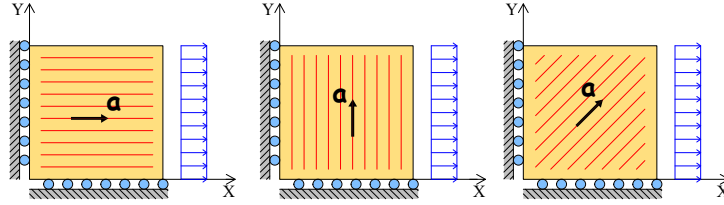


Figure 5.3: Traction test for anisotropic material, with fiber direction (left) $\mathbf{a} = (1, 0)$, (middle) $\mathbf{a} = (0, 1)$, (right) $\mathbf{a} = (\sqrt{2}/2, \sqrt{2}/2)$. The three tests are denoted, respectively, as T1, T2 and T3.

5.2.1 Isotropic material

Table 5.1 shows the displacement components varying the Poisson's ratio: we note that no locking phenomena occur. Experience shows that, a mesh sensitivity analysis would not be meaningful. Moreover, this observation is strengthened by the use of the well-known formulations discussed in Chapter 3, extensively tested in many works.

Table 5.1: Traction test numerical results: isotropic formulations.

Q1-DB			Q1-PS		Q1-E4	
ν	u_C	v_C	u_C	v_C	u_C	v_C
0.3	9.1000E-03	-3.9000E-03	9.1000E-03	-3.9000E-03	9.1000E-03	-3.9000E-03
0.49	7.5990E-03	-7.3010E-03	7.5990E-03	-7.3010E-03	7.5990E-03	-7.3010E-03
0.499	7.5100E-03	-7.4800E-03	7.5100E-03	-7.4800E-03	7.5100E-03	-7.4800E-03
0.4999	7.5010E-03	-7.4980E-03	7.5010E-03	-7.4980E-03	7.5010E-03	-7.4980E-03
0.49999	7.5001E-03	-7.4998E-03	7.5001E-03	-7.4998E-03	7.5001E-03	-7.4998E-03
0.499999	7.5000E-03	-7.5000E-03	7.5000E-03	-7.5000E-03	7.5000E-03	-7.5000E-03
Q1-E5			T1-DB		MINI	
ν	u_C	v_C	u_C	v_C	u_C	v_C
0.3	9.1000E-03	-3.9000E-03	9.1000E-03	-3.9000E-03	9.1000E-03	-3.9000E-03
0.49	7.5990E-03	-7.3010E-03	7.5990E-03	-7.3010E-03	7.5990E-03	-7.3010E-03
0.499	7.5100E-03	-7.4800E-03	7.5100E-03	-7.4800E-03	7.5100E-03	-7.4800E-03
0.4999	7.5010E-03	-7.4980E-03	7.5010E-03	-7.4980E-03	7.5010E-03	-7.4980E-03
0.49999	7.5001E-03	-7.4998E-03	7.5001E-03	-7.4998E-03	7.5001E-03	-7.4998E-03
0.499999	7.5000E-03	-7.5000E-03	7.5000E-03	-7.5000E-03	7.5000E-03	-7.5000E-03

5.2.2 Anisotropic material

Table 5.2 shows the obtained results. Regarding the Lagrange Multiplier formulation, we note that it provides correct results only with the Q2P1-LM element. Instead, if the Lagrange multiplier p is interpolated with a constant approximation throughout the element (Q2P0-LM and Q1P0-LM), the imposed constraint is ineffective. All the remaining cases (Q1P1-LM, Q1PL-LM, and Q2PL-LM) give completely incorrect results. It is evident that approximating p with constant and linear approximations is not enough accurate. Both the Penalty and Perturbed Lagrangian formulations do not show many problems in the results. In particular, both formulations provide an excellent behaviour even if we use the Q1 element (advantage in terms of computa-

tional cost). On the other hand, using the Q2 element and interpolating p constantly or linearly, the Perturbed Lagrangian formulation provides incorrect results.

Table 5.2: Traction test numerical results: anisotropic formulations. When the constraint is effective, the results are indicated in green, while the incorrect results are indicated in red. Instead, when the constraint is ineffective, the results are indicated in black.

		Q1P1-LM	Q1P0-LM	Q1PL-LM	Q2P1-LM	Q2P0-LM	Q2PL-LM
T1	u_C	Indet.	9.1000E-03	9.1000E-03	4.6923E-19	9.1000E-03	7.4957E-03
	v_C	Indet.	-3.9000E-03	-3.9000E-03	-3.2017E-19	-3.9000E-03	-9.8087E-04
T2	u_C	Indet.	9.1000E-03	9.1000E-03	7.4286E-03	9.1000E-03	1.2019E-02
	v_C	Indet.	-3.9000E-03	-3.9000E-03	5.1653E-19	-3.9000E-03	-5.5043E-03
T3	u_C	6.5000E-03	9.1000E-03	7.3491E-03	6.5000E-03	9.1000E-03	7.0870E-03
	v_C	-6.5000E-03	-3.9000E-03	-5.6509E-03	-6.5000E-03	-3.9000E-03	-5.9130E-03
Cc = 1.00E+11		Q1-PM			Q2-PM		
T1	u_C		1.0000E-10			1.0000E-10	
	v_C		-4.2857E-11			-4.2857E-11	
T2	u_C		7.4286E-03			7.4286E-03	
	v_C		-4.2857E-11			-4.2857E-11	
T3	u_C		6.5000E-03			6.5000E-03	
	v_C		-6.5000E-03			-6.5000E-03	
Cc = 1.00E+11		Q1P1-PLM	Q1P0-PLM	Q1PL-PLM	Q2P1-PLM	Q2P0-PLM	Q2PL-PLM
T1	u_C	1.0000E-10	1.0000E-10	1.0000E-10	1.0000E-10	1.0000E-10	-1.6043E-03
	v_C	-4.2857E-11	-4.2857E-11	-4.2857E-11	-4.2857E-11	-4.2857E-11	2.9191E-03
T2	u_C	7.4286E-03	7.4286E-03	7.4286E-03	7.4286E-03	7.4286E-03	1.0348E-02
	v_C	-4.2857E-11	-4.2857E-11	-4.2857E-11	-4.2857E-11	-4.2857E-11	-1.6043E-03
T3	u_C	6.5000E-03	6.5000E-03	6.5000E-03	6.5000E-03	6.94362E-03	5.5727E-03
	v_C	-6.5000E-03	-6.5000E-03	-6.5000E-03	-6.5000E-03	-6.0638E-03	-7.4273E-03

Now, we test the sensitivity to mesh and to parameter C_C for all the considered formulations.

5.2.2.1 Sensitivity to mesh

Experience shows that, carrying out a traction test with boundary conditions like in our case, the discretization of the problem is not necessary. Since the problem and its stress-strain relation is very simple, we should get the exact solution using only one element. Despite this, we want to verify this affirmation. We choose only the finite elements which provide correct results in Table 5.2, i.e., the Q2P1-LM, Q2-PM and Q2P1-PLM elements. We perform the traction test, meshing with 1×1 , 10×10 and 100×100 elements. The results are shown in Table 5.3. Concerning the Penalty

and Perturbed Lagrangian formulations, a penalty parameter $C_C = 10^{11}$ is used.

Table 5.3: Traction test numerical results: sensitivity to mesh.

		T1		T2		T3	
	Mesh	u_C	v_C	u_C	v_C	u_C	v_C
Q2P1-LM	1×1	4.6923E-19	-3.2017E-19	7.4286E-03	-5.1653E-19	6.5000E-03	-6.5000E-03
	10×10	4.0500E-19	1.6600E-19	7.4286E-03	5.4800E-20	6.7311E-03	-6.2689E-03
	100×100	-8.0300E-19	6.1900E-19	7.4286E-03	7.1400E-19	6.6374E-03	-6.3626E-03
Q2-PM	1×1	1.0000E-10	-4.2857E-11	7.4286E-03	-4.2857E-11	6.5000E-03	-6.5000E-03
	10×10	1.0000E-10	-4.2900E-11	7.4286E-03	-4.2900E-11	6.5000E-03	-6.5000E-03
	100×100	1.0000E-10	-4.2900E-11	7.4286E-03	-4.2900E-11	6.5000E-03	-6.5000E-03
Q2P1-PLM	1×1	1.0000E-10	-4.2857E-11	7.4286E-03	-4.2857E-11	6.5000E-03	-6.5000E-03
	10×10	1.0000E-10	-4.2900E-11	7.4286E-03	-4.2900E-11	6.7311E-03	-6.2689E-03
	100×100	1.0000E-10	-4.2900E-11	7.4286E-03	-4.2900E-11	6.6374E-03	-6.3626E-03

Therefore, the formulations developed in Chapter 4 are affected by the meshing only when the fibers are inclined at an angle of 45° .

5.2.2.2 Sensitivity to C_C

Here, we investigate the displacement components by varying the values assigned to the penalty parameter C_C . This analysis, whose results are shown in Figures 5.4 to 5.9, is carried out to establish the convergence value for the Penalty and Perturbed Lagrangian formulations. Generally, the convergence values are reached for $C_C = 10^5$.

The Penalty formulation appears to be stable because it does not show odd behaviours for both the developed elements (Q1-PM and Q2-PM). Regarding the Perturbed Lagrangian formulation, except for the Q1PL-PLM, Q2P0-PLM and Q2PL-PLM elements, all the developed elements show the same behaviour. Observing Figures 5.4 to 5.9, similarities between these two formulations are evident.

It is interesting to note that the vertical displacement component increases with increasing C_C in the T3 test. Contrary to what would be expected, it is evident that the value of the vertical displacement of point C increases with increasing C_C . Physically, this result is due to the presence of the constraint imposed by the fiber direction.

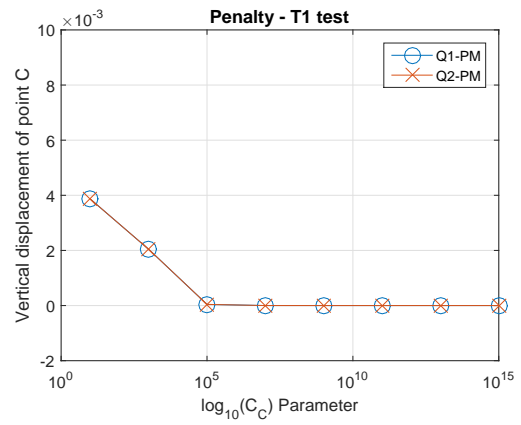
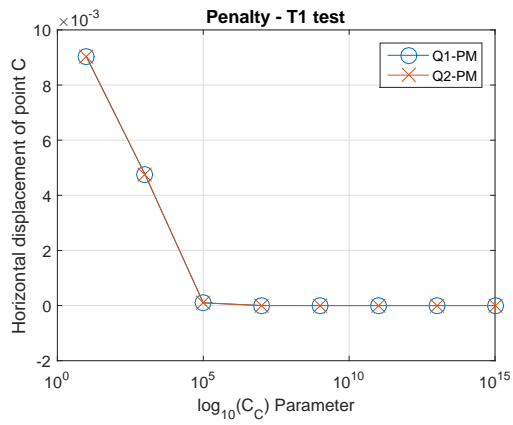


Figure 5.4: Traction test T1: sensitivity to C_C for the Penalty Formulation.

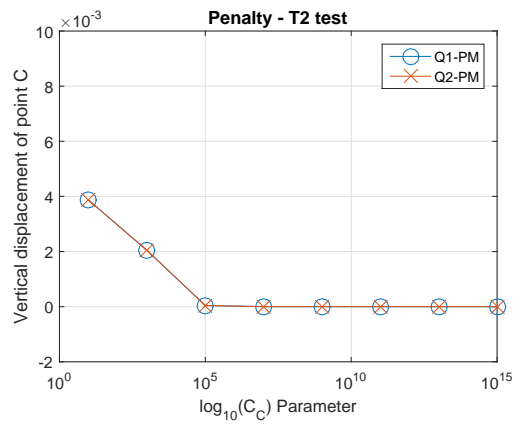
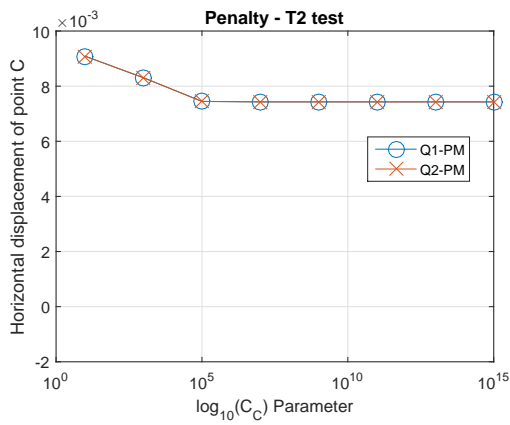


Figure 5.5: Traction test T2: sensitivity to C_C for the Penalty Formulation.

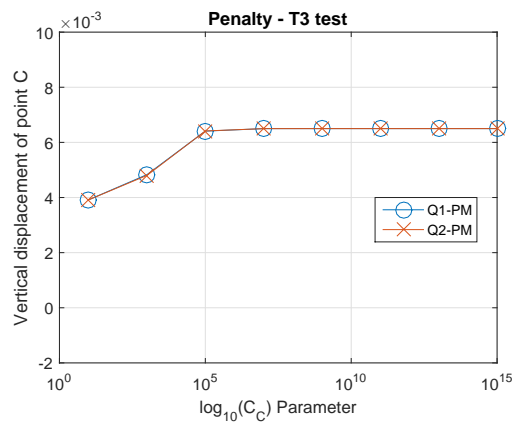
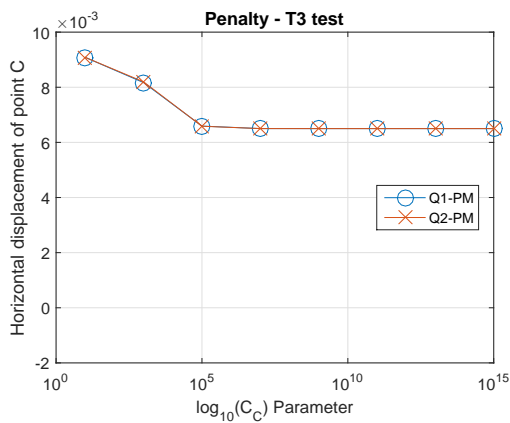


Figure 5.6: Traction test T3: sensitivity to C_C for the Penalty Formulation.

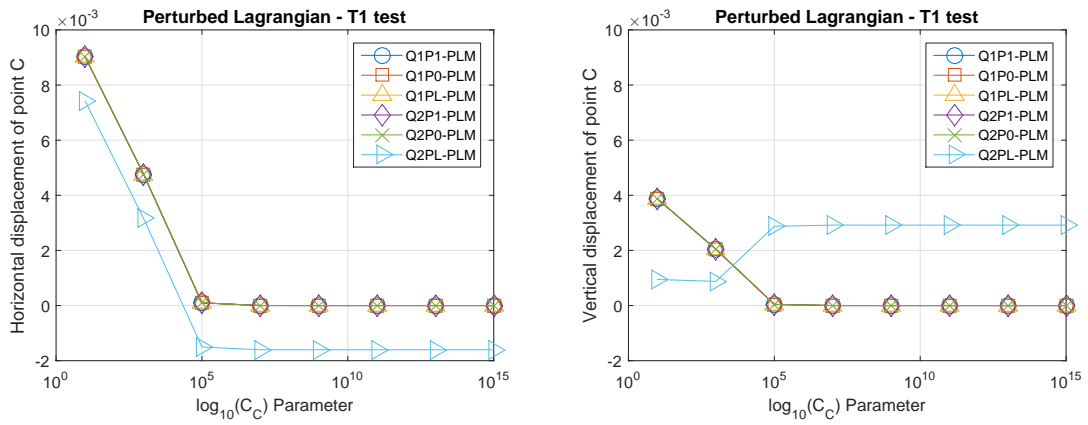


Figure 5.7: Traction test T1: sensitivity to C_C for the Perturbed Lagrangian Formulation.

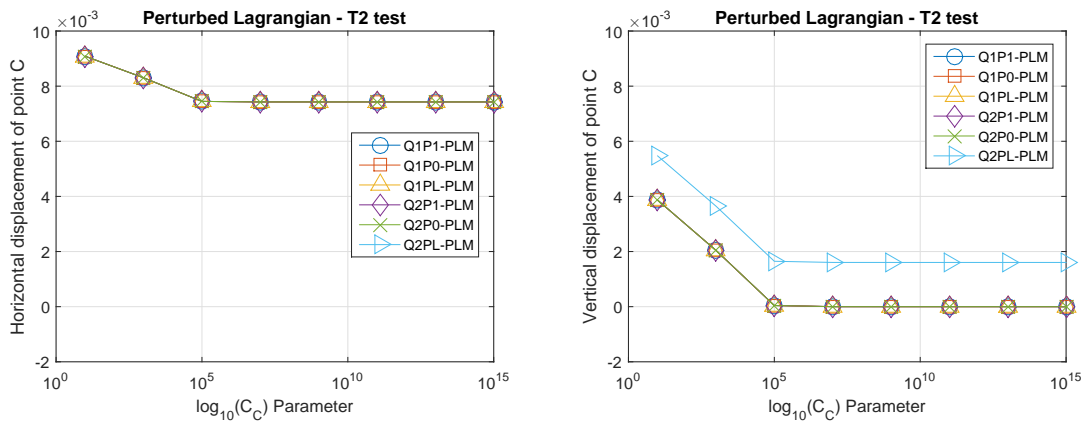


Figure 5.8: Traction test T2: sensitivity to C_C for the Perturbed Lagrangian Formulation.

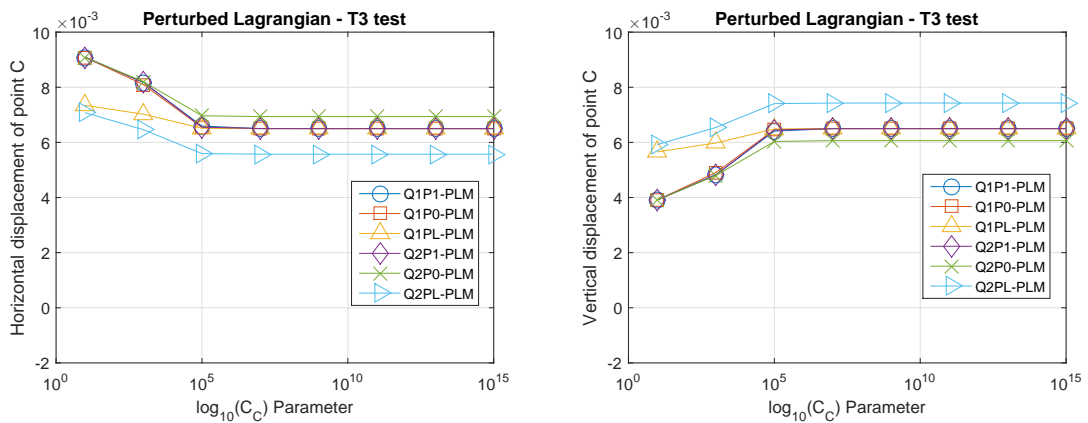


Figure 5.9: Traction test T3: sensitivity to C_C for the Perturbed Lagrangian Formulation.

5.3 Bending test

We consider a plane beam, subjected to a couple at one end as depicted in Figure 5.10. Along the edge AB , the horizontal displacement is set equal to zero, while the point A is constrained along both the directions. Along the edge CD a couple is applied to generate a bending state. We set: $L = 10$, $H = 2$, $E = 1500$, $\nu = 0.3$ and $f = 15$. Meshes of 5×1 , 10×2 , 40×8 and 80×16 elements are considered.

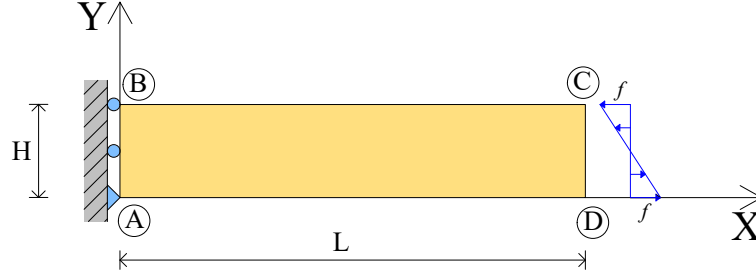


Figure 5.10: Bending test. Geometry and boundary conditions.

If we consider an isotropic material, the analytical solution is given by [21]:

$$\begin{cases} u(x, y) = \frac{2f(1 - \nu^2)}{EH} x \left(\frac{H}{2} - y \right) \\ v(x, y) = \frac{f(1 - \nu^2)}{EH} \left[x^2 + \frac{\nu}{1 - \nu} y(y - H) \right] \end{cases} \quad (5.5)$$

where $u(x, y)$ and $v(x, y)$ are the horizontal and vertical displacements, respectively. We focus on the displacement components of point D , where $x = L$ and $y = H$. Hence, using Equations (5.5), the displacement components of point D are the following:

$$\begin{cases} u_D = 9.10E - 02 \\ v_D = 4.55E - 01 \end{cases} \quad (5.6)$$

If we consider an anisotropic material (see Figure 5.10), the analytical solutions are respectively:

$$B1 \begin{cases} u_D = 0.00E + 00 \\ v_D = 0.00E + 00 \end{cases} \quad B2 \begin{cases} u_D = 7.43E - 02 \\ v_D = 3.71E - 01 \end{cases} \quad B3 \begin{cases} u_D = 8.36E - 02 \\ v_D = 4.18E - 01 \end{cases} \quad (5.7)$$

The explicit calculation of the bending test analytical solutions is shown in Appendix A.

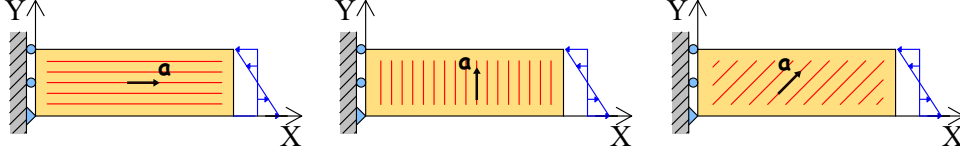


Figure 5.11: Bending test for anisotropic material, with fiber direction (left) $\mathbf{a} = (1, 0)$, (middle) $\mathbf{a} = (0, 1)$, (right) $\mathbf{a} = (\sqrt{2}/2, \sqrt{2}/2)$. The three tests are denoted, respectively, as B1, B2 and B3.

5.3.1 Isotropic material

Table 5.4 shows the displacement components of point D , obtained with a mesh composed of 80 elements in X -direction and varying the Poisson's ratio. We note that, as regards the displacement-based elements (Q1-DB and T1-DB), locking phenomena occur. Instead, all the other finite elements considered do not exhibit this numerical problem.

Moreover, it is interesting to evaluate the response of various considered finite elements, varying the mesh density. The results, assuming for example $\nu = 0.3$ (this value of Poisson's ratio does not expect locking phenomena) can be observed in Figure 5.12. We can see that the results for the hybrid assumed-stress and enhanced-strain elements (Q1-PS, Q1-E4, and Q1-E5) are not affected by a coarse mesh.

Table 5.4: Bending test numerical results: isotropic formulations.

Q1-DB		Q1-PS		Q1-E4		
ν	u_D	v_D	u_D	v_D	u_D	v_D
0.3	9.0769E-02	4.5396E-01	9.1000E-02	4.5500E-01	9.1000E-02	4.5500E-01
0.49	7.2285E-02	3.6244E-01	7.5990E-02	3.7995E-01	7.5990E-02	3.7995E-01
0.499	5.0031E-02	2.5211E-01	7.5100E-02	3.7550E-01	7.5100E-02	3.7550E-01
0.4999	1.2648E-02	6.3631E-02	7.5010E-02	3.7505E-01	7.5010E-02	3.7505E-01
0.49999	1.5012E-03	7.5190E-03	7.5001E-02	3.7501E-01	7.5001E-02	3.7501E-01
0.499999	1.5323E-04	7.6632E-04	7.5000E-02	3.7500E-01	7.5000E-02	3.7500E-01
Q1-E5		T1-DB		MINI		
ν	u_D	v_D	u_D	v_D	u_D	v_D
0.3	9.1000E-02	4.5500E-01	8.9653E-02	4.4870E-01	9.0057E-02	4.5063E-01
0.49	7.5990E-02	3.7995E-01	6.6277E-02	3.3324E-01	7.5311E-02	3.7683E-01
0.499	7.5100E-02	3.7550E-01	3.4202E-02	1.7383E-01	7.4429E-02	3.7243E-01
0.4999	7.5010E-02	3.7505E-01	1.1985E-02	5.8901E-02	7.4340E-02	3.7198E-01
0.49999	7.5001E-02	3.7501E-01	7.9808E-03	3.7551E-02	7.4331E-02	3.7194E-01
0.499999	7.5000E-02	3.7500E-01	7.5280E-03	3.5127E-02	7.4331E-02	3.7193E-01

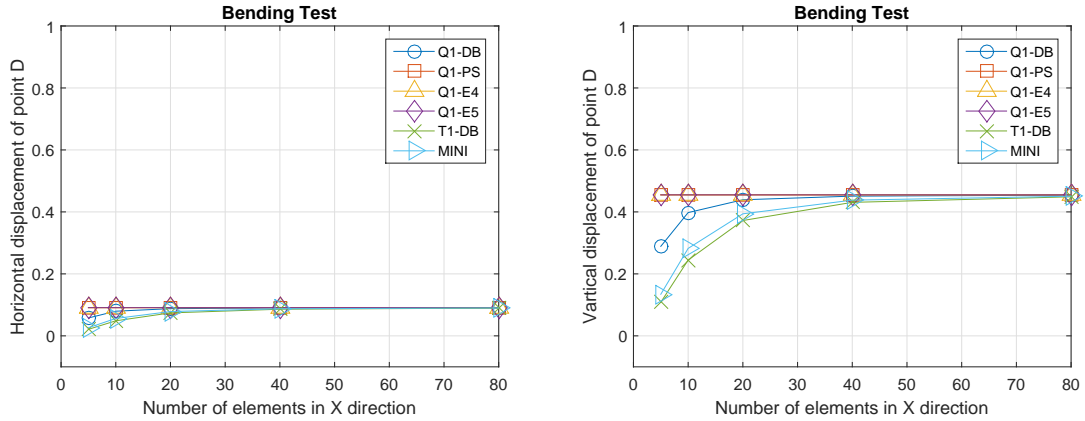


Figure 5.12: Bending test sensitivity to mesh setting $\nu = 0.3$: isotropic formulations.

5.3.2 Anisotropic material

For the considered anisotropic formulations, in the absence of constraint (i.e. setting $\mathbf{a} = (0, 0)$) and setting a 80×16 mesh, we obtain the solutions shown in Table 5.5.

Table 5.5: Bending test: solutions for anisotropic formulations setting $\mathbf{a} = (0, 0)$.

	Q1P1-LM	Q1P0-LM	Q1PL-LM	Q2P1-LM	Q2P0-LM	Q2PL-LM
u_D	9.0769E-02	9.0769E-02	9.0769E-02	9.0878E-02	9.1000E-02	9.1000E-02
v_D	4.5396E-01	4.5396E-01	4.5396E-01	4.5434E-01	4.5500E-01	4.5500E-01
	Q1-PM			Q2-PM		
u_D		9.0769E-02			9.1000E-02	
v_D		4.5396E-01			4.5500E-01	
	Q1P1-PLM	Q1P0-PLM	Q1PL-PLM	Q2P1-PLM	Q2P0-PLM	Q2PL-PLM
u_D	9.0769E-02	9.0769E-02	9.0769E-02	9.0878E-02	9.1000E-02	9.1000E-02
v_D	4.5396E-01	4.5396E-01	4.5396E-01	4.5434E-01	4.5500E-01	4.5500E-01

These results are useful for evaluation in which cases the imposed constraint is ineffective (i.e., when the implemented finite elements show an isotropic behaviour).

In the presence of the inextensibility constraint, the obtained results are shown in Table 5.6. For the meaning of the colors used in the table, see the Paragraph 5.2.2.

As in the previous benchmark test, in case of the Lagrange Multiplier formulation, we obtain correct results only with the Q2P1-LM element. Instead, the imposed constraint is ineffective with the Q1P0-LM and Q2P0-LM elements (compare this values with those shown in Table 5.5), while incorrect results are obtained with the Q1PL-LM and Q2PL-LM elements.

As regards the Penalty formulation, both the developed finite elements provide results correct and coherent with the inextensibility imposed constraint.

Leastly, for the Perturbed Lagrangian formulation, we obtain incorrect results only with the Q2P0-PLM and Q2P1-PLM elements.

Now, we analyze the behaviour of the considered finite elements, by performing a convergence analysis varying the mesh. Then, we analyze the same results (i.e., the displacement components of node D) varying the penalty parameter C_C .

Table 5.6: Bending test numerical results: anisotropic formulations. When the constraint is effective, the results are indicated in green, while the incorrect results are indicated in red. Instead, when the constraint is ineffective, the results are indicated in black.

		Q1P1-LM	Q1P0-LM	Q1PL-LM	Q2P1-LM	Q2P0-LM	Q2PL-LM
B1	u_D	0.0000E+00	9.0769E-02	9.0769E-02	-5.6900E-08	9.1000E-02	9.0973E-02
	v_D	0.0000E+00	4.5396E-01	4.5396E-01	-5.8525E-08	4.5500E-01	4.5492E-01
B2	u_D	7.5545E-03	9.0769E-02	9.0769E-02	7.4184E-02	9.1000E-02	9.0803E-02
	v_D	0.0000E+00	4.5396E-01	4.5396E-01	3.7089E-01	4.5500E-01	4.5416E-01
B3	u_D	-3.0789E+206	9.0769E-02	9.1101E-02	8.4483E-02	9.1000E-02	9.1092E-02
	v_D	6.7854E+206	4.5396E-01	4.5543E-01	4.1405E-01	4.5500E-01	4.5544E-01
Cc = 1.00E+11			Q1-PM		Q2-PM		
B1	u_D		1.5000E-09			1.5000E-09	
	v_D		7.5000E-09			7.5000E-09	
B2	u_D		7.4194E-02			7.4286E-02	
	v_D		3.7101E-01			3.7143E-01	
B3	u_D		8.3499E-03			8.4371E-02	
	v_D		3.8473E-02			4.14915E-01	
Cc = 1.00E+11		Q1P1-PLM	Q1P0-PLM	Q1PL-PLM	Q2P1-PLM	Q2P0-PLM	Q2PL-PLM
B1	u_D	1.5000E-09	1.9980E-09	1.9980E-09	-5.5400E-08	3.9246E-05	2.8329E-05
	v_D	7.5000E-09	1.0430E-08	1.0430E-08	-5.1018E-08	2.4033E-05	-4.17686E-05
B2	u_D	7.4194E-02	7.4194E-02	7.4194E-02	7.4184E-02	7.4351E-02	7.4189E-02
	v_D	3.7101E-01	3.7101E-01	3.7101E-01	3.7089E-01	3.7170E-01	3.7102E-01
B3	u_D	8.4098E-02	8.4423E-02	8.4732E-02	8.4483E-02	8.4631E-02	8.4717E-02
	v_D	4.1411E-01	4.1388E-01	4.1516E-01	4.1405E-01	4.1493E-01	4.1532E-01

5.3.2.1 Sensitivity to mesh

Figures 5.13 to 5.15 show the obtained results for the Lagrange multiplier formulation, varying the mesh density. As previously observed, the formulation provides incorrect results if interpolating p with constant or linear shape functions, and it is not affected by the imposed inextensibility constraint in the fiber direction in case of constant interpolation. On the other hand, the Q2P1-LM element provides the expected results with a fine mesh.

We now comment on the results obtained for the PM formulation, which are shown in Figures 5.16 to 5.18. Regarding the B1 test, we do not find any numerical pathology: the results obtained for the two types of finite element coincide and the imposed constraint is also effective for coarse meshes. No specific issue is found for the B2 test, but in this case, to obtain satisfactory results, it is advisable to use a fairly fine mesh.

Finally, the results obtained for the Perturbed Lagrangian formulation, are shown in Figures 5.19 to 5.21. Regarding the B1 test, we note that all the used finite elements reach convergence with a fairly coarse discretization. Also, with regard to the B2 test, all the elements reach the convergence with a finest discretization. The same considerations can be made for the B3 test.

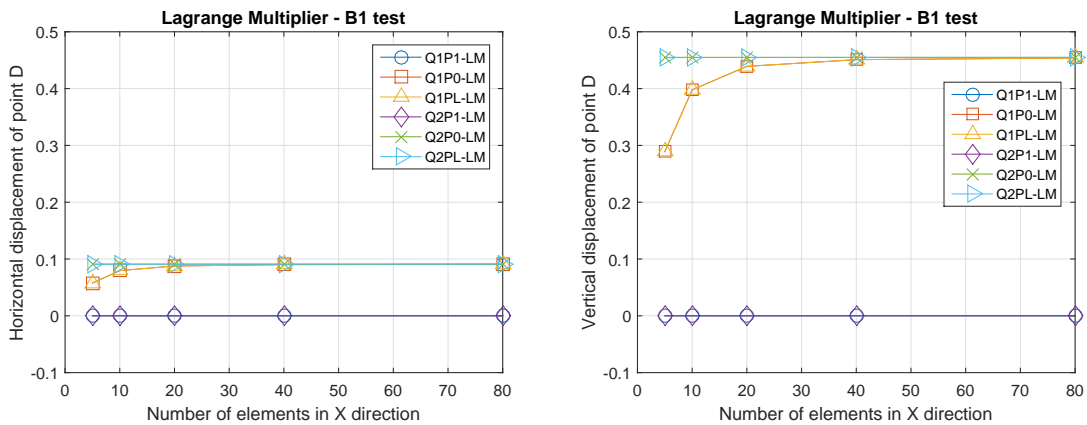


Figure 5.13: Bending test B1: sensitivity to mesh for the Lagrange Multiplier Formulation.

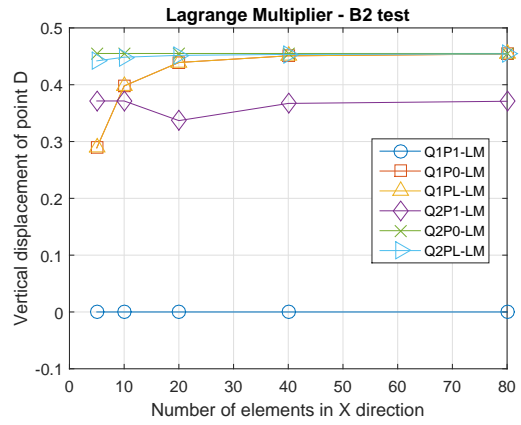
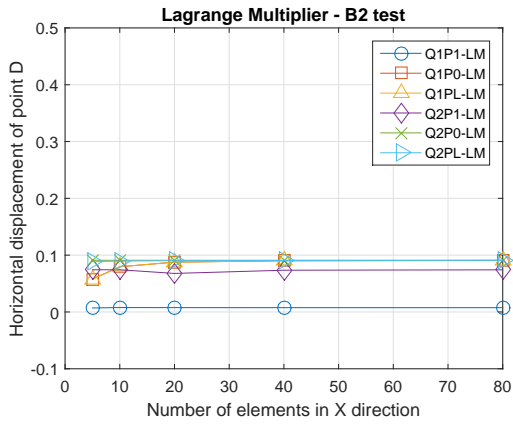


Figure 5.14: Bending test B2: sensitivity to mesh for the Lagrange Multiplier Formulation.

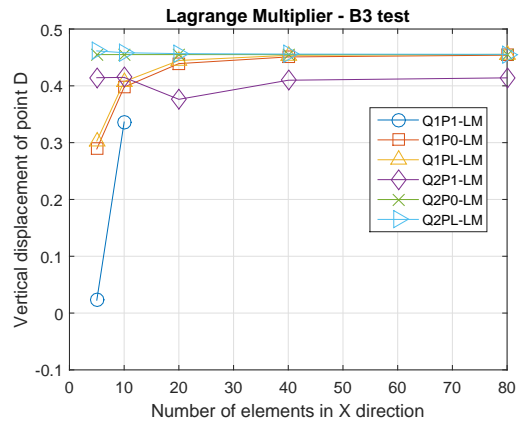
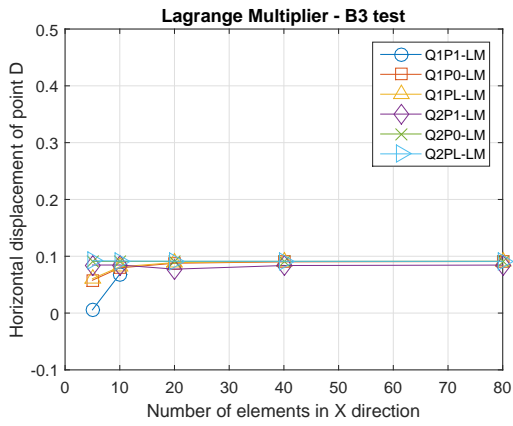


Figure 5.15: Bending test B3: sensitivity to mesh for the Lagrange Multiplier Formulation.

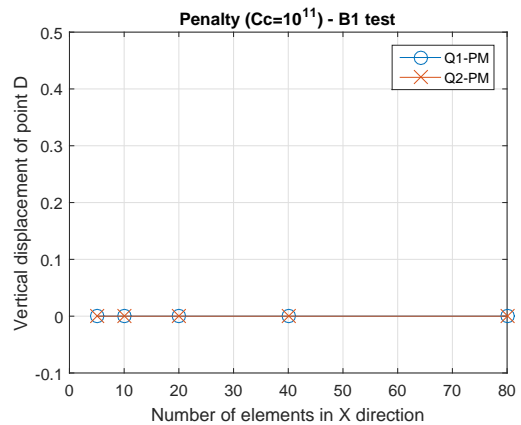
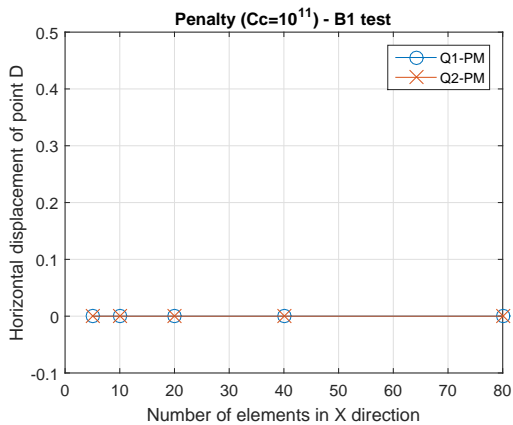


Figure 5.16: Bending test B1: sensitivity to mesh for the Penalty Formulation.

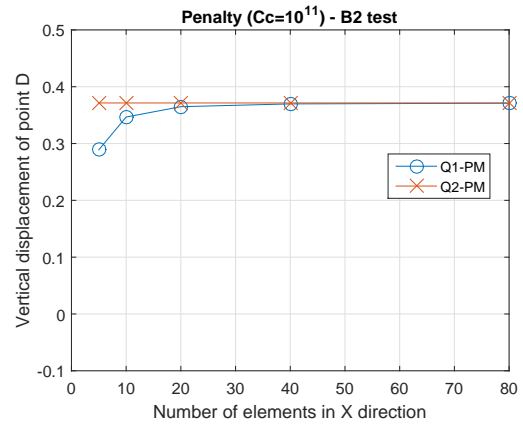
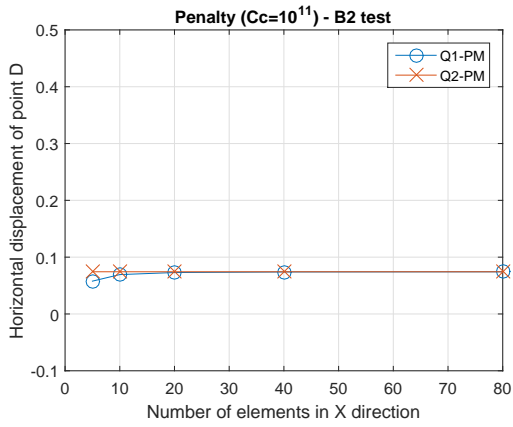


Figure 5.17: Bending test B2: sensitivity to mesh for the Penalty Formulation.

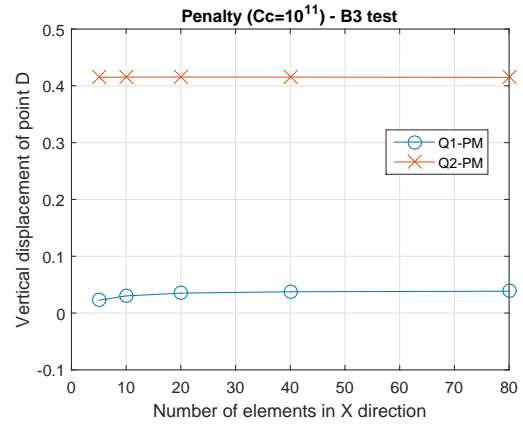
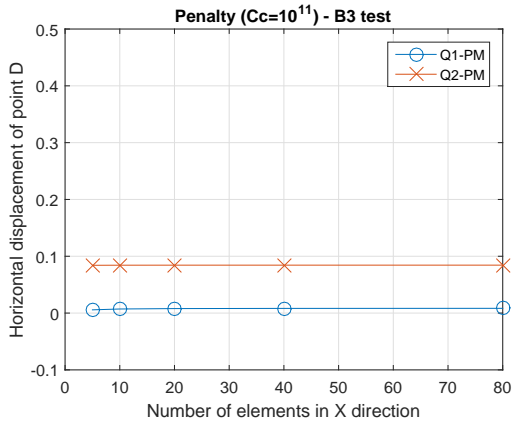


Figure 5.18: Bending test B3: sensitivity to mesh for the Penalty Formulation.

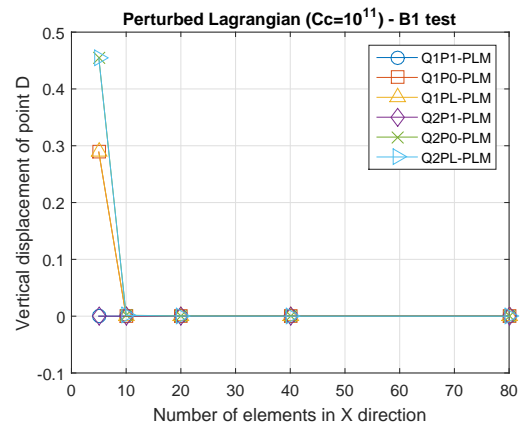
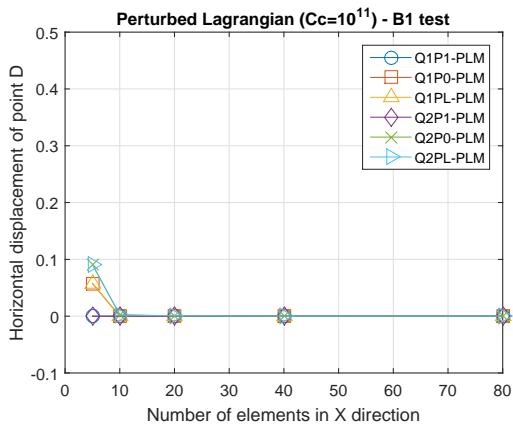


Figure 5.19: Bending test B1: sensitivity to mesh for the Perturbed Lagrangian Formulation.

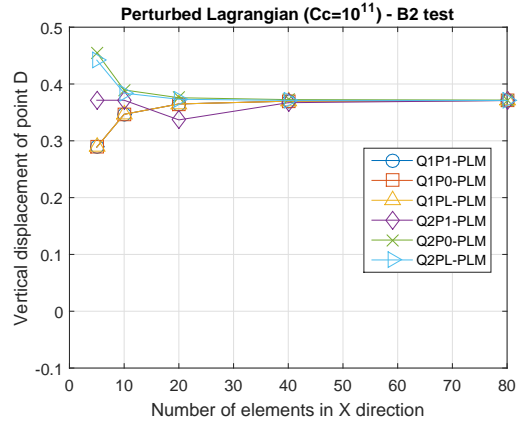
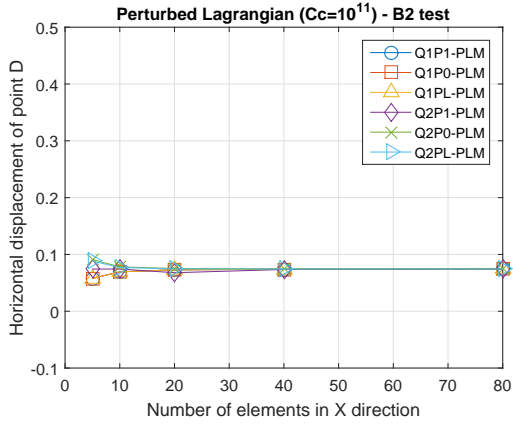


Figure 5.20: Bending test B2: sensitivity to mesh for the Perturbed Lagrangian Formulation.

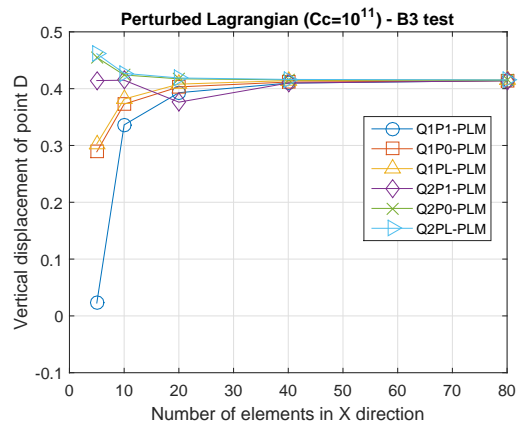
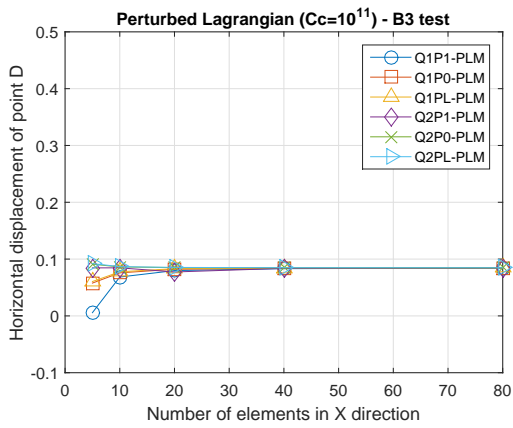


Figure 5.21: Bending test B3: sensitivity to mesh for the Perturbed Lagrangian Formulation.

5.3.2.2 Sensitivity to C_C

We now analyze the results by varying the penalty parameter C_C . We can affirm that, in general, the convergence is reached for $C_C = 10^7$.

We first focus on the Penalty Formulation results, shown in Figures 5.22 to 5.24. Regarding the B1 test, the results coincide for all the elements and converge with the value of the penalty parameter mentioned above. For the B2 test, instead, we note that satisfactory results are obtained with values of the penalty parameter up to 10^{13} . Beyond this value, ill-conditioning occurs. Regarding the B3 test, the results obtained with the Q1-PM element are different from those obtained with the other cases.

Finally, as regards the Perturbed Lagrangian formulation, we observe that the results coincide with those shown for the Penalty formulation. In particular, we can establish that the Q2P1-PLM element is the most performant, because it also provides results for high values of the C_C parameter.

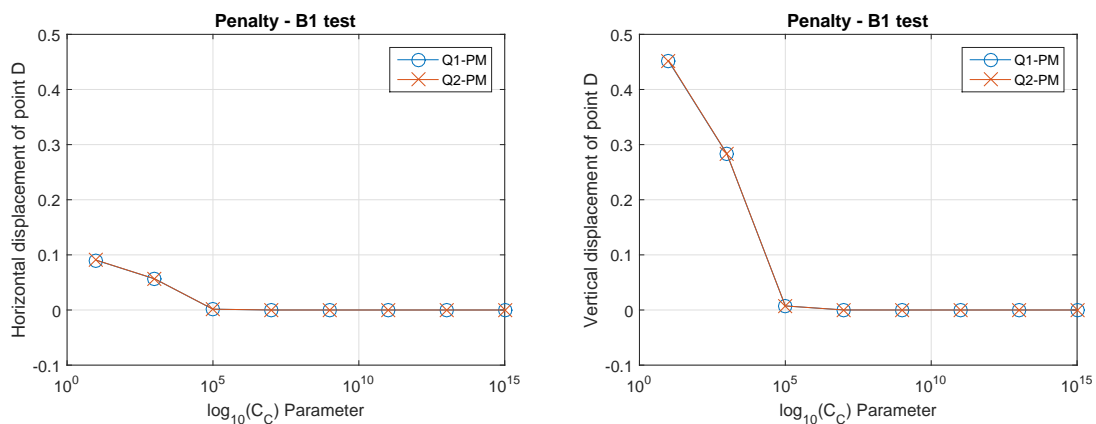


Figure 5.22: Bending test B1: sensitivity to C_C for the Penalty Formulation.

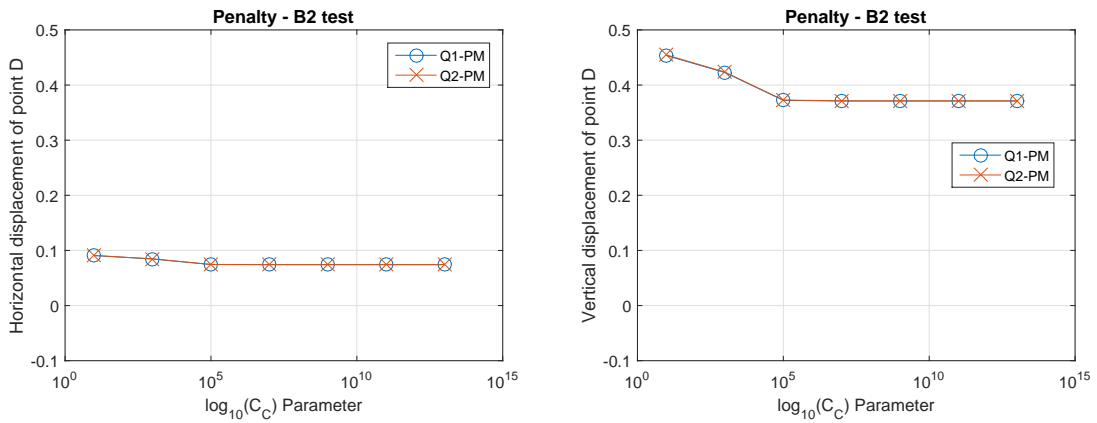


Figure 5.23: Bending test B2: sensitivity to C_C for the Penalty Formulation.

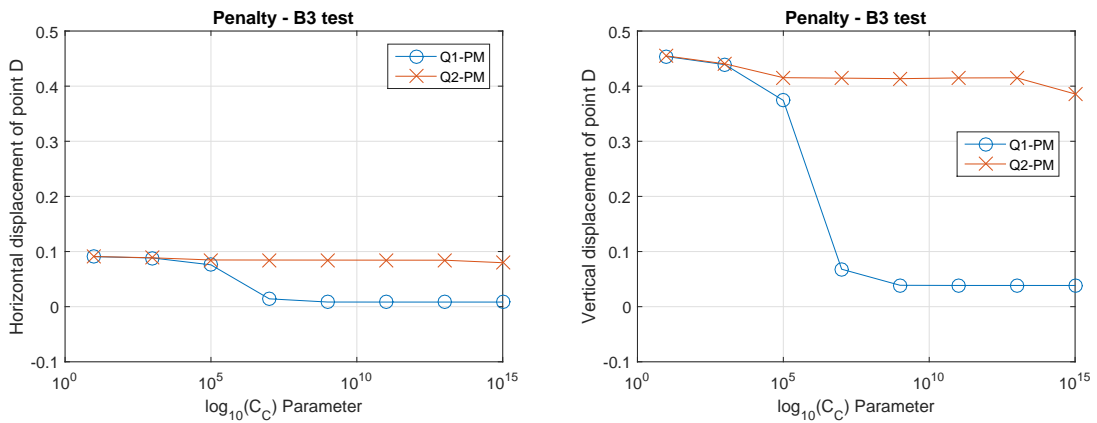


Figure 5.24: Bending test B3: sensitivity to C_C for the Penalty Formulation.

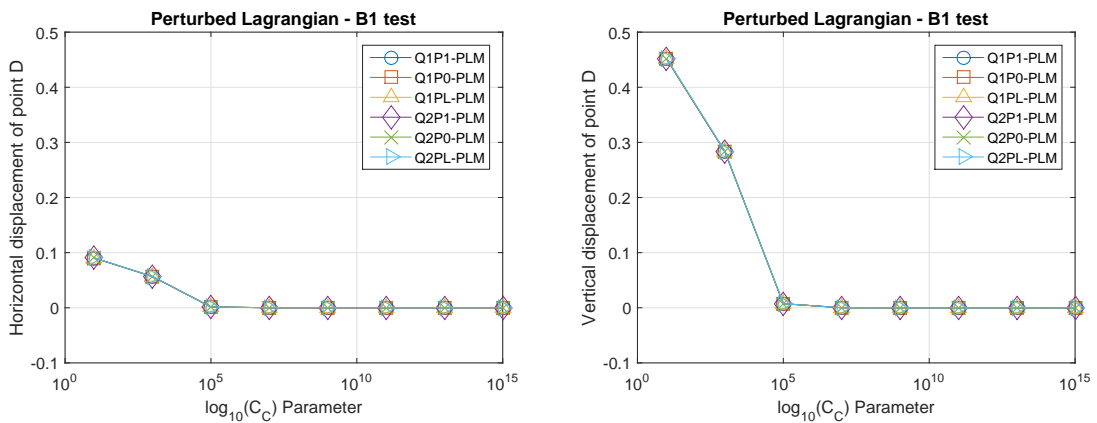


Figure 5.25: Bending test B1: sensitivity to C_C for the Perturbed Lagrangian Formulation.

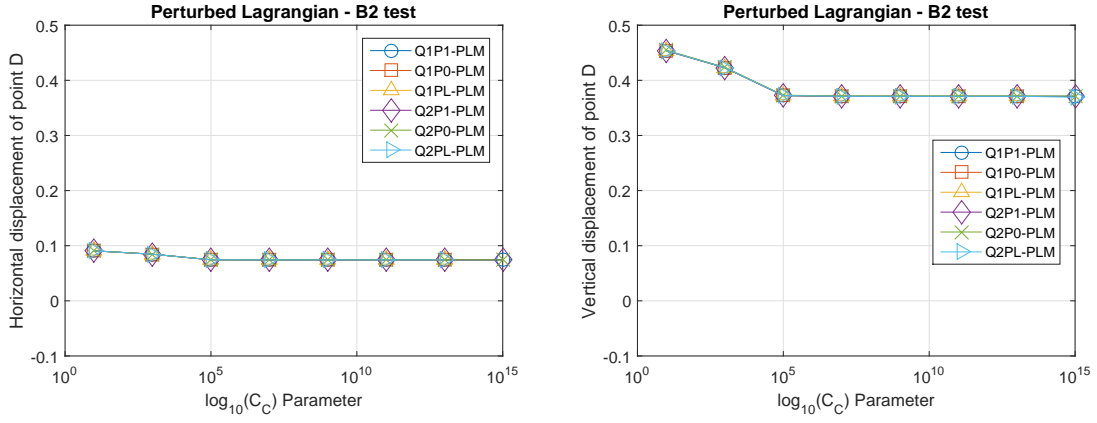


Figure 5.26: Bending test B2: sensitivity to C_C for the Perturbed Lagrangian Formulation.

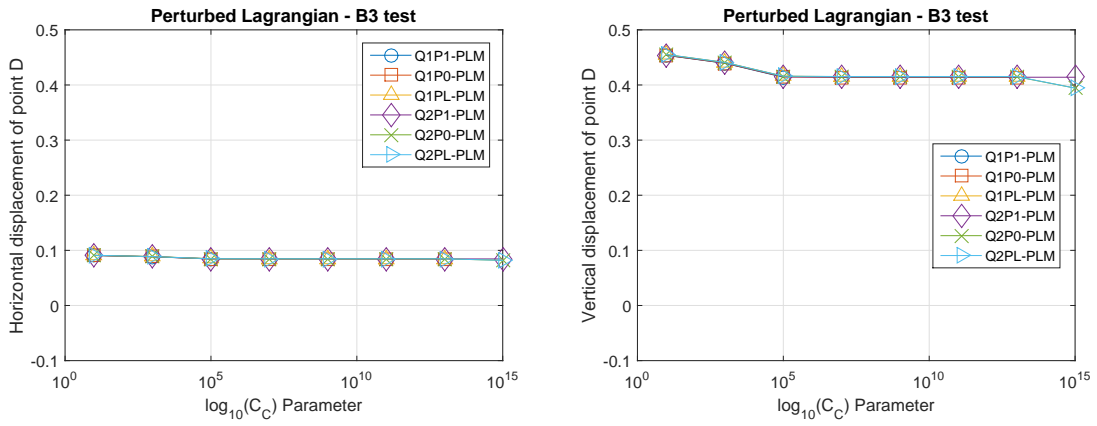


Figure 5.27: Bending test B3: sensitivity to C_C for the Perturbed Lagrangian Formulation.

5.4 Cook's membrane test

The Cook's membrane problem is a standard benchmark test for combined bending and shear response with moderate distortion, named after the author R. D. Cook who first reported it [26]. This test consists of a tapered panel clamped on the edge AB and subjected to a shearing load at the free end CD , resulting in a deformation dominated by a bending response, as shown in Figure 5.28. The analytical solution of this problem is unknown. Therefore, a reference solution is obtained using a fine mesh. We set: $E = 250$, $\nu = 0.3$ and $F = 100$. Meshes of 5×5 , 10×10 , 40×40 and 80×80 are considered. For this test, we consider the displacement components of point C .

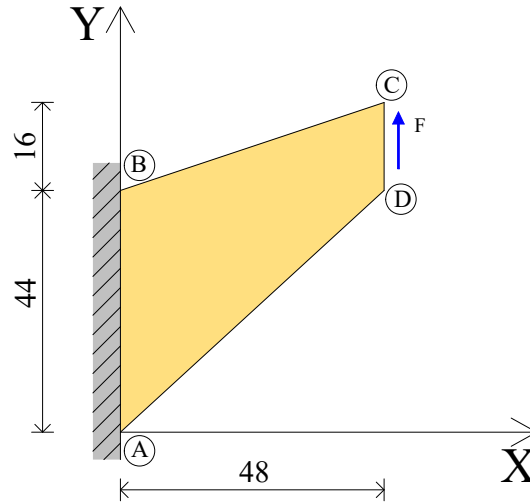


Figure 5.28: Cook's membrane test. Geometry and boundary conditions.

For the anisotropic material, we assume the configurations shown in Figure 5.29.

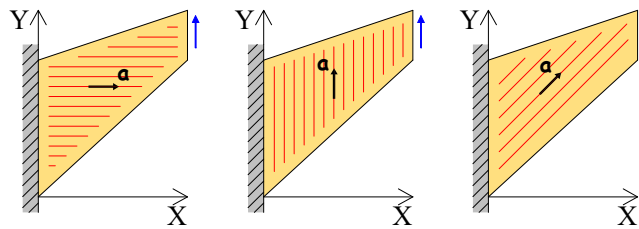


Figure 5.29: Cook's membrane test for anisotropic material, with fiber direction (left) $\mathbf{a} = (1, 0)$, (middle) $\mathbf{a} = (0, 1)$, (right) $\mathbf{a} = (\sqrt{2}/2, \sqrt{2}/2)$. The three tests are denoted, respectively, as C1, C2 and C3.

5.4.1 Isotropic material

Table 5.7 shows the displacement components of point C , obtained with a mesh composed of 80 elements in X-direction and varying the Poisson's ratio. Also in this case, as shown for the bending test, locking phenomena occur with the displacement-based elements (Q1-DB and T1-DB). Instead, all the other finite elements do not exhibit this numerical problem.

Table 5.7: Cook's membrane test numerical results: isotropic formulations.

Q1-DB		Q1-PS			Q1-E4	
ν	u_C	v_C	u_C	v_C	u_C	v_C
0.3	-6.8401E+00	9.1794E+00	-6.8639E+00	9.1989E+00	-6.8639E+00	9.1989E+00
0.49	-5.5126E+00	7.6704E+00	-5.6743E+00	7.8373E+00	-5.6743E+00	7.8373E+00
0.499	-4.7841E+00	6.8786E+00	-5.6002E+00	7.7503E+00	-5.6002E+00	7.7503E+00
0.4999	-2.6128E+00	4.5546E+00	-5.5926E+00	7.7414E+00	-5.5926E+00	7.7414E+00
0.49999	-6.1128E-01	2.5955E+00	-5.5918E+00	7.7405E+00	-5.5918E+00	7.7405E+00
0.499999	-7.7809E-02	2.1441E+00	-5.5918E+00	7.7404E+00	-5.5918E+00	7.7404E+00
Q1-E5		T1-DB			MINI	
ν	u_C	v_C	u_C	v_C	u_C	v_C
0.3	-6.8639E+00	9.1989E+00	-6.7643E+00	9.1079E+00	-6.7892E+00	9.1329E+00
0.49	-5.6743E+00	7.8373E+00	-5.1386E+00	7.2750E+00	-5.5999E+00	7.7641E+00
0.499	-5.6002E+00	7.7503E+00	-3.3232E+00	5.3227E+00	-5.5239E+00	7.6746E+00
0.4999	-5.592603905	7.741415142	-1.0030E+00	2.9349E+00	-5.5160E+00	7.6654E+00
0.49999	-5.5918E+00	7.7405E+00	-1.6422E-01	2.1951E+00	-5.5153E+00	7.6645E+00
0.499999	-5.5918E+00	7.7404E+00	-1.8050E-02	2.0890E+00	-5.5152E+00	7.6644E+00

Figure 5.30 shows the results by varying the mesh density. A 80×80 mesh and a Poisson's ratio equal to 0.3 are considered. We can note that all the formulations, as also seen for the bending test, converge with 80 elements per side.

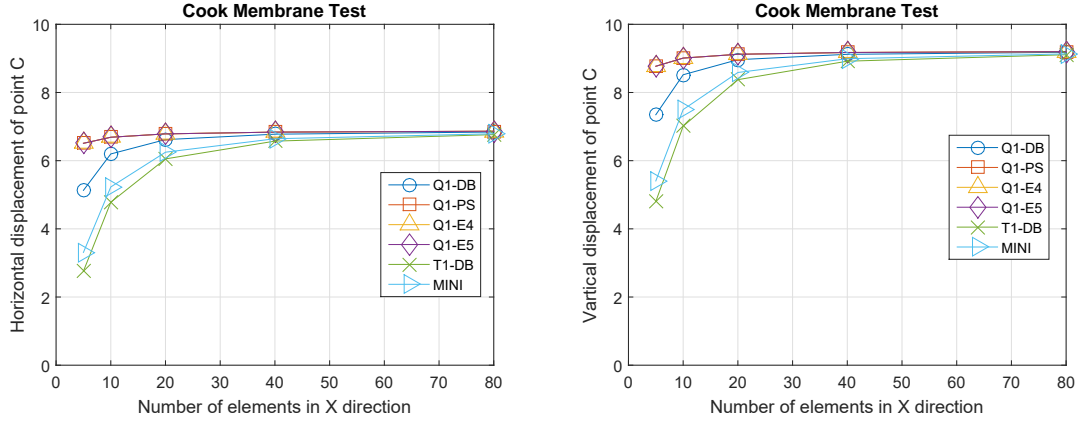


Figure 5.30: Cook's membrane test sensitivity to mesh setting $\nu = 0.3$: isotropic formulations.

5.4.2 Anisotropic material

Setting a 80×80 mesh, the obtained results for the Cook's membrane test are shown in Table 5.8. Using the Lagrange Multiplier formulation, if we approximate p with P0 or PL interpolations, the constraint is ineffective. Using the Penalty formulation, we get acceptable results only when the Q2-PM element is used. Finally, as regards the Perturbed Lagrangian formulation, we note that it provides comparable results with all the element used.

5.4.2.1 Sensitivity to mesh

Figures 5.31 to 5.33 show the results obtained with the Lagrange Multiplier formulation, varying the mesh size. Once again, if we interpolate the Lagrange multiplier p with constant or linear shape functions, the imposed constraint turns out to be ineffective. It remains to analyze the results concerning the Q1P1-LM and Q2P1-LM elements. As in the previous tests, using the Q2P1-LM element we obtain reliable results.

Regarding the results for the Penalty formulation, shown in Figures 5.34 to 5.36, we note that we have satisfactory results only using the Q2-PM element. The Q1-PM element would provide correct results only when C2 and C3 tests are performed.

Finally, we comment on the results obtained for the Perturbed Lagrangian formulation, shown in Figures 5.37 to 5.39. We note that, as regards this formulation, all

Table 5.8: Cook's membrane test numerical results: anisotropic formulations. When the constraint is effective, the results are indicated in **green**, while the incorrect results are indicated in **red**. Instead, when the constraint is ineffective, the results are indicated in black.

		Q1P1-LM	Q1P0-LM	Q1PL-LM	Q2P1-LM	Q2P0-LM	Q2PL-LM
C1	u_C	-6.5349E-319	-6.8401E+00	-6.8326E+00	-2.3032E+00	-6.8807E+00	-6.8827E+00
	v_C	2.0595E+00	9.1794E+00	9.1730E+00	4.3048E+00	9.2147E+00	9.2170E+00
C2	u_C	-3.6000E-19	-6.8401E+00	-6.8401E+00	-5.8835E+00	-6.8807E+00	-6.8798E+00
	v_C	-2.9628E-268	9.1794E+00	9.1794E+00	7.8872E+00	9.2147E+00	9.2142E+00
C3	u_C	5.4700E+158	-6.8401E+00	-6.8440E+00	-1.2975E+00	-6.8807E+00	-6.8831E+00
	v_C	-5.4700E+158	9.1794E+00	9.1826E+00	1.2981E+00	9.2147E+00	9.2165E+00
Cc = 1.00E+05		Q1-PM			Q2-PM		
C1	u_C		-1.7838E+00			-2.3189E+00	
	v_C		3.7896E+00			4.3253E+00	
C2	u_C		-5.8692E+00			-5.8843E+00	
	v_C		7.8786E+00			7.8898E+00	
C3	u_C		-1.3565E+00			-1.3602E+00	
	v_C		1.3578E+00			1.3615E+00	
		Q1P1-PLM	Q1P0-PLM	Q1PL-PLM	Q2P1-PLM	Q2P0-PLM	Q2PL-PLM
C1	u_C	-2.2698E+00	-2.3263E+00	-2.3234E+00	-2.3773E+00	-2.4646E+00	-2.4663E+00
	v_C	4.2714E+00	4.3380E+00	4.3355E+00	4.3982E+00	4.5126E+00	4.5146E+00
C2	u_C	-5.8692E+00	-5.8772E+00	-5.8772E+00	-5.8953E+00	-5.9210E+00	-5.9202E+00
	v_C	7.8786E+00	7.8829E+00	7.8829E+00	7.8963E+00	7.9151E+00	7.9147E+00
C3	u_C	-1.3587E+00	-1.3599E+00	-1.3600E+00	-1.3625E+00	-1.3794E+00	-1.3794E+00
	v_C	1.3600E+00	1.3612E+00	1.3613E+00	1.3643E+00	1.3822E+00	1.3816E+00

the developed finite elements provide correct results.

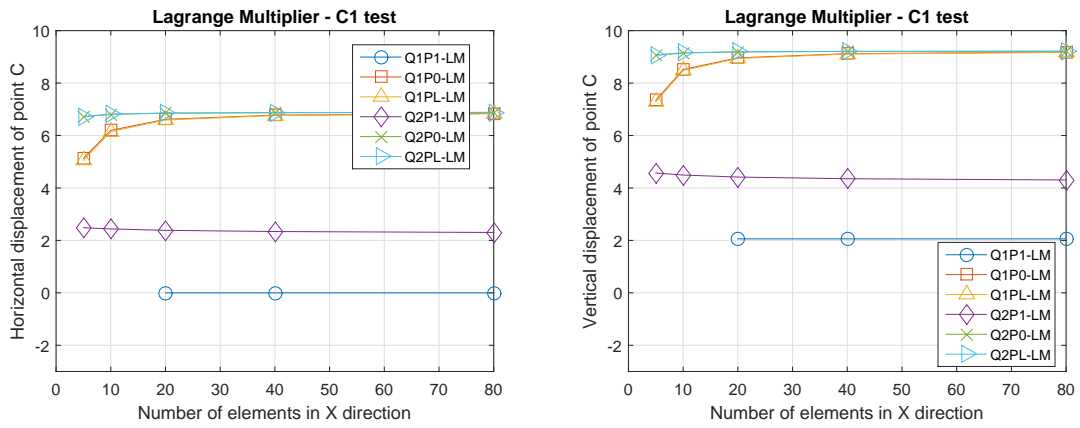


Figure 5.31: Cook's membrane test C1: sensitivity to mesh for the Lagrange Multiplier Formulation.

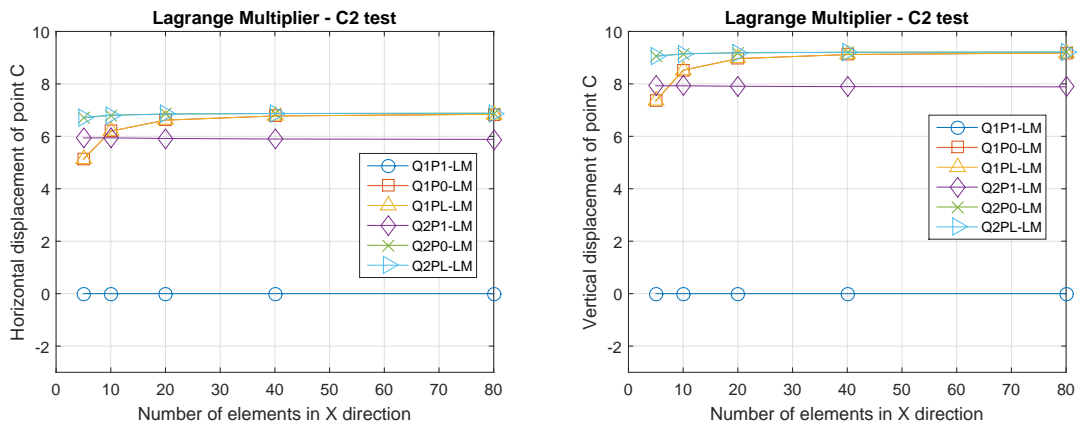


Figure 5.32: Cook's membrane test C2: sensitivity to mesh for the Lagrange Multiplier Formulation.

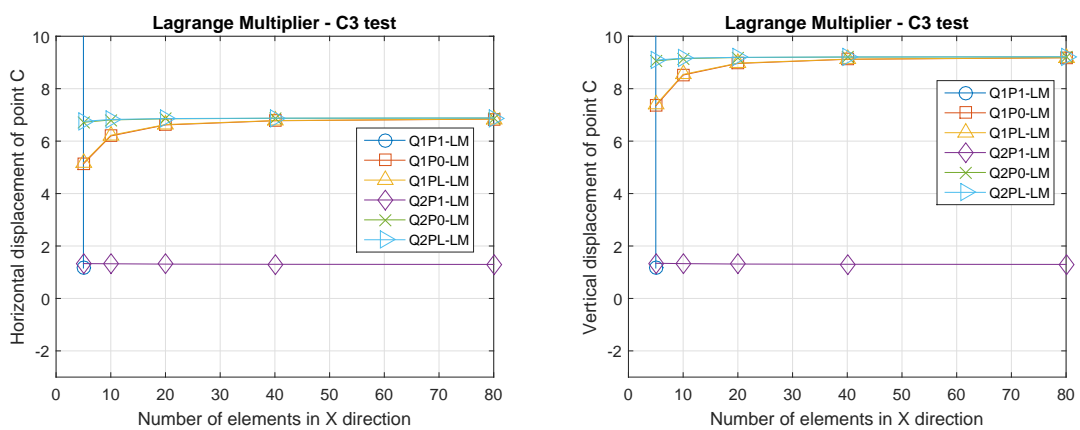


Figure 5.33: Cook's membrane test C3: sensitivity to mesh for the Lagrange Multiplier Formulation.

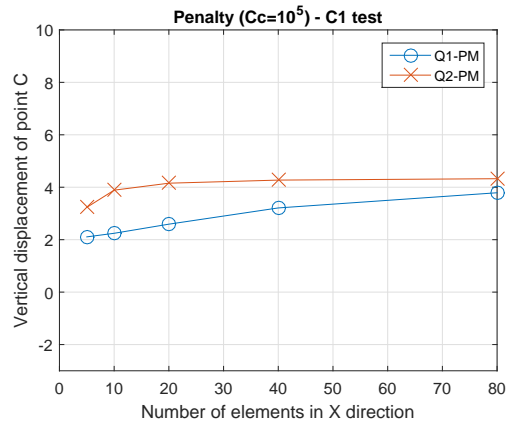
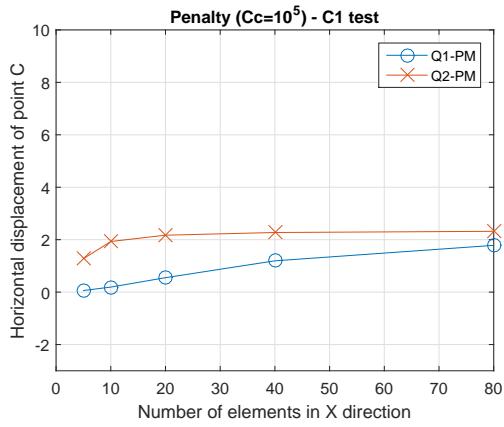


Figure 5.34: Cook's membrane test C1: sensitivity to mesh for the Penalty Formulation.

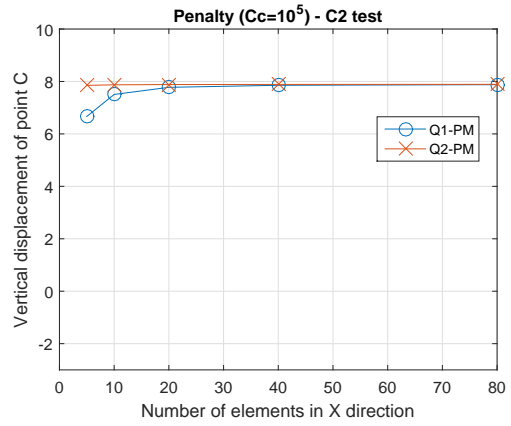
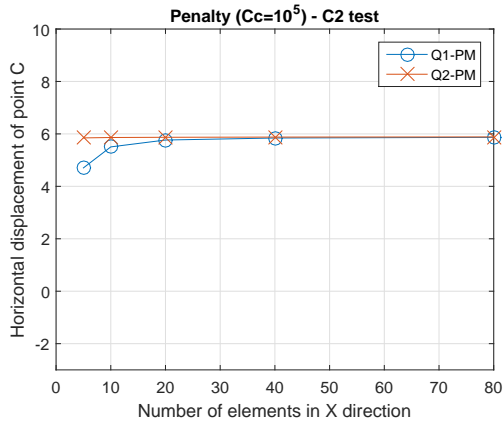


Figure 5.35: Cook's membrane test C2: sensitivity to mesh for the Penalty Formulation.

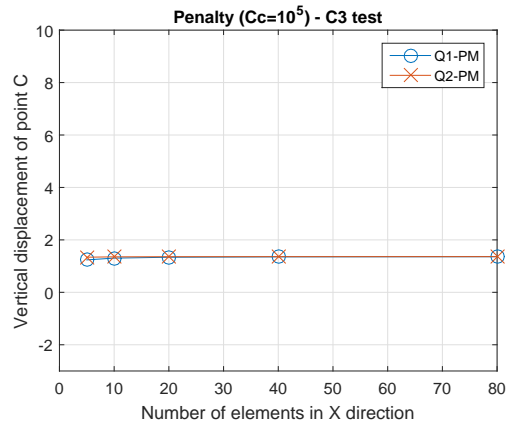
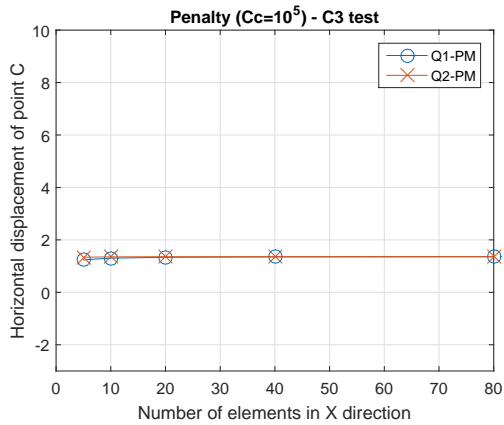


Figure 5.36: Cook's membrane test C3: sensitivity to mesh for the Penalty Formulation.

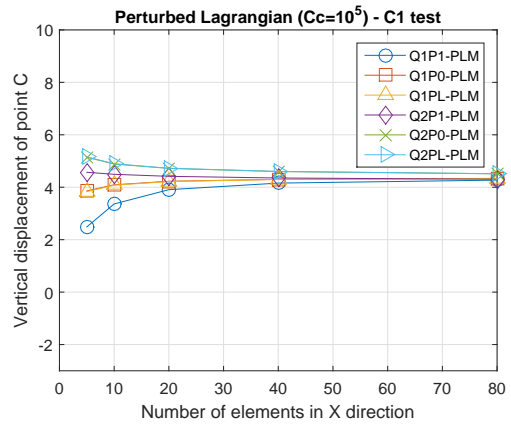
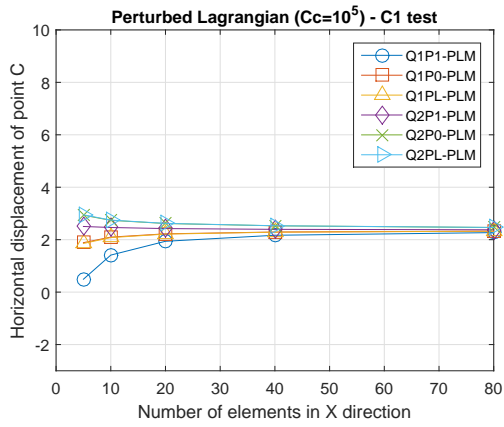


Figure 5.37: Cook's membrane test C1: sensitivity to mesh for the Perturbed Lagrangian Formulation.

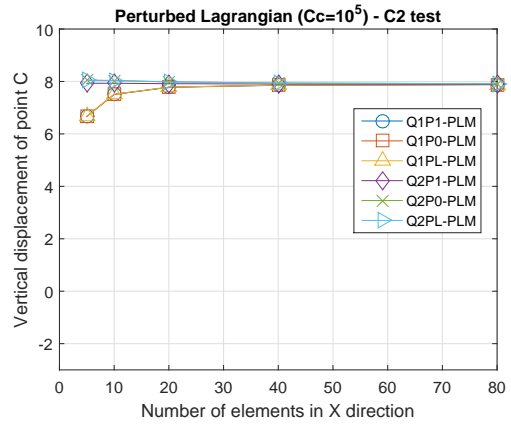
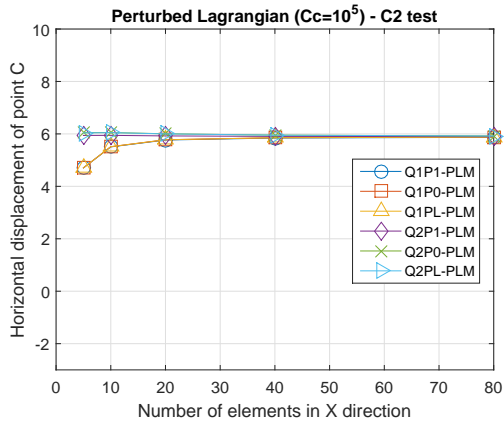


Figure 5.38: Cook's membrane test C2: sensitivity to mesh for the Perturbed Lagrangian Formulation.

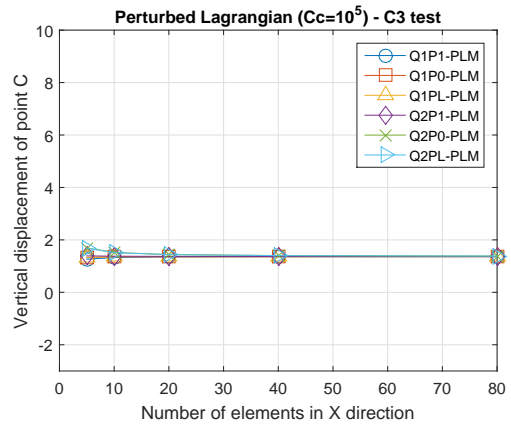
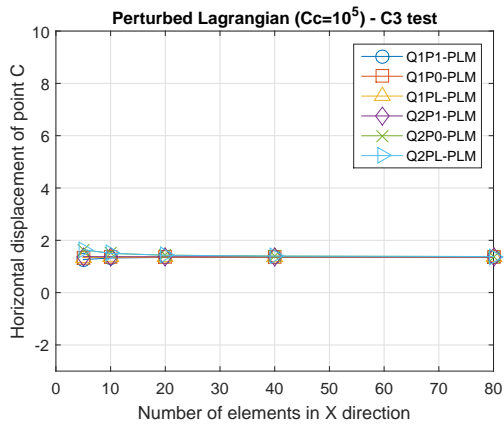


Figure 5.39: Cook's membrane test C3: sensitivity to mesh for the Perturbed Lagrangian Formulation.

5.4.2.2 Sensitivity to C_C

We analyze the values of the two displacement components of point D, varying the penalty parameter C_C . First, we consider the results shown in Figures 5.40 to 5.42, which concern the Penalty formulation. Regarding the C1 test we note that the behaviours of the Q1-PM and Q2-PM elements are different. The Q2-PM element provides reliable results only when $C_C = 10^5$. Instead, with regard to C2 and C3 tests, both the elements show the same results: the Q1-PM element provide, however, more stable results, while the Q2-PM element shows numerical issues after $C_C = 10^{13}$.

Now, we focus on the Perturbed Lagrangian formulation results, which are shown in Figures 5.43 to 5.45. First, we note that, concerning the C2 and C3 tests, both the formulations provide the same results. Rather, the C1 test is interesting. The Q1P1-PLM element shows the same behaviour of the Q2-PM element: this is an unexpected results. Instead, all the other elements show a similar behaviour and provide convergent results with $C_C = 10^5$.

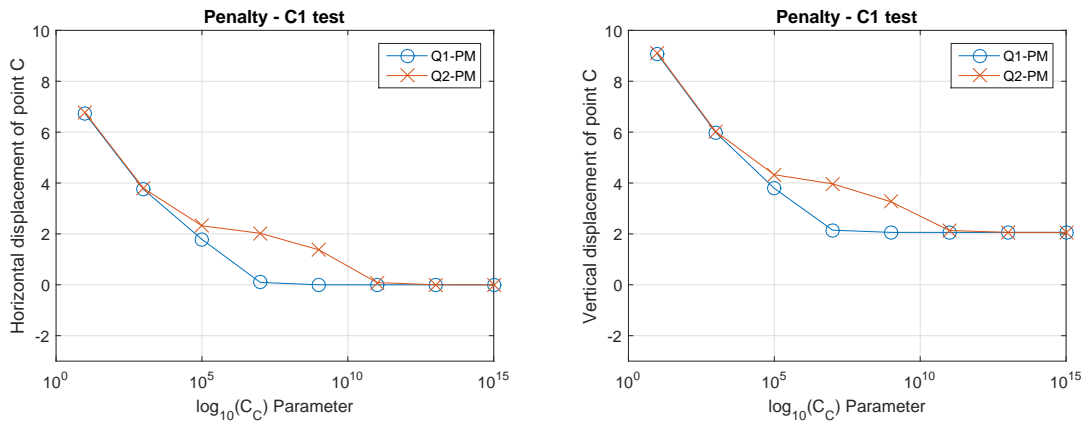


Figure 5.40: Cook's membrane test C1: sensitivity to C_C for the Penalty Formulation.

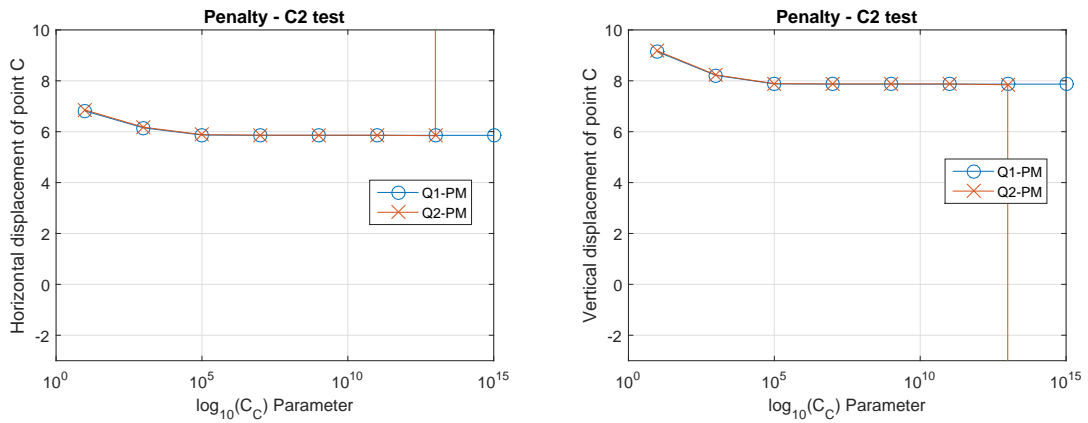


Figure 5.41: Cook's membrane test C2: sensitivity to C_C for the Penalty Formulation.

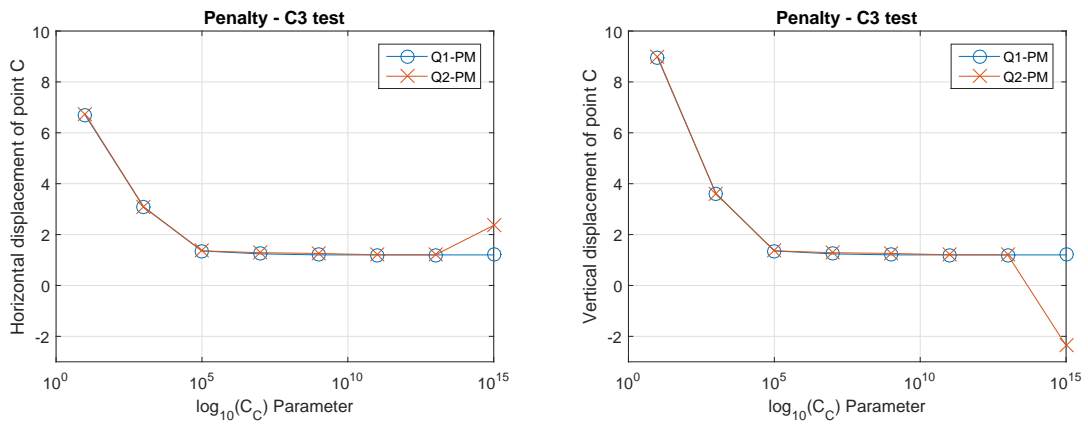


Figure 5.42: Cook's membrane test C3: sensitivity to C_C for the Penalty Formulation.

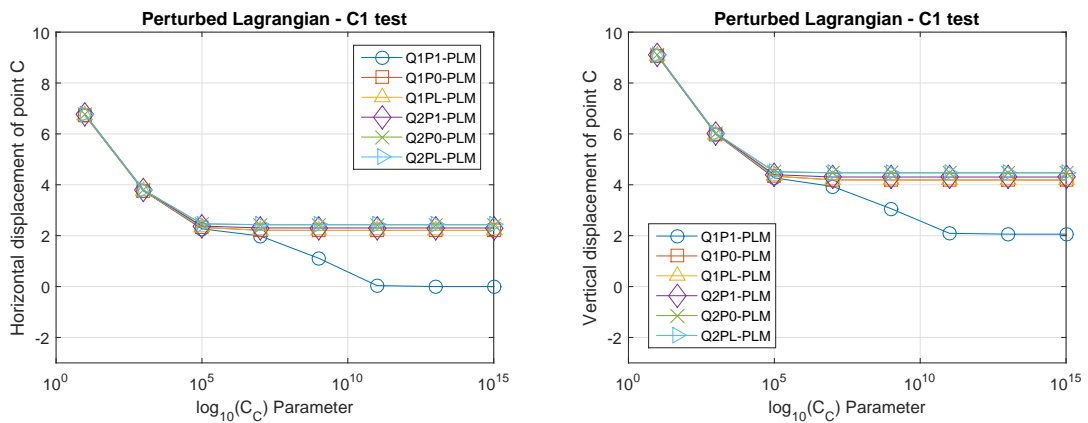


Figure 5.43: Cook's membrane test C1: sensitivity to C_C for the Perturbed Lagrangian Formulation.

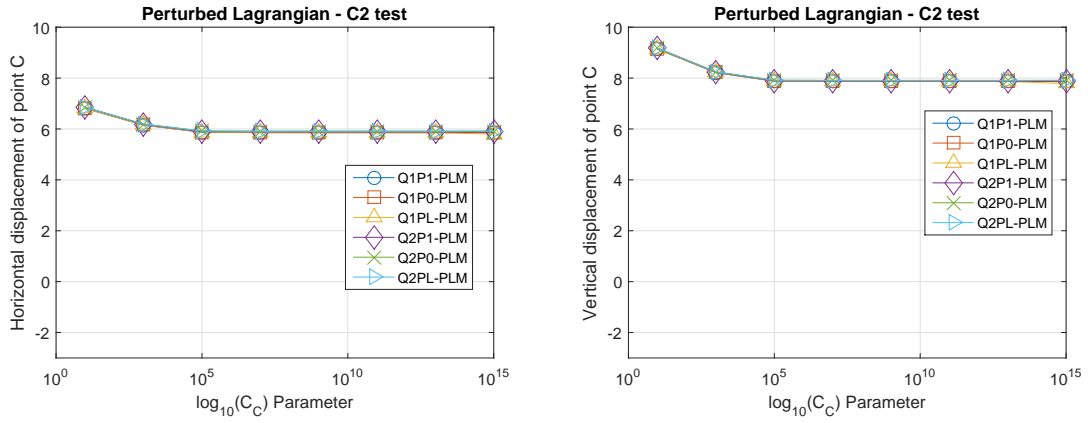


Figure 5.44: Cook's membrane test C2: sensitivity to C_C for the Perturbed Lagrangian Formulation.

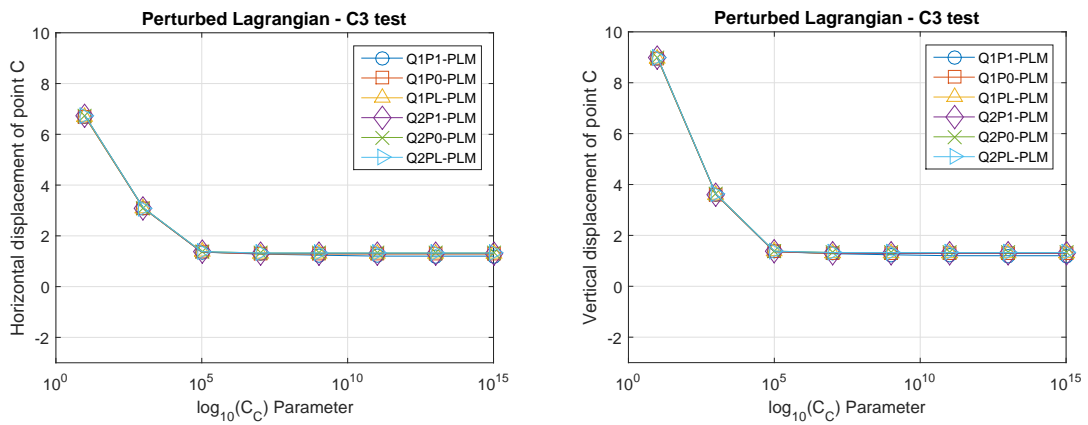


Figure 5.45: Cook's membrane test C3: sensitivity to C_C for the Perturbed Lagrangian Formulation.

5.5 Two-element distortion test

This test is conducted in order to demonstrate the sensibility against mesh distortion. We consider the cantilever beam depicted in Figure 5.46, subjected to a couple at the edge CD . Along the edge AB , the horizontal displacement is set equal to zero, while the point A is constrained along both the directions. The aim is to analyze how the displacements varies with respect to the distortion parameter d . We set: $L = 10$, $H = 2$, $E = 3000$, $\nu = 0$ and $f = 60$. We compare the results in terms of the displacement components of point D .

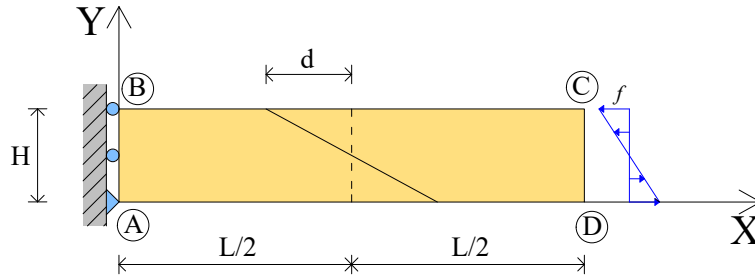


Figure 5.46: Two-element Distortion test. Geometry and boundary conditions.

In order to obtain acceptable results, Gifford suggested that element distortions should be limited to less than 45° [27]. Moreover, Lee and Bathe demonstrated that elements with internal nodes (in this case, the Q2 element) are not affected by the angular distortion [28].

For an isotropic material, referring to Equation (5.5), the horizontal and vertical displacements of point D are the following:

$$\begin{cases} u_D = 2.00E - 01 \\ v_D = 1.00E + 00 \end{cases} \quad (5.8)$$

If we consider an anisotropic material (see Figure 5.47), the analytical solutions are respectively:

$$D1 \begin{cases} u_D = 0.00E + 00 \\ v_D = 0.00E + 00 \end{cases} \quad D2 \begin{cases} u_D = 2.00E - 01 \\ v_D = 1.00E + 00 \end{cases} \quad D3 \begin{cases} u_D = 1.50E - 01 \\ v_D = 7.50E - 01 \end{cases} \quad (5.9)$$

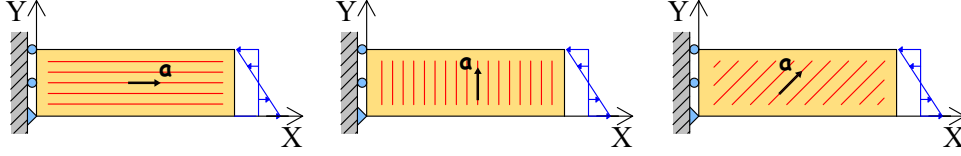


Figure 5.47: Two-elements distortion test for anisotropic material, with fiber direction (left) $\mathbf{a} = (1, 0)$, (middle) $\mathbf{a} = (0, 1)$, (right) $\mathbf{a} = (\sqrt{2}/2, \sqrt{2}/2)$. The three tests are denoted, respectively, as D1, D2 and D3.

5.5.1 Isotropic material

For the isotropic formulations, the test returns the results shown in Figure 5.48. Obviously, given the objectives of the test, only quadrilateral elements have been used, i.e., the Q1-DB, Q1-PS, Q1-E4 and Q1-E5 elements.

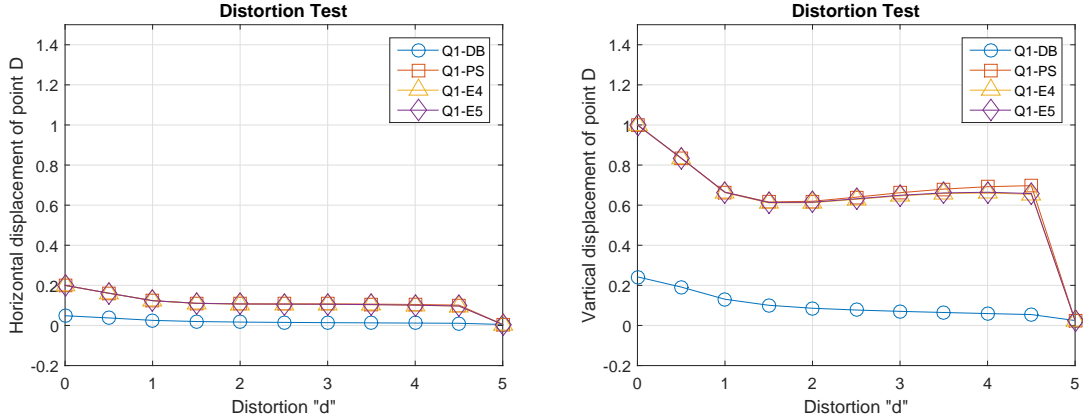


Figure 5.48: Two-elements distortion test sensitivity to mesh distortion: isotropic formulations.

Comparing the results with those available from the literature (see, e.g., [19]), we can observe that the performed two-element distortion test has been set correctly. For the case $d = 0$, the analytical result provided in Equation (5.8) is obtained for all the formulations, except for the Q1-DB element.

For this test, we decide to evaluate the results without varying the Poisson's ratio, because this analysis has already been made for the bending test (considering that these two tests have the same geometry and boundary conditions).

5.5.2 Anisotropic material

To determine the effect that the imposed inextensibility constraint produces on the developed finite elements, we need only to observe the results obtained without

distortion. Hence, setting $d = 0$, the results are shown in Table 5.9.

Table 5.9: Two-elements distortion test numerical results: anisotropic formulations. When the constraint is effective, the results are indicated in green, while the incorrect results are indicated in red. Instead, when the constraint is ineffective, the results are indicated in black.

		Q1P1-LM	Q1P0-LM	Q1PL-LM	Q2P1-LM	Q2P0-LM	Q2PL-LM
D1	u_D	0.0000E+00	4.8485E-02	4.8485E-02	-1.7900E-18	2.0000E-01	2.0000E-01
	v_D	0.0000E+00	2.4242E-01	2.4242E-01	-9.1500E-19	1.0000E+00	1.0000E+00
D2	u_D	8.0134E-03	4.8485E-02	4.8485E-02	2.0000E-01	2.0000E-01	2.0000E-01
	v_D	0.0000E+00	2.4242E-01	2.4242E-01	1.0000E+00	1.0000E+00	1.0000E+00
D3	u_D	5.5749E-03	4.8485E-02	4.9485E-02	1.5168E-01	2.0000E-01	2.0113E-01
	v_D	2.2300E-02	2.4242E-01	2.4759E-01	7.3091E-01	1.0000E+00	1.0062E+00
Cc=1.00E+11		Q1-PM			Q2-PM		
D1	u_D		6.0000E-09		6.0000E-09		
	v_D		3.0000E-08		3.0000E-08		
D2	u_D		4.8485E-02		2.0000E-01		
	v_D		2.4242E-01		1.0000E+00		
D3	u_D		5.5749E-03		1.4862E-01		
	v_D		2.2300E-02		7.2703E-01		
Cc=1.00E+11		Q1P1-PLM	Q1P0-PLM	Q1PL-PLM	Q2P1-PLM	Q2P0-PLM	Q2PL-PLM
D1	u_D	6.0000E-09	4.8485E-02	4.8485E-02	6.0000E-09	2.0000E-01	2.0000E-01
	v_D	3.0000E-08	2.4242E-01	2.4242E-01	3.0000E-08	1.0000E+00	1.0000E+00
D2	u_D	4.8485E-02	4.8485E-02	4.8485E-02	2.0000E-01	2.0000E-01	2.0000E-01
	v_D	2.4242E-01	2.4242E-01	2.4242E-01	1.0000E+00	1.0000E+00	1.0000E+00
D3	u_D	5.5749E-03	4.8485E-02	4.9485E-02	1.5168E-01	2.0000E-01	2.0113E-01
	v_D	2.2300E-02	2.4242E-01	2.4755E-01	7.3091E-01	1.0000E+00	1.0062E+00

Observing the values, we note that the conducted test returns the same results only with the Q2P1-LM, Q2-PM and Q2P1-PLM elements.

5.5.2.1 Sensitivity to mesh distortion

Now we evaluate how the results vary with the mesh distortion parameter d .

Figures 5.49 to 5.51 show the displacement components of point D , for the Lagrange Multiplier formulation. We can observe that the Q2P1-LM element is the most performing. It is interesting to note that the Q1P0-LM and Q1PL-LM elements, provide the same results obtained with the isotropic Q1-DB element, shown in the previous section. Instead, all the other elements provide incorrect results.

With regard to the Penalty formulation, the results are shown in Figures 5.52 to 5.54. We can note that the Q2-PM element is the most performing.

Finally, with reference to the results shown in Figures 5.55 to 5.57, we comment on the Perturbed Lagrangian formulation. As seen for the LM formulation, we note that, in general, for the elements Q1P0-PLM and Q1PL-PLM, the constraint is ineffective and the results coincide with those obtained with the Q1-DB isotropic element.

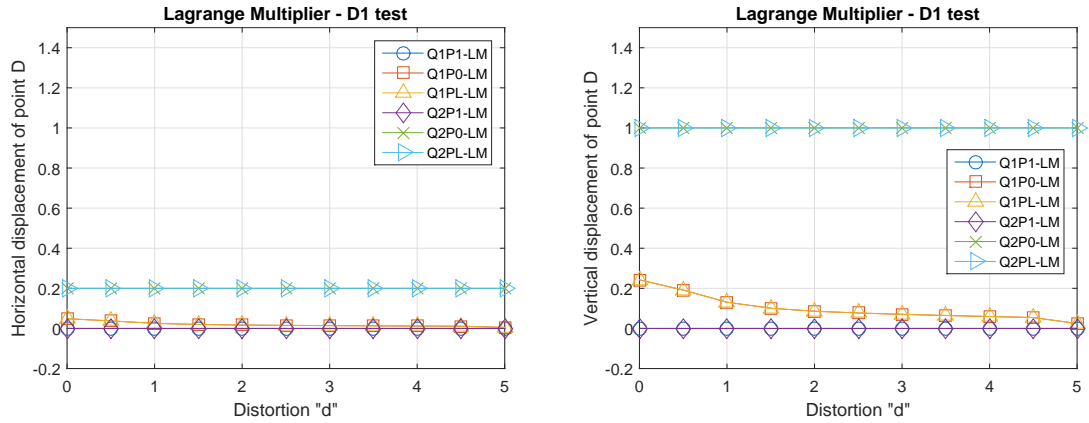


Figure 5.49: Distortion test D1: sensitivity to mesh distortion for the Lagrange Multiplier Formulation.

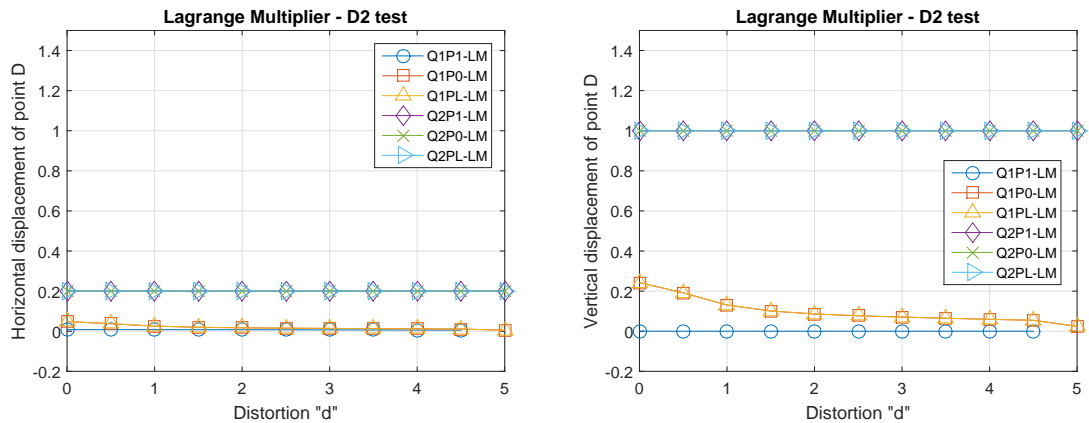


Figure 5.50: Distortion test D2: sensitivity to mesh distortion for the Lagrange Multiplier Formulation.

5.5.2.2 Sensitivity to C_C

We analyze now how the results vary with respect to the penalty parameter C_C . We set $d = 5$, namely the maximum possible distortion.

Observing Figures 5.58 to 5.60, we note that, as regards the Penalty formulation, we obtain converged results between the Q1-PM and Q2-PM elements used, only

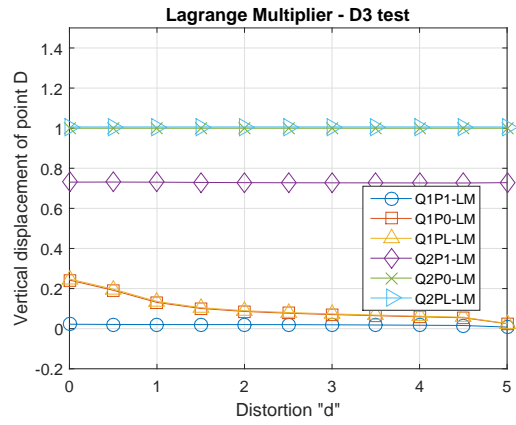
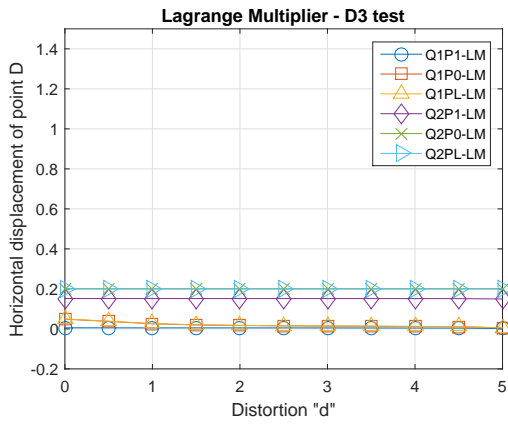


Figure 5.51: Distortion test D3: sensitivity to mesh distortion for the Lagrange Multiplier Formulation.

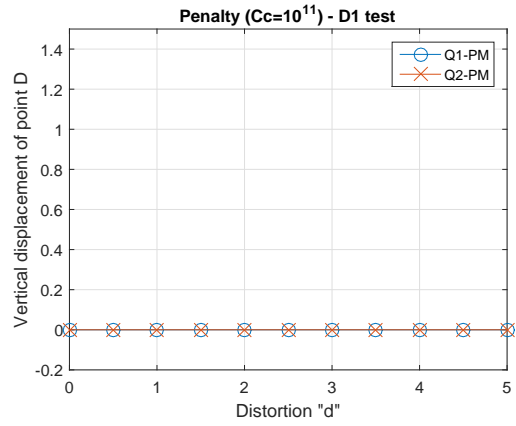
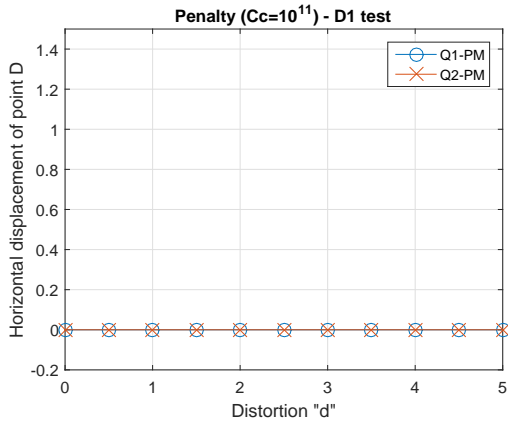


Figure 5.52: Distortion test D1: sensitivity to mesh distortion for the Penalty Formulation.

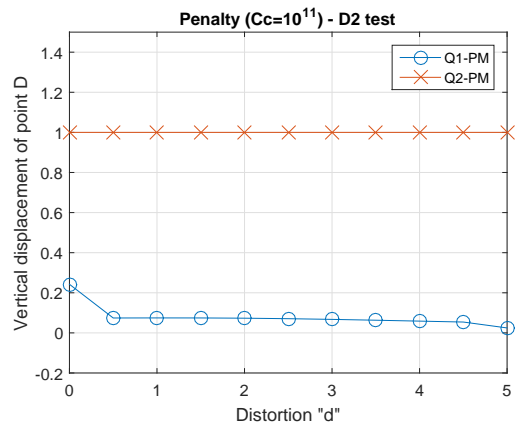
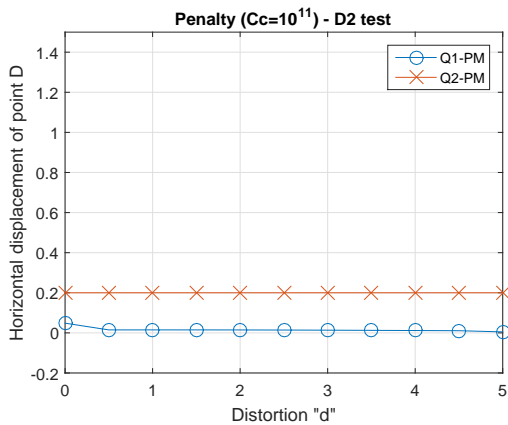


Figure 5.53: Distortion test D2: sensitivity to mesh distortion for the Penalty Formulation.

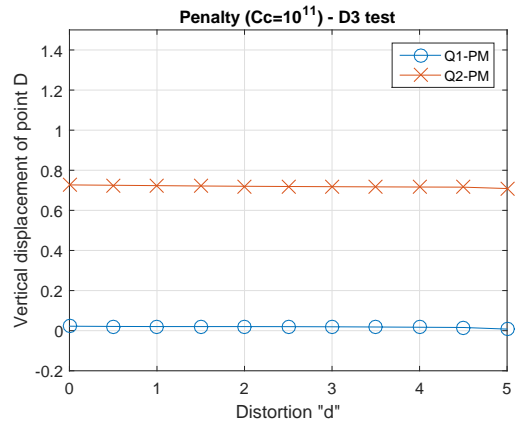
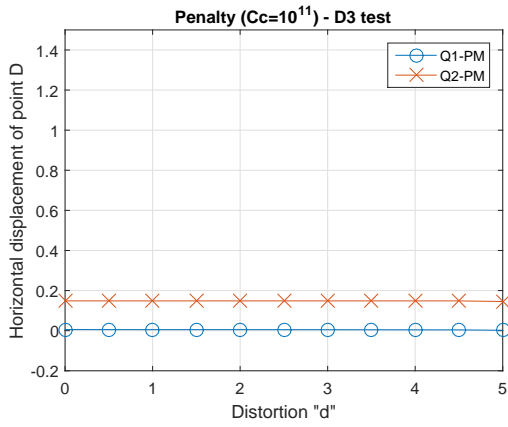


Figure 5.54: Distortion test D3: sensitivity to mesh distortion for the Penalty Formulation.

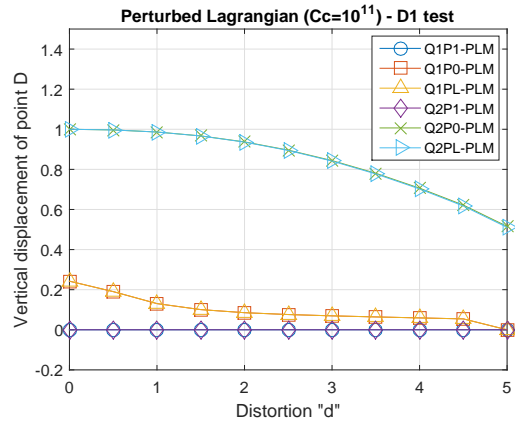
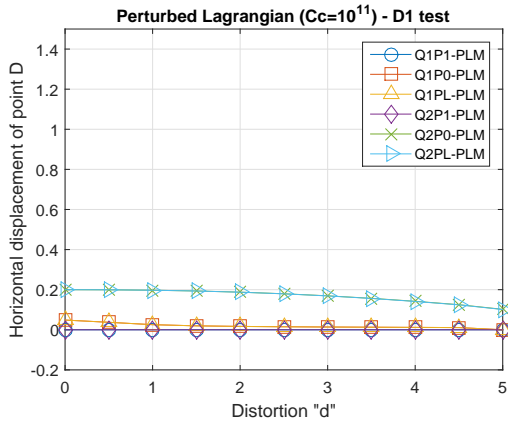


Figure 5.55: Distortion test D1: sensitivity to mesh distortion for the Perturbed Lagrangian Formulation.

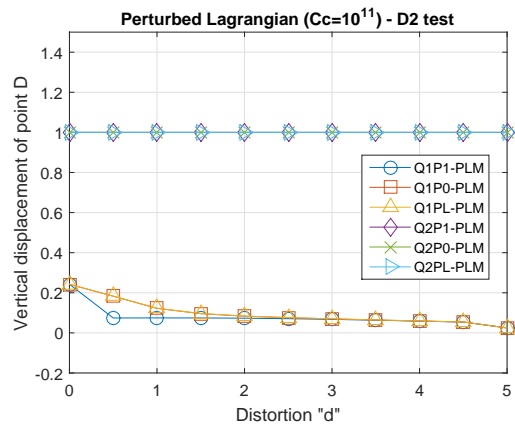
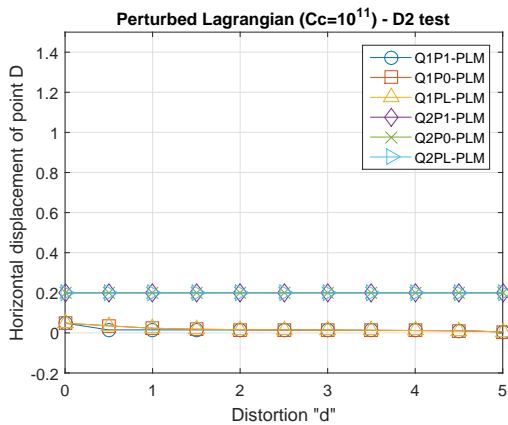


Figure 5.56: Distortion test D2: sensitivity to mesh distortion for the Perturbed Lagrangian Formulation.

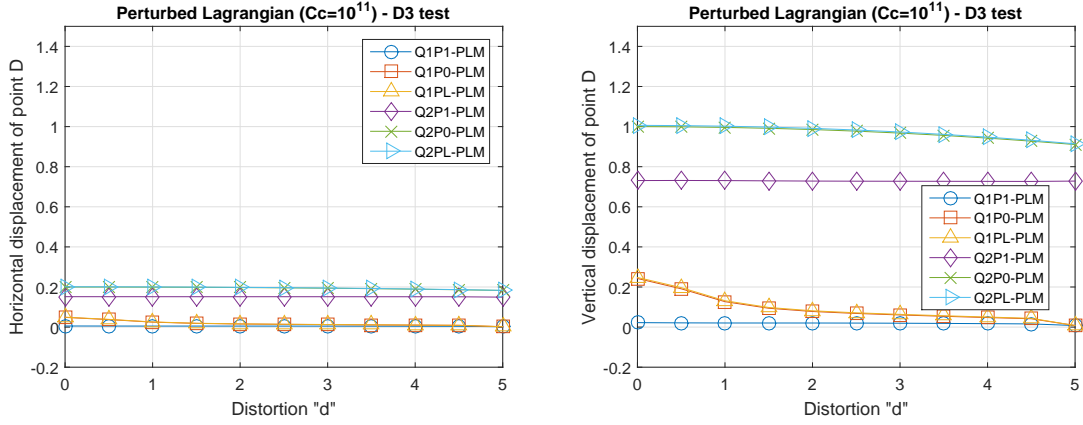


Figure 5.57: Distortion test D3: sensitivity to mesh distortion for the Perturbed Lagrangian Formulation.

when the fibers are arranged horizontally. Convergence is reached for $C_C = 10^7$. In the other cases, instead, the results are not convergent.

Finally, we analyze the results obtained regarding the Perturbed Lagrangian formulation, which are shown in Figures 5.61 to 5.63. As already mentioned in the previous paragraph, the Q1 elements provide incorrect results. Instead, setting $d = 5$, we note that varying C_C , the Q1 elements provide almost coincident results.

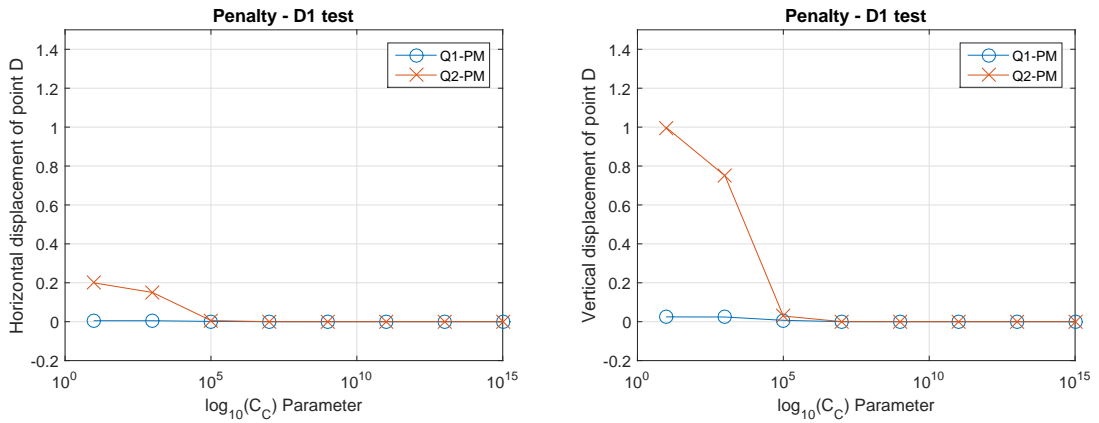


Figure 5.58: Distortion test D1: sensitivity to C_C for the Penalty Formulation.

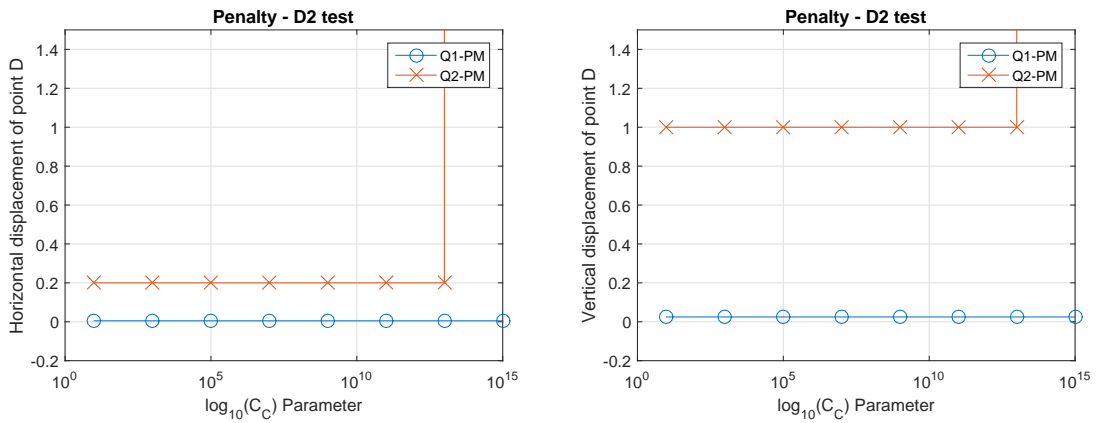


Figure 5.59: Distortion test D2: sensitivity to C_C for the Penalty Formulation.

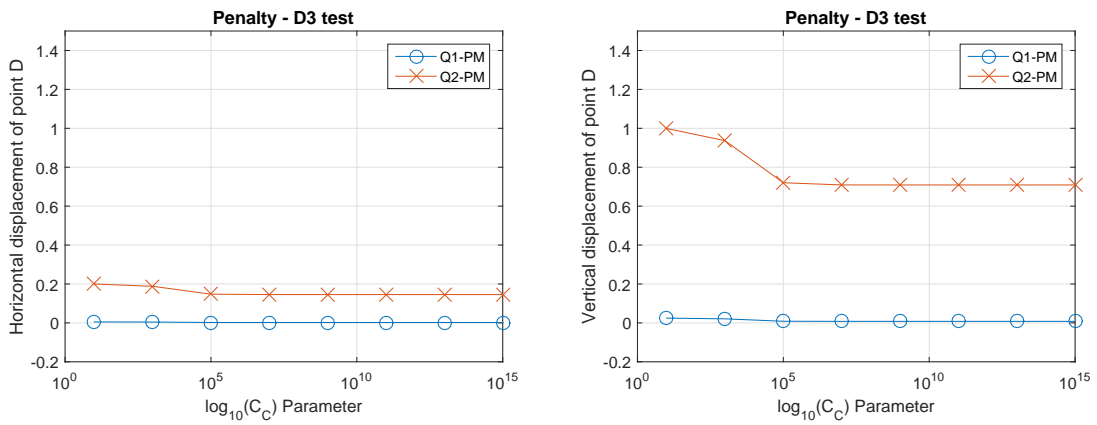


Figure 5.60: Distortion test D3: sensitivity to C_C for the Penalty Formulation.

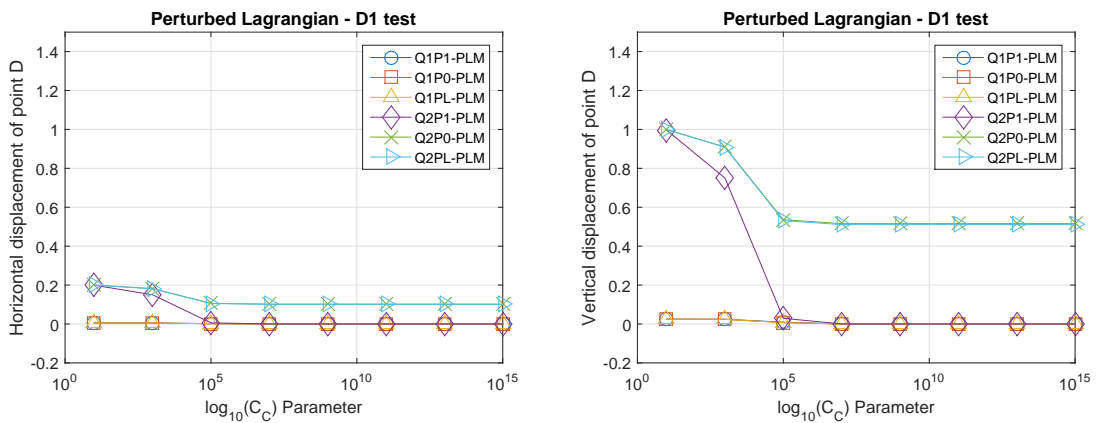


Figure 5.61: Distortion test D1: sensitivity to C_C for the Perturbed Lagrangian Formulation.

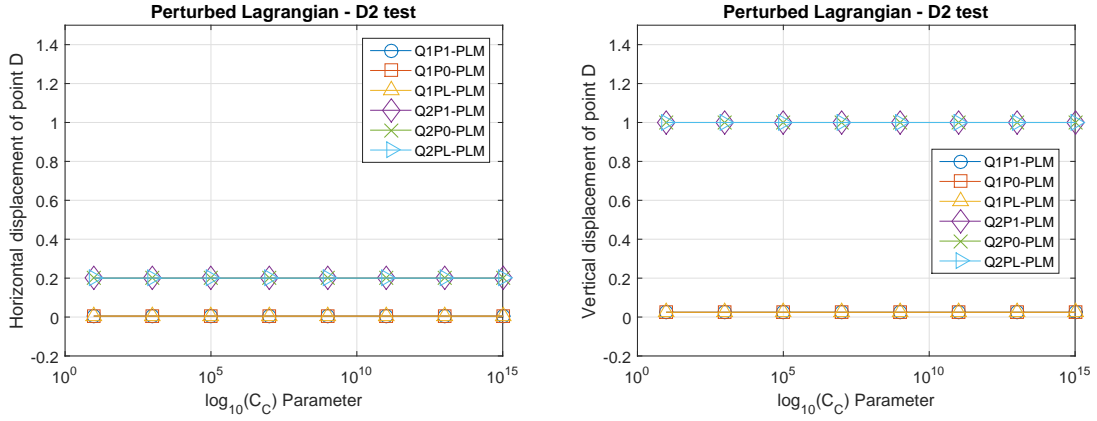


Figure 5.62: Distortion test D2: sensitivity to C_C for the Perturbed Lagrangian Formulation.

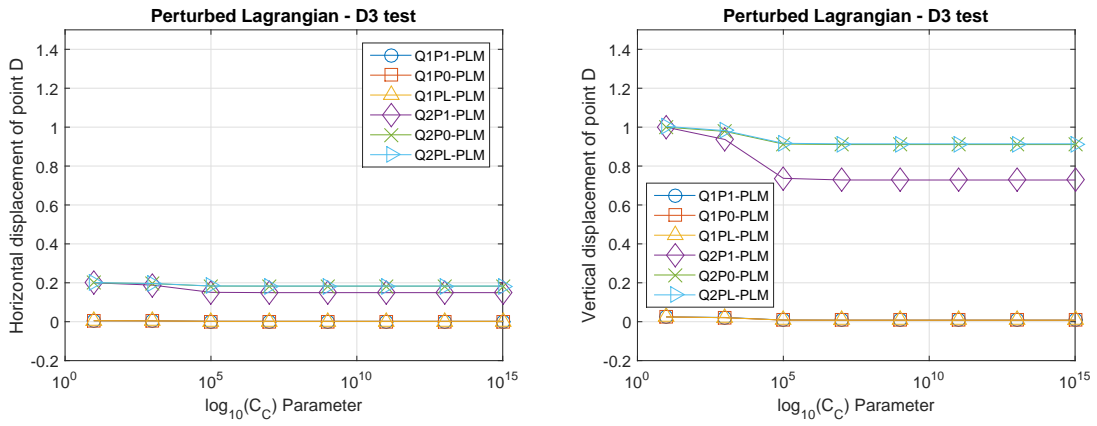


Figure 5.63: Distortion test D3: sensitivity to C_C for the Perturbed Lagrangian Formulation.

Chapter 6

Conclusions and future work

The aim of this thesis was to propose a new possible approach, based on constrained optimization methods, for the modeling of anisotropic materials. In particular, we limit our analysis to linear elastic materials reinforced by a family of parallel inextensible fibers. We proposed different types of finite elements, that differ in the chosen Lagrange multiplier and displacement interpolation.

Element Type	Interpolations	Strain Energy Function
Q2P1-LM		$W = \frac{\lambda}{2}[tr(\boldsymbol{\varepsilon})]^2 + \mu tr(\boldsymbol{\varepsilon}^2) + tr(\boldsymbol{\varepsilon}\mathbf{M})p$
Q2-PM		$W = \frac{\lambda}{2}[tr(\boldsymbol{\varepsilon})]^2 + \mu tr(\boldsymbol{\varepsilon}^2) + \frac{1}{2}C_C[tr(\boldsymbol{\varepsilon}\mathbf{M})]^2$
Q2P1-PLM		$W = \frac{\lambda}{2}[tr(\boldsymbol{\varepsilon})]^2 + \mu tr(\boldsymbol{\varepsilon}^2) + tr(\boldsymbol{\varepsilon}\mathbf{M})p - \frac{1}{2C_C}p^2$
<ul style="list-style-type: none"> • Displacements node ○ Lagrange Multiplier node 		

Figure 6.1: Finite elements for anisotropic materials.

In view of the numerical results presented in Chapter 5, we can affirm that the application of constrained optimization methods to the modeling of anisotropic materials turns to be an excellent implementation strategy. We note that the use of biquadratic shape functions for the displacement field interpolation and of bilinear

shape functions for the Lagrange multiplier interpolation allows to obtain the best performances. Figure 6.1 summarizes the three elements.

Now, for the chosen elements, we can summarize and compare the numerical test results. As regards the Traction test, the results shown in Table 6.1 turn to be consistent with those that we expect. In particular, we note that, when the fibers are arranged horizontally (i.e. in the same direction of the applied tensile load), the imposed inextensibility constraint has effects on both the displacement components of point C (see Figure 5.2). Instead, when the fibers are arranged vertically, the only displacement component tending to zero is the vertical one. Finally, in case of fibers inclined at an angle of 45° , the point C is constrained to move in the fiber direction.

Table 6.1: Traction test results.

		Q2P1-LM	Q2-PM	Q2P1-PLM
T1	u_C	4.6923E-19	1.0000E-10	1.0000E-10
	v_C	-3.2017E-19	-4.2857E-11	-4.2857E-11
T2	u_C	7.4286E-03	7.4286E-03	7.4286E-03
	v_C	-5.1653E-19	-4.2857E-11	-4.2857E-11
T3	u_C	6.5000E-03	6.5000E-03	6.5000E-03
	v_C	-6.5000E-03	-6.5000E-03	-6.5000E-03

Table 6.2 shows the Bending test results. This test results in a bending-dominated response, thus we expect greater constraint effects when the fibers are arranged horizontally (we make a comparison with a reinforced concrete cantilever beam, where the longitudinal reinforcements are represented by the fibers). On the contrary, we expect minimal constrained effects if the fibers are arranged in vertical or inclined direction. The results confirm what we expect.

Table 6.2: Bending test results.

		Q2P1-LM	Q2-PM	Q2P1-PLM
B1	u_D	-5.6900E-08	1.5000E-09	-5.5400E-08
	v_D	-5.8525E-08	7.5000E-09	-5.1018E-08
B2	u_D	7.4184E-02	7.4286E-02	7.4184E-02
	v_D	3.7089E-01	3.7143E-01	3.7089E-01
B3	u_D	8.4483E-02	8.4371E-02	8.4483E-02
	v_D	4.1405E-01	4.1491E-01	4.1405E-01

For the Cook's membrane test, the results are shown in Table 6.3. This test,

like the previous one, provides a bending-dominated response. We obtain a good correspondence with the expected behaviour. Indeed, analyzing the results, we note that the imposed constraint is more effective when the fibers are inclined at an angle of 45° . In the other cases, the considerations done previously are still valid.

Table 6.3: Cook's membrane test results.

		Q2P1-LM	Q2-PM	Q2P1-PLM
C1	u_C	-2.3032E+00	-2.3189E+00	-2.3773E+00
	v_C	4.3048E+00	4.3253E+00	4.3982E+00
C2	u_C	-5.8835E+00	-5.8843E+00	-5.8853E+00
	v_C	7.8872E+00	7.8898E+00	7.8963E+00
C3	u_C	-1.2975E+00	-1.3602E+00	-1.3625E+00
	v_C	1.2981E+00	1.3615E+00	1.3643E+00

We now come to the two-element distortion test, whose results are shown in Table 6.4. Since we consider a cantilever beam, the same considerations of the effects produced by the imposed constraint varying the fiber direction, made for the Bending test, are valid. Observing the results shown in Figures 5.49 to 5.57, it is interesting to note that the chosen Q2P1-LM, Q2-PM, and Q2P1-PLM elements, are not affected by the mesh distortion.

Table 6.4: Two-element distortion test results.

		Q2P1-LM	Q2-PM	Q2P1-PLM
D1	u_D	-1.7900E-18	6.0000E-09	6.0000E-09
	v_D	-9.1500E-19	3.0000E-08	3.0000E-08
D2	u_D	2.0000E-01	2.0000E-01	2.0000E-01
	v_D	1.0000E+00	1.0000E+00	1.0000E+00
D3	u_D	1.5168E-01	1.4862E-01	1.5168E-01
	v_D	7.3091E-01	7.2703E-01	7.3091E-01

In this thesis we provided the basis for a new approach to the modeling of anisotropic materials. Since we have shown the good quality of the proposed formulations, it could be useful to extend the present work to the following research fields:

- *Three-dimensional fiber-reinforced linear elastic materials.* The generalization of the proposed formulations to the three-dimensional case should be a natural

extension of this work. The unit vector that indicates the fiber directions, will take the form:

$$\mathbf{a} = (a_x, a_y, a_z)^T$$

Appropriate interpolations have to be considered.

- *Two fiber-family anisotropic materials.* It will be necessary to introduce an additional unit vector \mathbf{b} , indicating the direction of the second family of fibers, such that the strain energy will be assumed to be a function of strain tensor $\boldsymbol{\varepsilon}$ and of unit vectors \mathbf{a} and \mathbf{b} :

$$W = W(\boldsymbol{\varepsilon}, \mathbf{a}, \mathbf{b})$$

Therefore, the function W will include two directional inextensibility constraints.

- *Finite strain.* At present, an important field concerning anisotropic materials is certainly that inherent materials with large rotations and strains (e.g., elastomers, plastically-deforming materials, and biological soft tissues). For this reason, the application of the proposed formulations to these materials would be very interesting.

Appendix A

Analytical solutions

A.1 Traction test

In the context of plane strain and small displacements, the horizontal and vertical displacement fields of a continuous domain Ω subjected to an uniaxial pure traction state can be written as follows:

$$\begin{aligned}u(x, y) &= \varepsilon_{xx} x + \varepsilon_{xy} y \\v(x, y) &= \varepsilon_{xy} x + \varepsilon_{yy} y\end{aligned}\tag{A.1}$$

where ε_{xx} , ε_{yy} , ε_{xy} are the strain tensor components and x and y are the Cartesian coordinates of the generic point in the domain Ω . Therefore, considering Equations (A.1) and the constitutive relations (4.25) concerning the Lagrange Multiplier formulation, we can provide the following analytical solutions:

$$\begin{aligned}u(x, y) &= q \left[\frac{a_y[a_y^3\mu + a_x^2a_y(\lambda + 2\mu)]x}{(a_x^2 + a_y^2)^2\mu(\lambda + 2\mu)} + \frac{[a_xa_y^3\lambda - (2\mu + \lambda)a_x^3a_y]y}{2(a_x^2 + a_y^2)^2\mu(\lambda + 2\mu)} \right] \\v(x, y) &= q \left[\frac{[a_xa_y^3\lambda - (2\mu + \lambda)a_x^3a_y]x}{2(a_x^2 + a_y^2)^2\mu(\lambda + 2\mu)} + \frac{a_x[-a_xa_y^2(\lambda + \mu)]y}{(a_x^2 + a_y^2)^2\mu(\lambda + 2\mu)} \right]\end{aligned}\tag{A.2}$$

where q is the uniformly distributed tensile load, $\mathbf{a} = (a_x, a_y)$ is the unit vector that identify the fiber direction, and λ and μ are the Lamé constants.

A.2 Bending test

The Bending test carried out in Section 5.3 can be seen as a simplified representation of the pure bending of a beam (see Figure A.1). The elementary beam theory predicts that the stress σ_{xx} varies linearly with y . Then, we consider the following Airy stress function:

$$\phi = Ay^3 \quad (\text{A.3})$$

where A is a constant to be determined.

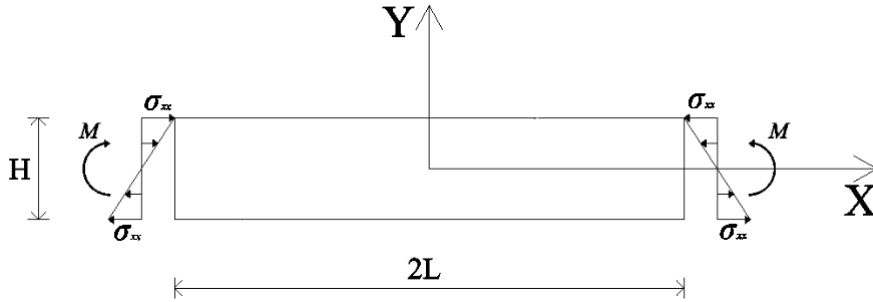


Figure A.1: Pure bending of a beam

The Airy stress function enable us to determine the stress components by applying the following relations:

$$\begin{aligned} \sigma_{xx} &= \frac{\partial^2 \phi}{\partial y^2} = 6Ay \\ \sigma_{yy} &= \frac{\partial^2 \phi}{\partial x^2} = 0 \\ \sigma_{xy} &= -\frac{\partial^2 \phi}{\partial x \partial y} = 0 \end{aligned} \quad (\text{A.4})$$

Now we want to establish a relation between the moment M and the stress distribution at the beam ends in integral form to fully define the stress field in terms of problem parameters. Particularly, setting $h = H/2$:

$$M = \int_{-h}^h \sigma_{xx} y dy = 6A \int_{-h}^h y^2 dy = 4Ah^3 \Rightarrow A = \frac{M}{4h^3} \quad (\text{A.5})$$

and, therefore, then the stress component σ_{xx} , which defines the bending state,

becomes:

$$\sigma_{xx} = \frac{3M}{2h^3}y \quad (\text{A.6})$$

By applying the strain-displacement conditions and the strain-stress relationship, we obtain that:

$$\begin{aligned} \varepsilon_{xx} &= \frac{\partial u}{\partial x} = \mathbb{S}_{11}\sigma_{xx} = \mathbb{S}_{11}\frac{3M}{2h^3}y \\ \varepsilon_{yy} &= \frac{\partial v}{\partial y} = \mathbb{S}_{21}\sigma_{xx} = \mathbb{S}_{21}\frac{3M}{2h^3}y \\ \varepsilon_{xy} &= \frac{1}{2}\left(\frac{\partial u}{\partial y} + \frac{\partial v}{\partial x}\right) = \mathbb{S}_{31}\sigma_{xx} = \mathbb{S}_{31}\frac{3M}{2h^3}y \end{aligned} \quad (\text{A.7})$$

After integrating, we obtain the following displacement field:

$$\begin{aligned} u(x, y) &= \mathbb{S}_{11}\frac{3M}{2h^3}xy + g(y) \\ v(x, y) &= \mathbb{S}_{12}\frac{3M}{4h^3}y^2 + h(x) \end{aligned} \quad (\text{A.8})$$

Equation (A.7)₃, can be separated into two independent relations in x and y . The first relation is:

$$\mathbb{S}_{11}\frac{3M}{2h^3}x + g'(y) + h'(x) - \mathbb{S}_{31}\frac{3M}{h^3}y = 0 \Rightarrow \begin{cases} h'(x) + \mathbb{S}_{11}\frac{3M}{2h^3}x = C_1 \\ g'(y) - \mathbb{S}_{31}\frac{3M}{h^3}y = -C_1 \end{cases} \quad (\text{A.9})$$

which leads to:

$$g(y) = \mathbb{S}_{31}\frac{3M}{2h^3}y^2 - C_1y + C_3 \quad (\text{A.10})$$

while the second one is:

$$h(x) = -\mathbb{S}_{11}\frac{3M}{4h^3}x^2 + C_1x + C_2 \quad (\text{A.11})$$

By replacing Equations (A.10) and (A.11) into Equations (A.8), we obtain:

$$\begin{aligned}
u(x, y) &= \frac{3M}{2h^3} (\mathbb{S}_{11}xy + \mathbb{S}_{31}y^2) - C_1y + C_3 \\
v(x, y) &= \frac{3M}{2h^3} \left(\frac{1}{2}\mathbb{S}_{21}y^2 - \mathbb{S}_{11}x^2 \right) + C_1x + C_2
\end{aligned} \tag{A.12}$$

If we consider the following boundary conditions

$$\begin{aligned}
u(0, -h) &= \mathbb{S}_{31} \frac{3M}{2h} + C_1h + C_3 = 0 \\
v(0, -h) &= \mathbb{S}_{21} \frac{3M}{4h} + C_2 = 0 \\
u(0, h) &= \mathbb{S}_{31} \frac{3M}{2h} - C_1h + C_3 = 0
\end{aligned} \tag{A.13}$$

we can compute the constants of integration:

$$\begin{aligned}
C_1 &= 0 \\
C_2 &= -\mathbb{S}_{21} \frac{3M}{4h} \\
C_3 &= -\mathbb{S}_{31} \frac{3M}{2h}
\end{aligned} \tag{A.14}$$

Now, setting $M = \frac{fH^2}{6}$ and replacing the constants of integration in Equations (A.12), we obtain the following analytical solutions:

$$\begin{aligned}
u(x, y) &= \frac{2f}{H} \left[\mathbb{S}_{11}xy + \mathbb{S}_{31} \left(y^2 - \frac{H^2}{4} \right) \right] \\
v(x, y) &= \frac{2f}{H} \left[\frac{\mathbb{S}_{21}}{2} \left(y^2 - \frac{H^2}{4} \right) - \mathbb{S}_{11}x^2 \right]
\end{aligned} \tag{A.15}$$

Finally, using the Lagrange Multiplier formulation, we provide the generic expressions of the components \mathbb{S}_{11} and \mathbb{S}_{21} of the \mathbb{S} tensor:

$$\begin{aligned}
\mathbb{S}_{11} &= \frac{a_y^4\mu + a_x^2a_y^2(\lambda + 2\mu)}{(a_x^2 + a_y^2)^2\mu(\lambda + 2\mu)} \\
\mathbb{S}_{21} &= -\frac{a_x^2a_y^2(\lambda + \mu)}{(a_x^2 + a_y^2)^2\mu(\lambda + 2\mu)}
\end{aligned} \tag{A.16}$$

Bibliography

- [1] George Lubin. *Handbook of composites*. Van Nostrand Reinhold Company, New York, Cincinnati, Toronto, London, Melbourne, 1969.
- [2] D. P. Bertsekas. *Constrained Optimization and Lagrange Multiplier Methods*. Athena Scientific, Belmont, Massachusetts, 1996.
- [3] O.C. Zienkiewicz. Constrained variational principles and penalty function methods in the finite element analysis. *Lecture Notes in Mathematics*, 363:207–214, 1974.
- [4] I. Babuska and M. Suri. Locking effects in the finite element approximation of elasticity problems. *Numerische Mathematik*, 62:439–463, 1992.
- [5] H.C. Martin M.J. Turner, R.W. Clough and L.C. Topp. Stiffness and deflection analysis of complex structures. *Journal of the Aeronautical Sciences*, 23:805–882, 1956.
- [6] O. C. Zienkiewicz and R. L. Taylor. *The Finite Element Method. Volume 1: The Basis*. Butterworth Heinemann, 2000.
- [7] K. J. Bathe. *Finite Element Procedures in Engineering Analysis*. Prentice-Hall, 1982.
- [8] K. Washizu. *Variational methods in elasticity and plasticity*. Pergamon Press, Oxford - New York - Toronto - Sydney, 1968.
- [9] E. Hellinger. *Die allgemeine Ausetze der Mechanik der Kontinua*. in *Encyclopedia der Matematischen Wissenschaften*, Vol. 4, 1914.
- [10] E. Reissner. On a variational theorem in elasticity. *J. Math. Phys.*, 29:90–95, 1950.
- [11] P. J. Davis and P. Rabinowitz. *Methods of numerical integration*. Academic Press, 1975.
- [12] T. T. H. Pian and K. Sumihara. Rational approach for assumed stress finite elements. *Int. J. Num. Meth. Eng.*, 20:1685–1695, 1984.
- [13] J. C. Simo and M. S. Rifai. A class of mixed assumed strain methods and the method of incompatible modes. *Int. J. Num. Meth. Eng.*, 29:1595–1683, 1990.

- [14] F. Brezzi D.N. Arnold and M. Fortin. A stable finite element for the stokes equations. *Calcolo*, 21:337–344, 1984.
- [15] T. T. H. Pian. Derivation of element stiffness matrices by assumed stress distribution. *AAIA J.*, 2:1333–1336, 1964.
- [16] A.J.M. Spencer. *Deformations of Fiber-reinforced Materials*. Oxford University Press, London, 1972.
- [17] A.J.M. Spencer. *Large Deformations of Solids: Physical Basis and Mathematical Modelling*, chapter 3: Modelling of Finite Deformations of Anisotropic Materials, pages 41–52. Elsevier Applied Science - London and New York, 1986.
- [18] S. Kolling M. Volger and R. Rolfes. Transversely isotropic plasticity with application to fiber-reinforced plastics. In *Material II*. DYNAmore GmbH, 2007.
- [19] J. Korelc and P. Wriggers. Improved enhanced strain four-node element with taylor expansion of the shape functions. *Int. J. Num. Meth. Eng.*, 40:407–421, 1997.
- [20] A. Chama and B.D. Reddy. New stable mixed finite element approximations for problems in linear elasticity. *Comput. Methods Appl. Mech. Engrg.*, 256:211–223, 2013.
- [21] B.D. Reddy J.K. Djoko, B.P. Lamichhane and B.I. Wohlmuth. Conditions for equivalence between the hu-washizu and related formulation, and computational behavior in the incompressible limit. *Comput. Methods Appl. Mech. Engrg.*, 195:4161–4178, 2006.
- [22] J. Korelc. *AceGen Manual*. University of Ljubljana, Slovenia, 2015.
- [23] J. Korelc. *AceFem Manual*. University of Ljubljana, Slovenia, 2015.
- [24] J. Korelc. Automatic generation of finite-element code by simultaneous optimization of expressions. *Theoretical Computer Science*, 187:231–248, 1997.
- [25] J. Korelc. Multi-language and multi-environment generation of nonlinear finite element codes. *Engineering with Computers*, 18:312–327, 2002.
- [26] R. D. Cook. Improved two-dimensional finite element. *ASCE J. Struct. Div.*, ST9:1851–1863, 1974.
- [27] L. N. Gifford. More on distorted isoparametric elements. *Int. J. Num. Meth. Eng.*, 14:290–291, 1979.
- [28] N. S. Lee and K. J. Bathe. Effects of element distortion on the performance of isoparametric elements. *Int. J. Num. Meth. Eng.*, 36:3553–3576, 1993.